

Radiative mean lifetime measurement in N=2 hydrogen
by Edward Frank Kelley

A thesis submitted in partial fulfillment of the requirements for the degree of DOCTOR OF PHILOSOPHY in Physics
Montana State University
© Copyright by Edward Frank Kelley (1977)

Abstract:
We measure the lifetime of the(formula not captured in OCR)state in hydrogen by monitoring the Lyman-a radiation produced from the decay of the p-state atoms in a fast beam of hydrogen atoms (~OlOOkeV). The p atoms are produced from metastable 22S1/2 atoms via Stark mixing. The metastable atoms are obtained from proton impact on a gas target. Information obtained from observations of the field-free decay and the field-induced decay of the p state in a uniform field (giving rise to quantum beats) is combined to yield a value for the lifetime without measuring the beam velocity independently. The quantum-beat curves are fit taking into account contributions from both the fringe field and the hyperfine structure. The fringe field of the uniform field region is treated approximately using an analytical solution of the problem for a hyperbolic-secant-model fringe field. The resulting value of the lifetime is three percent lower than theory and previous experiment. Possible sources of error are discussed.

STATEMENT OF PERMISSION TO COPY

In presenting this thesis in partial fulfillment of the requirements for an advanced degree at Montana State University, I agree that the Library shall make it freely available for inspection. I further agree that permission for extensive copying of this thesis for scholarly purposes may be granted by my major professor, or, in his absence, by the Director of Libraries. It is understood that any copying or publication of this thesis for financial gain shall not be allowed without my written permission.

Signature Edward D. Kelley

Date March 10, 1978

RADIATIVE MEAN LIFETIME MEASUREMENT IN N=2 HYDROGEN

by

EDWARD FRANK KELLEY

A thesis submitted in partial fulfillment
of the requirements for the degree

of

DOCTOR OF PHILOSOPHY

in

Physics

Approved:

R.T. Robiscoe (15 Feb. 78)
Chairman, Graduate Committee

Head, Major Department

Graduate Dean

MONTANA STATE UNIVERSITY
Bozeman, Montana

December, 1977

ACKNOWLEDGMENT

Space will not permit a full disclosure of my gratitude to those mentioned here, nevertheless please accept this brief thanks.

I wish to extend my thanks to Montana State University and the Physics Department for their support and to the National Bureau of Standards for the funds for the experiment; to Dr. R. D. Hight for his kind oversight and support during the early days; to Gregg Taylor, Richard Green, and Fred Zarndt for their assistance in the laboratory; to Mark Baldwin for his execellent workmanship; to Bill Schwalm for help with the computer; to Dr. L. D. Kirkpatrick, Dr. M. A. Hamilton, and Dr. D. A. Pierre for help in data handling; to Jay Walker (electronics), Mike Kelly (computer), and to Rosemary Gilbert (typing). I am indebted to Mark Franz for his unselfish help during the last months.

I thank Dr. J. E. Drumheller, my surrogate adviser, for his valuable suggestions; Dr. J. D. Hermanson and Dr. R. E. Lund for their time; and the rest fo my committee, Dr. K. L. Nordtvedt and Dr.P.J.Burfening.

I am especially grateful to Dr. R. T. Robiscoe, my adviser, for that part of his life, skills, style, and attitude which he imparted to me knowingly or not; also for his patience, friendship, and counsel.

A warm thanks must also be extended to my wife, Marva, for her patience and support throughout the seven years of graduate school; much of the credit for this work must go to her.

And finally, I wish to thank Albert.

TABLE OF CONTENTS

Chapter

I. INTRODUCTION 1

II. TWO-LEVEL THEORY 11

Two-Level System and Its Appropriateness 11

Uniform-Field Amplitude Solutions 15

Small-field approximation 17

P-population radiation profile 18

Contribution from the $2^2P_{3/2}$ state 19

Exact quantum-beat radiation profile 21

High-frequency approximation 22

Analytical Fringe-Field Model 24

Hyperfine Complications 26

Contribution from Window 31

III. EXPERIMENTAL APPARATUS AND DATA 34

Production of a Pure Metastable Beam 34

Experimental Chamber and Radiation Detection 39

Sources of Difficulties 52

Final Data 58

IV. ANALYSIS OF DATA 84

Least-Squares Fitting 84

Analysis of Free-Decay Data: Determination of γ/v . . . 87

Quantum-Beat Data 87

Calculation of window, velocity dispersion, and $2^2P_{3/2}$ contribution 102

Fitting function and results 109

Independent check with profile fit 120

Possible Systematic Errors and Improvements 122

V. CONCLUSION 130

. . . . . .

Appendix

1. CALCULATION OF LIFETIME 133

2. HYPERFINE STRUCTURE OF THE N=2 LEVEL 137

FOOTNOTES 146

LIST OF TABLES

1. Hyperfine Dipole Matrix Elements 28
2. Free-Decay Data: Run T18 68
3. Free-Decay Data: Run T19 69
4. Free-Decay Data: Run T22 70
5. Free-Decay Data: Run T23 71
6. Quantum-Beat Data: Run T18 77
7. Quantum-Beat Data: Run T19 78
8. Quantum-Beat Data: Run T22 79
9. Quantum-Beat Data: Run T23 80
10. Typical Operating Conditions: Run T23 83
11. Fit Results for Free-Decay Data 88
12. Fitting-Function Initialization 112
13. Quantum-Beat Fit Results: Run T18 113
14. Quantum-Beat Fit Results: Run T19 114
15. Quantum-Beat Fit Results: Run T22 115
16. Quantum-Beat Fit Results: Run T23 116
17. Quantum-Beat Profile Fits 121
18. Fine-Structure Dipole Matrix Elements 141
19. Hyperfine Wavefunctions 143
20. Hyperfine-Structure Dipole Matrix Elements 144

LIST OF ILLUSTRATIONS

1. Free Decay of Excited Atom 6
2. Field-Induced Quantum Beats 9
3. Allowed Hyperfine Transitions 30
4. Layout of Apparatus 36
5. Electrode Geometry in Experimental Chamber 41
6. Faraday Cup 44
7. Lyman-α Detector 47
8. Counting Electronics 49
9. Counts vs Charge-Exchange-Cell Pressure 57
10. Sweep-Field Signal Quenching 60
11. Decay-Induction Sandwich 62
12. Verification of Field-Free Region 65
13. Free-Decay Radiation vs Conversion Voltage 67
14. Free-Decay Data: Run T18 74
15. Quantum-Beat Modulation 76
16. Quantum-Beat Data: Run T23 82
17. Parallel-Plate-Capacitor Field Map 91
18. Uniform-Field Fringe Fields along Beam 94
19. Uniform-Field Fringe Field across Beam 96
20. First Radiation Peak in Fringe Field 98
21. Analytical and Actual Fringe-Field Comparison 101

22. Detector-Window Geometry 104

23. Detector-Window Profile 107

24. Fit for Run T23 119

25. Quasi-Free Decay 125

ABSTRACT

We measure the lifetime of the $2^2P_{1/2}$ state in hydrogen by monitoring the Lyman-α radiation produced from the decay of the p-state atoms in a fast beam of hydrogen atoms ($\sim$100keV). The p atoms are produced from metastable $2^2S_{1/2}$ atoms via Stark mixing. The metastable atoms are obtained from proton impact on a gas target. Information obtained from observations of the field-free decay and the field-induced decay of the p state in a uniform field (giving rise to quantum beats) is combined to yield a value for the lifetime without measuring the beam velocity independently. The quantum-beat curves are fit taking into account contributions from both the fringe field and the hyperfine structure. The fringe field of the uniform field region is treated approximately using an analytical solution of the problem for a hyperbolic-secant-model fringe field. The resulting value of the lifetime is three percent lower than theory and previous experiment. Possible sources of error are discussed.

CHAPTER I

INTRODUCTION

The radiative mean lifetime of an excited atomic state is the average time one would have to wait before the excited atom makes a transition to lower energy levels by giving off energy in the form of electromagnetic radiation. The following analysis attempts to measure the lifetime of the $2^2P_{\frac{1}{2}}$ (or 2p) state in hydrogen which decays to the ground state ($1^2S_{\frac{1}{2}}$ or 1s) emitting ultraviolet, Lyman-α radiation.

Measurements of atomic lifetimes began with Wien [1] from 1919 to 1927, and it was at this time that the first n = 2 lifetime measurement in hydrogen was made. Lifetime measurements received little interest until the 1960's when an increase in activity resulted from the discovery of the beam-foil light source by Kay and further development by Bashkin.[2] Beam-foil spectroscopy has since become one of the most important branches of atomic physics as it provides a means of exciting many different atomic states. When a beam of atoms, molecules, or ions pass through a thin foil (usually carbon) the emergent beam consists of atoms which have essentially been coherently excited. The coherence has been useful in time-resolution experiments, for it allows the observation of modulated radiation (beats) and other phenomena which would not be seen if the excitation was of longer length. We do not intend

to review beam-foil spectroscopy or lifetime measurements in general, however, the reader is referred to review articles for further information.[3]

At the time of this writing there appear only two modern measurements of the 2p lifetime in hydrogen in the literature, though many more measurements have been reported for $n > 2$ lifetimes. In 1966 Bickel and Goodman reported a measurement of the radiative mean lives of both the 2p and 2p levels in hydrogen by using beam-foil methods.[4] They quote a value for the 2p lifetime of $\tau = (1.600 \pm 0.004) \times 10^{-9}$ s. This precision (0.25%) is likely an underestimate because it is essentially a computer fitting error and not a standard deviation of several runs. Then in 1968 Chupp, Dotchin, and Pegg report mean lives for the 2p, 3p levels in hydrogen also using beam-foil methods.[5] They pay considerable attention to the effects of foil thickness as well as the best fitting function to account for the cascades. They quote a 2p lifetime of $\tau = (1.60 \pm 0.01) \times 10^{-9}$ s ($\pm 0.625\%$) which represents the weighted standard deviation of five runs. Their paper contains a history of lifetime measurements for $n > 2$ levels in hydrogen as well. All these results agree with the theoretical value of $\tau = 1.5961$ns as calculated in appendix 1.

Our interest in this lifetime measurement is twofold: 1.) For the purposes of testing any theory an accurate measurement must be pro-

vided, a measurement which refrains from oversimplifications and honestly examines all peculiarities of the equipment and analyses of data. 2.) A careful examination of the 2p lifetimes in hydrogen is free from complicated decay schemes characteristic of higher levels; indeed, since the hydrogen atom provides us with the most complete quantum mechanical description, when we make measurements upon it we test our fundamental understandings of atomic systems and the applicability of approximations used to describe such systems.

Our understanding of spontaneous decay parallels our understanding of the quantum theory of radiation. Although semiclassical theories avoid the problem of vacuum-field fluctuations they don't provide decay from a pure state.[6] More often, the vacuum fluctuations are considered to be the mechanism for triggering the emission of radiation.[7] Thus by careful observation of the 2p decay radiation we peer at some of the simplest manifestations of these vacuum fluctuations or whatever other mechanisms might produce the decay.

In this analysis we choose to use the damped, two-level theory of Bethe and Lamb which phenominologically provides for the decay of the excited state in the manner of Weisskopf-Wigner theory--described in detail in chapter two. This two-level theory provides the basis for several experiments, the most notable of which are the Lamb-shift experiments.[8] In our case we examine the field-free and Stark-coupled

2p-2s system and the resulting decay of the 2p state.

Probably the simplest way to make a lifetime measurement is to excite the atomic state of interest at some point along the beam and then monitor the decay radiation as a function of distance from the point of excitation. In Fig. 1 we show a beam of hydrogen metastables which enters a short electric field region converting some of the metastables ($2^2S_{\frac{1}{2}}$ or 2s) to 2p atoms via Stark coupling. Upon leaving the field region the remaining p-state atoms exponentially decay emitting Lyman-α radiation. The observed radiation profile exhibits the same exponential decay (neglecting background)

$$I(z) = I_o e^{-mz}, \quad m = \gamma/v = 1/v\tau . \tag{1}$$

Here the position z is related to the time after excitation by $t = z/v$ where v is the beam velocity. In this way the temporal evolution is observed as a spatial profile. The quantity $1/\tau$ is known as the decay rate γ. The natural logarithm of this profile will be a straight line

$$\ln I(z) = \ln I_o - mz \tag{2}$$

the slope of which gives the ratio $\gamma/v = m$. If the beam velocity can be measured separately then the decay rate may be determined. Assuming that the data can be obtained to any requisite precision the ultimate accuracy of lifetime measurements made in this manner depends upon the

Fig. 1. Free decay of excited atom. An electric field provided by the conversion electrodes converts metastable H_{2s} to H_{2p}. The H_{2p} atoms decay to the ground state emitting Lyman-α radiation. The resulting radiation profile exhibits simple exponential damping in the field-free region.

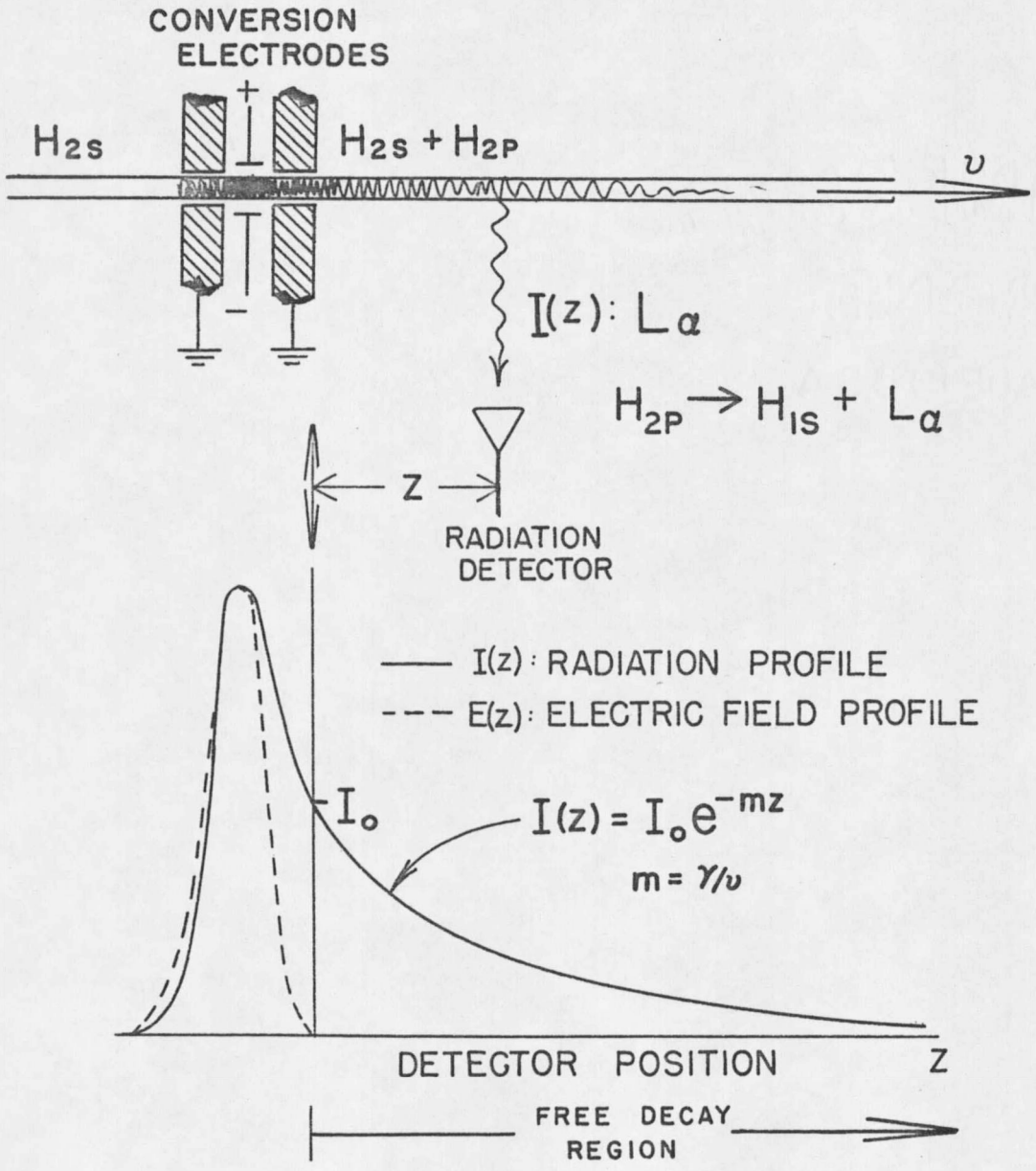

CONVERSION
ELECTRODES
+
H2S
H2S + H2P
v
−
I(z): Lα
H2P → H1S + Lα
z
RADIATION
DETECTOR
I(z): RADIATION PROFILE
E(z): ELECTRIC FIELD PROFILE
Io
I(z) = Ioe−mz
m = γ/v
DETECTOR POSITION
z
FREE DECAY
REGION

FIG. 1

accuracy with which the velocity can be measured. In the past, velocity measurements were only accurate to 0.5% or greater imposing a similar inaccuracy upon the lifetime. Progress has recently been made in the area of velocity measurements because of observations of zero-field quantum beats (QB), and velocity uncertainties of 0.1% or less are being claimed. It is now apparent that beam-foil spectroscopy is claimed to be capable of producting lifetime measurements to an accuracy of less than 0.3%.[9]

In Fig. 2 we show the effects of sending a beam of metastable hydrogen atoms into a uniform field region. The electric field couples the 2s metastable state to the 2p state, but rather than a simple decay profile, QB are observed in the radiation profile as long as the beam remains in the uniform field.[10] In the theory describing such modulated decay the beam velocity υ is found to occur always in the ratio γ/υ--the same ratio found in the description of the free-decay data--while the decay rate γ is found parametrically in combination with other factors describing the QB profile. We can use the ratio γ/υ obtained from the free-decay data to eliminate the velocity dependence in the QB theory and then by adjusting γ fit the QB theory to the data. The observation of field-induced QB will similarly allow a determination of the velocity. The theory of such observations also permits a formulation of the problem so that the velocity need not be

Fig. 2. Field-induced quantum beats. Under the application of a uniform electric field the Lyman-α radiation from the decay of the 2p state exhibits a modulated decay.

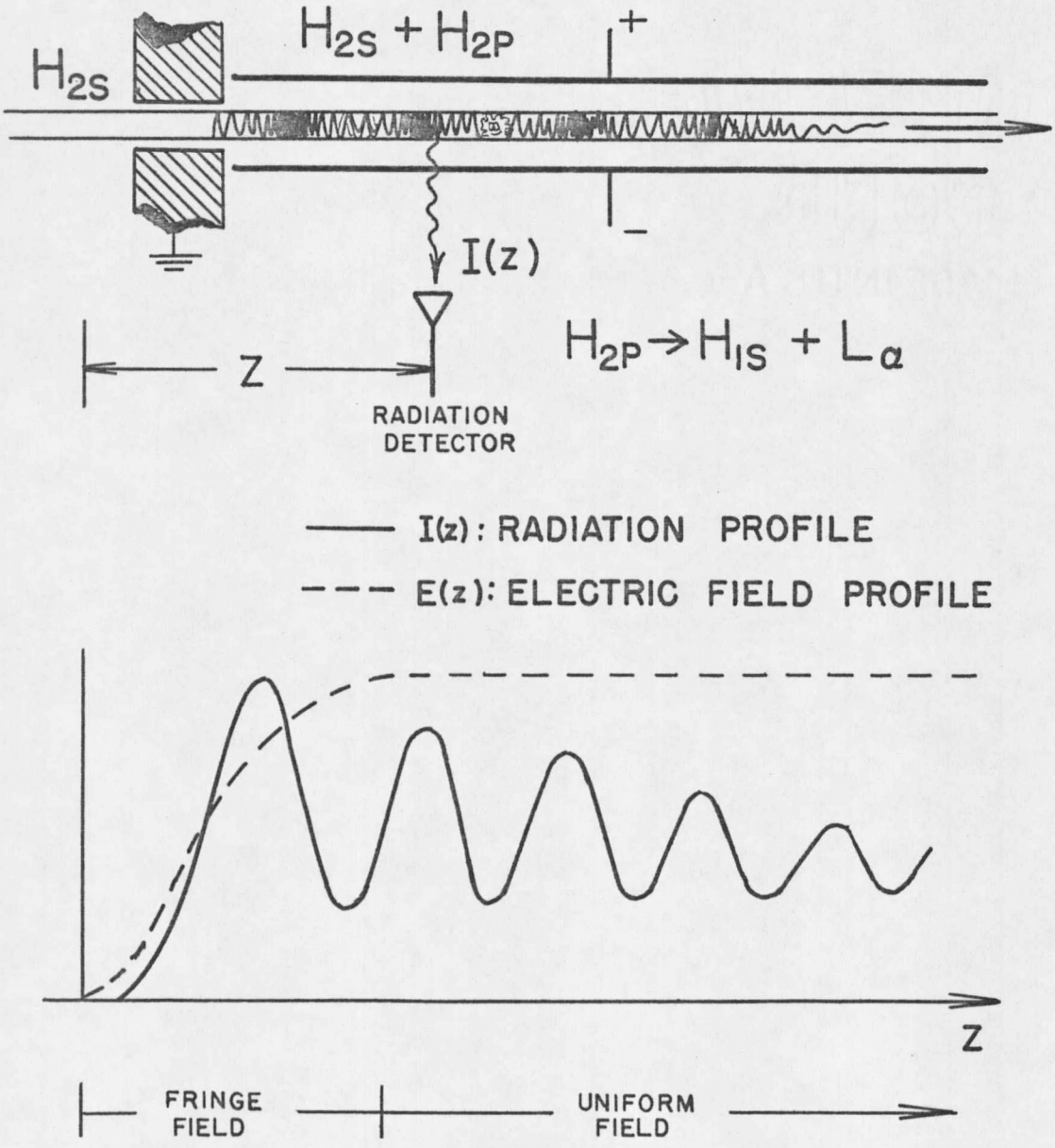

H2S
H2S + H2P
+
−
I(z)
z
RADIATION DETECTOR
H2P → H1S + Lα
I(z): RADIATION PROFILE
E(z): ELECTRIC FIELD PROFILE
z
FRINGE FIELD
UNIFORM FIELD

FIG. 2

measured directly.

Our handling of the QB data in this manner is not the only unique feature of this lifetime measurement. Serious attempt is made to analyze the QB curve in detail. Not only do we account for hyperfine structure, but we also pay considerable attention to the effects of the fringe field upon the QB radiation profile.

The theoretical details are discussed in the next chapter. There we develop the two-level problem with phenomenological damping and apply it to the hyperfine states. The theoretical machinery needed to estimate the effects of the fringe field and other factors which modify the QB profile are also developed. In chapter 3 we provide a description of the experimental apparatus and discuss the manner in which the data are collected. The chapter ends with a presentation of the final data. Chapter 4 gives the details of the analysis of these data. It is in the analysis section that we attempt to specify all factors which could affect the QB curves. They include fringe-field effects, demodulation from a detector window, influence of other excited states, and beam velocity dispersion. The value of the lifetime is presented and its accuracy is discussed along with possible improvements for a future continuation of this work and improvement in accuracy. Finally we discuss possible implications of our result.

CHAPTER II

TWO-LEVEL THEORY

Measurement of the $2^2P_{\frac{1}{2}}$ lifetime begins with a beam of metastable hydrogen atoms. This metastable or $2^2S_{\frac{1}{2}}$ state of hydrogen has a lifetime of $\tau_s=0.126s$.[11] Because of this long lifetime essentially none of the metastable atoms will decay as they travel through the experimental chamber--a trip which takes about 75ns to travel the 30cm of the chamber at beam velocities of 1.3% the velocity of light. Upon the application of an electric field the s state couples to the p state ($2^2P_{\frac{1}{2}}$) via an electric dipole (or Stark) coupling. In this way the rapidly decaying p state may be populated from the nondecaying s state reservoir providing us with a two-level problem.

Because there are four hyperfine sublevels associated with the s state and also the p state a two-level problem seems suspiciously simple. We show later, however, that the hyperfine problem reduces to four two-level problems; so the two-level theory is sufficient.

Two-Level System and Its Appropriateness

Consider a two-level system in which the levels (denoted by s and p) are separated by an energy $\mathcal{E}=\hbar\omega$. In our case this level separation is known as the n=2 Lamb shift in hydrogen having the value $\nu=1057.893(20)$MHz.[8] The electronic states of the unperturbed atom are

described by Schrödinger's equation

$$H\Psi = i\hbar\,\partial\Psi/\partial t\ , \tag{3}$$

where $H = H_A$ is the unperturbed atomic Hamiltonian. The stationary s and p states associated with the unperturbed atom are denoted by

$$\Psi_s = \varphi_s(\underset{\sim}{r})e^{-i\omega_s t}\ ,\quad \Psi_p = \varphi_p(\underset{\sim}{r})e^{-i\omega_p t}\ . \tag{4}$$

Here ω_s and ω_p represent the energy levels of the unperturbed s and p states respectively in units of angular frequency ($\omega_i = \mathcal{E}_i/\hbar$).

In the manner of time-dependent perturbation theory we consider the application of an electric field to this two-level system. The Hamiltonian now becomes

$$H = H_A + H_S \tag{5}$$

where

$$H_S = e\underset{\sim}{r}\cdot\underset{\sim}{E} \tag{6}$$

is the Stark (electric field) Hamiltonian which will couple the states. We write the wavefunction as a linear superposition of s and p wavefunctions

$$\Psi = s(t)\Psi_s + p(t)\Psi_p\ . \tag{7}$$

Normally, we would write the system wavefunction as a linear superposition of all the stationary state wavefunctions. If we assume that only the s state is occupied upon entry into the fringe field then to first order the amplitude of any other state m will be given by[12]

$$a_{sm}(t) = (1/i\hbar)\int_0^t \langle s|H_S|m\rangle\, e^{i\omega_{sm}t'}dt'\ . \tag{8}$$

The matrix elements which couple the s state to other states are not necessarily small when compared to the $2^2P_{\frac{1}{2}}$-$2^2S_{\frac{1}{2}}$ coupling. For example, the $2^2P_{3/2}$ - $2^2S_{\frac{1}{2}}$ coupling has the same magnitude and the 3P - 2S coupling is roughly 0.6 times as strong.[13] However, the integral is nontrivial only when the period characterizing the interaction ω_{sm}^{-1} is of the same order as the time necessary for the interaction to turn on. Because of the length of the fringe fields encountered in this measurement only the transitions to the $2^2P_{\frac{1}{2}}$ state are nontrivial--the interaction is essentially adiabatic for all other transitions. The period associated with $\omega_{\frac{1}{2}}$ is about 2×10^{-10} s while the period associated with $\omega_{3/2}$ is a factor of ten smaller. Even if we assumed a sudden turn on of the field we would find that transitions were predominantly to the $2^2P_{\frac{1}{2}}$ states. The transition probability in the sudden approximation is given by[14]

$$\Pi_{sm} \simeq |\langle s|H_s|m\rangle|^2/\hbar^2\omega_{sm}^2. \tag{9}$$

Since the energy separation between the $2^2S_{\frac{1}{2}}$ and $2^2P_{3/2}$ levels is roughly ten times the $2^2S_{\frac{1}{2}}$ - $2^2P_{\frac{1}{2}}$ separation the transition probability to this next nearest level ($2^2P_{3/2}$) is roughly 1% of that to the $2^2P_{\frac{1}{2}}$ level. This is not to say that the effects of the $2^2P_{3/2}$ state may be completely ignored. We will later develop corrections in the theory to account for the presence of the $2^2P_{3/2}$ state. For now, however, it is sufficient to consider only the $2^2P_{\frac{1}{2}}$ - $2^2S_{\frac{1}{2}}$ two-level system.

Requiring the system wavefunction to be a solution of Schrödinger's equation and utilizing the orthogonality of the unperturbed wavefunctions we can derive equations governing the time evolution of the amplitudes

$$i\hbar\dot{s} = V^* p\, e^{i\omega t}$$
$$i\hbar\dot{p} = V s\, e^{-i\omega t}, \tag{10}$$

where ω is the (unperturbed) state separation in angular frequency units and $V = \langle\varphi_p|H_s|\varphi_s\rangle$ represents the dipole matrix element which couples the states. H_s is non-diagonal in this representation as it only couples states of opposite parity.

Decay of the p state is provided for in the theory by the addition of a phenomenological damping term to the equation for the p amplitude

$$i\hbar\dot{p} = V s\, e^{-i\omega t} - i\hbar(\gamma/2)p\,, \tag{11}$$

where γ is the decay rate of the p state ($\gamma=1/\tau$). In the absence of coupling the p state will now decay exponentially $|p|^2 \sim e^{-\gamma t}$. A similar term could be added to the s-amplitude equation, but, as mentioned earlier, it is unnecessary to do so since the s state is so long lived ($\gamma_s \sim 8s^{-1}$) compared to the p state ($\gamma_p \sim 6\times10^8 s^{-1}$). This addition of phenomenological, radiative damping amounts to adding a non-Hermetian decay Hamiltonian H_D to the total Hamiltonian

$$H = H_A + H_S + H_D \tag{12}$$

whose only nonzero matrix element is $\langle\varphi_p|H_D|\varphi_p\rangle=-i\hbar\gamma/2$. With such an inclusion we no longer have conservation of probability $|S|^2+|p|^2<1$. Phenomenological damping was first introduced by Weisskopf and Wigner[15] and has been successfully tested both experimentally and theoretically[16] and found to be an excellent approximation for atomic beam work of this type. In fact, it is exact for hydrogen.[17]

Uniform-Field Amplitude Solutions

We now wish to solve these amplitude equations for an actual electric field, e.g., that produced by a parallel plate capacitor. If we could produce an electric field which turned on and reached its maximum value instantly at t=0 (a rectangular field profile) then the equations may be straightforwardly solved for a uniform field. Such a field cannot be produced in the laboratory so we have the problem of dealing with fringe fields.

Prior to entering the fringe field we may assume that the beam is purely metastable

$$S(t=-\infty)=1\ , \quad p(t=-\infty)=0\ . \tag{13}$$

The beam atoms pass through the fringe field whereby the amplitudes change $|S|^2<1$, $|p|^2>0$ and accumulate phases. Eventually the atoms reach a region where the field may be considered to be uniform. If we could determine the amplitudes upon reaching this uniform field region then we could follow the remaining time evolution of the amplitudes us-

ing the solution of the amplitude equations for a rectangular field, i.e., uniform field. We need only specify the amplitudes and not also their derivatives since Schrödinger's equation is first order in its time derivative. We will investigate two methods of estimating the fringe-field amplitudes after we more fully explore the solution to the uniform field region with arbitrary initial conditions.

If we decouple the damped amplitude equations and solve the resulting second order equations subject to the initial conditions

$$S(0)=A_S e^{i\theta_s}\,, \qquad p(0)=A_p e^{i\theta_p} \tag{14}$$

the amplitudes for t>0 will be given by

$$S(t)=S(0)\left[\frac{1+U}{2U}e^{-\mu_1 t}+\frac{U-1}{2U}e^{-\mu_2 t}\right] + p(0)\frac{iq^*}{(1-i\kappa)U}\left[e^{-\mu_2 t}-e^{-\mu_1 t}\right], \tag{15a}$$

$$p(t)=S(0)e^{-i\omega t}\frac{iq}{(1-i\kappa)U}\left[e^{-\mu_2 t}-e^{-\mu_1 t}\right] + p(0)e^{-i\omega t}\left[\frac{U-1}{2U}e^{-\mu_1 t}+\frac{1+U}{2U}e^{-\mu_2 t}\right], \tag{15b}$$

where

$$\mu_{1,2}=\gamma(1-i\kappa)(1\mp U)/4\,, \qquad U=\left[1-4|q|^2/(1-i\kappa)^2\right]^{1/2}$$
$$\kappa=2\omega/\gamma\,, \qquad q=2V/\hbar\gamma\,, \qquad \gamma=1/\tau\,. \tag{15c}$$

Although these solutions for the uniform field are exact they are by no means instructive. In way of clarification consider the temporal evolution of the amplitudes under the application of small electric

fields.

Small-Field Approximation

By requiring the fields to be small we mean $q<<1$, however, if $\kappa^2>>1$ we could equivalently require q/κ to be small. We will later find that q may be written as $q = E/E_o$ where $E_o = \hbar\gamma/2\sqrt{3}\,a\,e = 22.5 V/cm$ (assuming $\gamma=6.27\times10^8 s^{-1}$). The amplitudes with arbitrary initial conditions to lowest order in q may be written as

$$s(t) \simeq s(0)e^{-\gamma Q^2(1+i\kappa)t/2} - ip(0)q^*\frac{1+i\kappa}{1+\kappa^2}e^{-\gamma Q^2(1+i\kappa)t/2}\left[1-e^{-\frac{\gamma t}{2}+i\omega t}\right] \tag{16a}$$

$$p(t) \simeq -is(0)q\,\frac{1+i\kappa}{1+\kappa^2}\,e^{-\gamma Q^2(1+i\kappa)t/2-i\omega t}\left[1-e^{-\frac{\gamma t}{2}+i\omega t}\right]+ \tag{16b}$$

$$+\,p(0)\,e^{-i\omega t}\left[e^{-\frac{\gamma t}{2}+i\omega t}-\frac{1}{2}Q^2\,\frac{1+i\kappa}{1+\kappa^2}\,e^{-\gamma Q^2(1+i\kappa)t/2}\right],$$

where

$$Q^2 = |q|^2/(\kappa^2+1). \tag{16c}$$

As we will ultimately need to know $|p|^2$ we quote for later purposes the p population for $p(0)=0$

$$|p(t)|^2 \simeq Q^2 e^{-\gamma Q^2 t}\left[1+e^{-\gamma t}-2e^{-\gamma t/2}\cos\omega t\right]. \tag{17}$$

Further clarification of these complicated expressions may be obtained by considering short and long time behavior starting with a pure s state initially, $s(0)=1$, $p(0)=0$; then

$$s(t) = \exp\left[-\gamma Q^2 t/2 - i\omega Q^2 t\right] \tag{18a}$$

and

$$p(\Delta t) \simeq -iq(\gamma\Delta t/2)e^{-i\omega\Delta t} \qquad \text{(short times, } \Delta t\text{)} \quad (18b)$$

$$p(t) \simeq (q/\sqrt{\kappa^2+1})\exp\left\{-\gamma Q^2 t/2 + i[\theta-\omega(1+Q^2)t]\right\} \qquad \text{(long times)} \quad (18c)$$

where $\theta = \tan^{-1}(-1/\kappa)$. For zero magnetic field the level splitting is the fine-structure (or hyperfine) splitting giving a value for $\kappa \simeq 21$ and $\theta \simeq -0.043$rad which is negligible. Note that there is a $-\pi/2$ phase difference (from the s state) introduced in the p state upon entrance into the field (short times) and that the phase accumulates essentially as ωt whereas in the s state the phase more slowly accumulates as ωt times the square of the applied field (a slower rate since q is small). Also note that both states decay as the p-state decay rate times the square of the field, i.e., more slowly than the free decay of the p state. If we expand the most general small-fields approximation for the p state, Eq. (16b), we would obtain interference terms providing quantum beats as in the p-population expression Eq. (17). This small-field approximation will be found to be useful in estimating the effects of the $2^2P_{3/2}$ state.

P-Population Radiation Profile

Before proceeding further we must determine exactly what gives rise to the observed radiation. The decrease in population of the p state by its decay to the ground state provides the monitorable Lyman-α

radiation. We cannot, however, claim that the time derivative of the p-state population is proportional to the Lyman-α radiation since the p-population changes result from repopulation of the s state as well as decay to the ground state. Consistent with the assumption that the s state does not spontaneously decay compared with the p state, the only means that the total population $|s|^2 + |p|^2$ can change is by decay to the ground state through the p state. Referring to the amplitude equations with p-state damping it is simple to show that

$$d(|s|^2 + |p|^2)/dt = -\gamma|p|^2. \tag{19}$$

Hence the decay radiation intensity is proportional to the p-population.

Contribution from the $2^2P_{3/2}$ State

We can now use the small-field approximation to estimate the effects of the $2^2P_{3/2}$ state which have previously been ignored. The $2^2S_{1/2} - 2^2P_{3/2}$ Stark coupling is just as strong as the $2^2S_{1/2} - 2^2P_{1/2}$ coupling, however, the level separation is larger $\nu_{3/2} = 9911$MHz whereas $\nu_{1/2} = 1058$MHz.[18] Since the decay rate γ is essentially the same for both p states we find

$$\kappa_{1/2} / \kappa_{3/2} \equiv \eta = 0.0167 \tag{20}$$

with $\kappa_i = 2\omega_i/\gamma$, $\kappa_{1/2} = 21.2$ for zero magnetic field. Usually our electric fields were small $q \simeq 4.5$ so that the ratio $q/\kappa_{3/2} \simeq 0.02$ ($q/\kappa_{1/2} \simeq 0.21$) suggests using the small-field approximation to anticipate the effects of the $2^2P_{3/2}$ state. We now have two decaying states both producing

Lyman-α radiation roughly proportional to their population sum

$$R \propto |\rho_{1/2}|^2 + |\rho_{3/2}|^2. \tag{21}$$

Assuming $|s(0)| = 1$, $|p(0)| = 0$ the $2^2P_{3/2}$ population will be given by

$$|\rho_{3/2}|^2 \simeq \eta^2 Q^2 e^{-\gamma\eta^2 Q^2 t}\left[1 + e^{-\gamma t} - 2e^{-\gamma t/2}\cos\omega t\right], \tag{22}$$

where we have taken advantage of the fact that for zero magnetic fields

$$Q_{3/2}^2 \simeq \eta^2 Q^2$$

(Q is in terms of the $2^2S_{\frac{1}{2}} - 2^2P_{\frac{1}{2}}$ separation $\omega_{\frac{1}{2}}$). Similarly the s-state population will be given by

$$|s(t)|^2 = \exp\left(-\gamma\eta^2 Q^2 t\right). \tag{23}$$

To account for the effects of the $2^2P_{3/2}$ state we will employ the small-field approximation to express the $2^2P_{\frac{1}{2}}$ population as well, only rather than using $|s(0)|=1$ we will allow the s state to de-populate via the $2^2P_{3/2}$ state; then the $p_{\frac{1}{2}}$ population will be

$$|\rho_{1/2}|^2 = Q^2 \exp\left[-(1+\eta^2)\gamma Q^2 t\right]\left[1 + e^{-\gamma t} - 2e^{-\gamma t/2}\cos\omega t\right]. \tag{24}$$

The total radiation then appears as

$$\begin{aligned} |\rho|^2 = &\left\{\exp\left[-(1+\eta^2)\gamma Q^2 t\right] + \eta^2 \exp\left[-\gamma\eta^2 Q^2 t\right]\right\} \\ &\times Q^2\left[1 + e^{-\gamma t} - 2e^{-\gamma t/2}\cos\omega t\right]. \end{aligned} \tag{25}$$

This equation is yet incomplete, for we have neglected the hyperfine contributions. There are twice as many couplings to the hyperfine states in the $2^2p_{3/2}$ level as in the $2^2P_{\frac{1}{2}}$ level. Replacing η^2 by $2\eta^2$ accounts for the increased number of decay channels The $2^2P_{3/2}$ state is then seen to manifest itself by increasing the effective decay rate of the p state as well as providing a small signal-proportional cor-

rection. To the extent $\gamma\eta^2Q^2t<<1$ and Q^2 is small the simplest correction made is

$$|p|^2 \rightarrow |p[\gamma \rightarrow \gamma(1+2\eta^2)]|^2 \tag{26}$$

where the contribution η^2Q^2 has been neglected.

Exact Quantum-Beat Radiation Profile

With no approximations other than letting the decay rate of the s state be zero, the p-state population as derived from Eqs. (15) and hence the Lyman-α radiation profile produced by the two level system with arbitrary initial conditions and under the application of a uniform field will be given by

$$|p(z)|^2 = \frac{1}{u}\left[A'e^{-\alpha z} + B'e^{-\beta z} - Ce^{-az}\cos(\delta z - \phi)\right], \tag{27}$$

where

$$\begin{aligned}
&a = \gamma/2v, \quad \alpha = a(1-\xi), \quad \beta = a(1+\xi), \quad \delta = a\zeta, \quad \Delta = \theta_p - \theta_s, \\
&\xi = R - \kappa S, \quad \zeta = \kappa R + S, \quad R = \sqrt{u}\cos(\theta/2), \quad S = \sqrt{u}\sin(\theta/2), \\
&u = \sqrt{x^2+y^2}, \quad x = 1 + 4|q|^2\frac{\kappa^2-1}{(1+\kappa^2)^2}, \quad y = 8|q|^2\kappa/(1+\kappa^2)^2, \\
&\theta = \tan^{-1}(y/x), \quad \kappa = 2\omega/\gamma, \quad q = 2V/\hbar\gamma, \quad \omega = \omega_s - \omega_p,
\end{aligned} \tag{28}$$

and

$$\begin{aligned}
A' &= A_s^2\frac{|q|^2}{1+\kappa^2} + A_p^2\frac{u+1-2R}{4} + A_sA_p\frac{|q|}{1+\kappa^2}\left[(\zeta-\kappa)\cos\Delta + (1-\xi)\sin\Delta\right], \\
B' &= A_s^2\frac{|q|^2}{1+\kappa^2} + A_p^2\frac{u+1+2R}{4} - A_sA_p\frac{|q|}{1+\kappa^2}\left[(\zeta+\kappa)\cos\Delta - (1+\xi)\sin\Delta\right], \\
C &= 2A_s^2\frac{|q|^2}{1+\kappa^2} - A_p^2\frac{u-1}{2} - 2A_sA_p\frac{|q|}{1+\kappa^2}\left[\kappa\cos\Delta - \sin\Delta\right],
\end{aligned} \tag{29}$$

$$D = A_p^2 S + 2A_s A_p \frac{|q|}{1+\kappa^2}\left[\xi\cos\Delta + \zeta\sin\Delta\right],$$

$$G = \sqrt{C^2 + D^2}, \quad \phi = \cos^{-1}(C/G).$$

Here, as before, we've replaced t by its equivalent $t=z/v$. This somewhat complicated expression provides a complete description of quantum beat phenomena in a two-level system under the application of a uniform electric field. Note the appearance of the γ/v factor in the expression for $\mathfrak{a}$ and how the factors which provide for the predominant decay structure, viz., α,β,δ are proportional to $\mathfrak{a}$. Note also how γ enters elsewhere through κ and q. Such independence provides us with the means of using the value of γ/v obtained from the analysis of the free decay data yet provide remaining freedom to fit the QB curve by adjusting γ.

High-Frequency Approximation

It is instructive to examine an approximation at this point. Using the fine-structure splitting angular frequency $\omega=6.6469\times10^9\,s^{-1}$ and decay rate $\gamma=6.27\times10^8\,s^{-1}$ we find $\kappa=2\omega/\gamma=21.2$. If we make an expansion of the p-state probability in terms of $1/\kappa$ and keep terms to order $1/\kappa^2$ (since for zero magnetic fields $1/\kappa^2=0.0022$ we expect this approximation to be quite good) we obtain

$$|\rho(z)|^2 = \frac{1}{4}\left[A'e^{-\alpha z} + B'e^{-\beta z} - Ge^{-\mathfrak{a}z}\cos(\delta z - \phi)\right] \tag{30}$$

where

$$u = 1+4\epsilon^2, \quad a = \gamma/2\upsilon, \quad \alpha = a\left(1-\frac{1}{\sqrt{u}}\right), \quad \beta = a\left(1+\frac{1}{\sqrt{u}}\right), \quad \delta = \omega\sqrt{u}/\upsilon,$$

$$A' = A_s^2\epsilon^2 + \tfrac{1}{2}A_p^2\left(1+2\epsilon-\sqrt{u}\right) + A_sA_p\epsilon\left[\left(\sqrt{u}-1\right)\cos\Delta + \left(1-\frac{1}{\sqrt{u}}\right)\frac{\sin\Delta}{\kappa}\right],$$

$$B' = A_s^2\epsilon^2 + \tfrac{1}{2}A_p^2\left(1+2\epsilon+\sqrt{u}\right) - A_sA_p\epsilon\left[\left(1+\sqrt{u}\right)\cos\Delta - \left(1+\frac{1}{\sqrt{u}}\right)\frac{\sin\Delta}{\kappa}\right],$$

$$C = 2A_s^2\epsilon^2 - 2A_p^2\epsilon^2 - 2A_sA_p\epsilon\left(\cos\Delta - \frac{\sin\Delta}{\kappa}\right), \tag{31}$$

$$D = \frac{4A_p^2\epsilon^2}{\kappa\sqrt{u}} + 2A_sA_p\epsilon\left(\frac{\cos\Delta}{\kappa\sqrt{u}} + \sqrt{u}\sin\Delta\right),$$

$$G = \sqrt{C^2+D^2}, \quad \phi = \cos^{-1}(C/G).$$

Here ϵ is a measure of the electric field

$$\epsilon = |q|/\kappa = |V|/\hbar\omega \tag{32}$$

It will later be shown that $V = \sqrt{3}\,a_o\,eE$ where E is the applied field and where a_o and e are the Bohr radius and electronic charge respectively. We can then write

$$\epsilon = \frac{E}{E_o}, \quad E_o = \hbar\omega/\sqrt{3}\,a_o e = 477.345 \text{ volts/cm} \tag{33}$$

Typically we use electric fields of about 324volts/cm. Here ω is the fine-structure splitting. We include this high frequency approximation ($1/\kappa^2 \ll 1$) because it demonstrates the general features of the radiation profile. Note that γ appears only in the form γ/υ (in the factor a) which is the ratio provided by the free-decay analysis. The oscillatory term may be written as

$$\cos\left(z\omega\sqrt{1+4\epsilon^2}/v - \phi\right) \tag{34}$$

which, aside from the phase factor ϕ, lacks any dependence upon γ; rather, it exhibits only a dependence upon the state separation ω, the field strength ϵ and the (unknown) velocity v. What this tells us is that any dependence upon γ in the exact expression for the p population, aside from the ratio γ/v, will be small. Hence, we will have to be very careful in selecting the amplitude initial conditions for the uniform field in order to expect to extract meaningful values for γ.

Now that we have a means of following the quantum beat (QB) profile when the beam is in the uniform field region we must provide a means of establishing the initial amplitude magnitudes A_s, A_p and the initial phase difference $\Delta = \theta_p - \theta_s$ produced as the beam travels through the fringe field. These results must then be extended to account for hyperfine structure, the effects of a beam velocity dispersion, and detector's observation of a finite portion of the beam (detector window).

Analytical Fring-Field Model

Probably the most direct way to estimate the amplitudes after they've passed through the fringe field would be to measure the fringe field and then provide for a computer integration of Schrödinger's equation, i.e., the amplitudes equations of Eqs. (10) and (11), as the atoms were through the nonuniform field. We do this in the analysis

chapter (Chap.4).

Such computer solutions may become expensive if high accuracy and large quantities are required. If a model of a fringe field could be developed for which analytical solutions to the amplitude equations could be found then analysis of the effects of the fringe field would be greatly facilitated. Such a model first developed by Rosen and Zener has recently been extended by Robiscoe to include decaying levels as well as a rotating field.[19] The following is an outline of some of the results as applied to our problem.

Consider subjecting our two-level system to a coupling of the form

$$W(t)=V\,\mathrm{sech}(\pi t/T),\quad \int_{-\infty}^{\infty} W(t)dt = VT. \tag{35}$$

Writing $p(t)=P(t)e^{-\gamma t/2}$ the new amplitude equations will be

$$i\hbar\dot{s} = W^{*}(t)\,P\,e^{i\Omega t},\qquad i\hbar\dot{P} = W(t)\,s\,e^{-i\Omega t} \tag{36}$$

where $\Omega = \omega + i\gamma/2$. Uncoupling these equations and making the transformation

$$x(t) = \tfrac{1}{2}\left[\tanh(\pi t/T) + 1\right] \tag{37}$$

the uncoupled amplitude equations are each transformed into a hypergeometric equation. Subjecting the solution to the initial conditions

$$|s(t\to-\infty)| = 1\ ,\qquad P(t\to-\infty) = 0 \tag{38}$$

the following amplitudes are obtained

$$p(t) = (a/|\phi|)\,x^{\phi}\,e^{-\gamma t/2}\,F(\phi+a,\phi-a;\phi+1;z) \tag{39}$$

$$s(t) = (i\phi/|\phi|)\, x^{\phi} \exp\left[-\left(\frac{\pi}{T} + \tfrac{1}{2}\gamma - i\omega\right)t\right] F(\phi+a, \phi-a; \phi; z),$$

where

$$a = VT/\pi\hbar, \quad \phi = \tfrac{1}{2} + (\gamma T/4\pi) - i(\omega T/2\pi), \quad t = z/v, \tag{40}$$

and F is the hypergeometric function.[20]

These results provide us with a model for a fringe field of a parallel plate capacitor configuration; for we can use the results for the fringe field amplitudes as initial conditions for a uniform field region. Note that at t=0, z=0 and x=½. The total field profile is then

$$W = \begin{cases} V \operatorname{sech}(\pi z/vT) & \text{for } z \le 0 \\ V & \text{for } z \ge 0 \end{cases} \tag{41}$$

The length of the fringe field may be established by its half-width-half-maximum which is related to T by

$$\Delta z_{HWHM} = (0.419201)\, Tv \tag{42}$$

This completes our development of a model fringe field for estimating initial amplitudes. We must now examine the complications arising from the hyperfine structure.

Hyperfine Complications

A discussion of the hyperfine problem details are given in appendix 2. Here we will only be concerned with the results.

Resolving the electric field into Cartesian components and defining

$$E_{\pm} = E_x \pm iE_y, \tag{43}$$

the dipole matrix elements between hyperfine states may all be written in terms of three scalar products involving the elementary n,ℓ,m_ℓ wavefunctions

$$V_{-1} = (3/\sqrt{2})\, a_o e\, E_- = \langle 2P(m_\ell=+1)|H_s|2S\rangle \tag{44}$$

$$V_{+1} = -(3/\sqrt{2})\, a_o e\, E_+ = \langle 2P(m_\ell=-1)|H_s|2S\rangle \tag{45}$$

$$V_o = -3a_o e\, E_z = \langle 2P(m_\ell=0)|H_s|2S\rangle \tag{46}$$

The first two V_{+1}, V_{-1} involve electric fields perpendicular to the quantization axis while the last one, V_o, involves electric fields parallel to the quantization axis. In table 1 we show the dipole coupling between hyperfine states. Note that there are two types of transitions allowed by the coupling, ones for which $\Delta m_f = \pm 1$ and ones for which $\Delta m_f = 0$. Which transitions occurs depends upon the electric field orientation

$\Delta m_f = 0$ $\quad$ σ-Transitions $\quad$ $E_z \neq 0$ $\quad$ $(E_{\parallel} \neq 0)$

$\Delta m_f = \pm 1$ $\quad$ π-Transitions $\quad$ $E_x, E_y \neq 0$ $\quad$ $(E_{\perp} \neq 0)$

In figure 3 we illustrate the transitions which may occur for dipole

TABLE 1

HYPERFINE DIPOLE MATRIX ELEMENTS

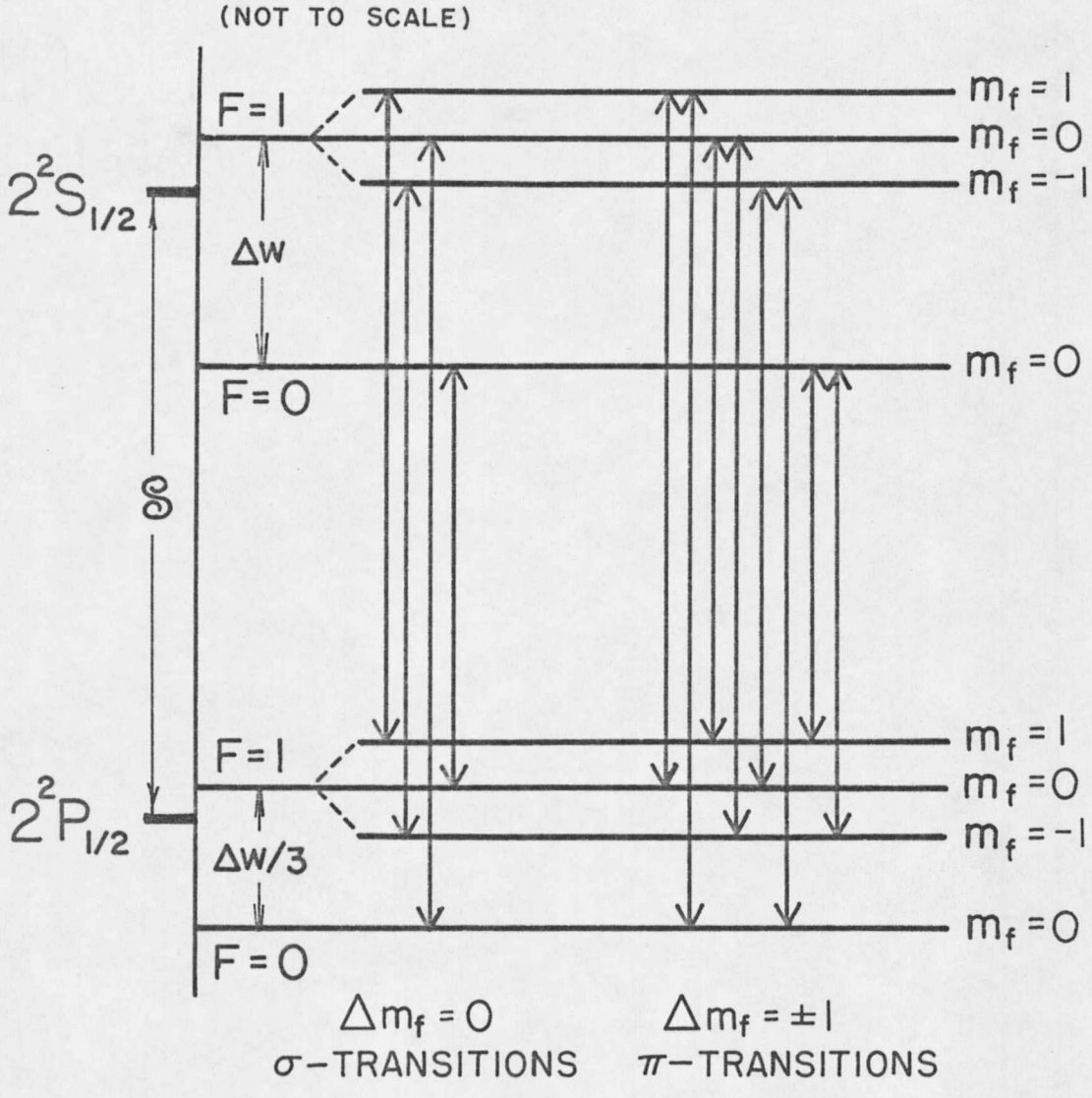
$\langle 2^2P_{1/2}(f,m_f)|e\mathbf{r}\cdot\mathbf{E}|2^2S_{1/2}(f,m_f)\rangle$

$2^2S_{1/2}$ / $2^2P_{1/2}$			ℓ	0			
			j	1/2			
			f	1			0
ℓ	j	f	m_f / m_f	1	0	-1	0
1	1/2	1	1	Σ	Π_-	0	$-\Pi_-$
			0	Π_+	0	Π_-	Σ
			-1	0	Π_+	$-\Sigma$	Π_+
		0	0	$-\Pi_+$	Σ	Π_-	0

$$\Sigma = \sqrt{3}\, a_e E_0 = -V_0$$

$$\Pi_\pm = \sqrt{9/2}\, a_e E_\pm = \mp V_\pm$$

Fig. 3. Allowed hyperfine transitions. For dipole coupling σ-transitions arise from components of the electric field parallel to the quantization axis; π-transitions, from E-field components perpendicular to the quantization axis.



$\mathcal{S} = 1057.893(20)\,\text{MHz}$

$\Delta W = 177.55686(53)\,\text{MHz}$

FIG. 3

coupling. Depending upon how the orientation of the electric field is chosen the hyperfine problem can be reduced to four two-level problems when the electric field is parallel to the quantization axis, two four-level problems when perpendicular to the quantization axis, or a single twelve-level problem for arbitrary electric field direction.

By choosing the z axis to lie in the direction of the electric field the otherwise complicated coupling between the hyperfine levels reduces to four independent two-level problems. We may, therefore, write the total population as an average of the hyperfine state populations (characterized by $\omega_{1,\ldots,4}$)

$$|p(z)|^2 = \frac{1}{4}\left[2|p(\omega_1;z)|^2 + |p(\omega_3;z)|^2 + |p(\omega_4;z)|^2\right] \tag{47}$$

where the ω_i are the hyperfine level separations ($\omega_1=\omega_2=6.832875\times10^9\,s^{-1}$, $\omega_3=7.204749\times10^9\,s^{-1}$, and $\omega_4=5.71725\times10^9\,s^{-1}$).

Contributions from Window

Up to now the expressions for $|p(z)|^2$ represent the population of the p state at a point z. No attempt has been made to account for the fact that a real detector obtains its signal from a finite portion of the beam. It is a simple matter to calculate the effects of such a window if we assume that the window has a rectangular profile. Consider, then, a rectangular window which observes a length w of the beam. The radiation observed for detector position z will be proportional to

$$\overline{|p(z)|^2} = \frac{1}{w}\int_{-w/2}^{w/2} |p(z+z')|^2 dz', \tag{48}$$

where w is assumed to be small compared to the detector-beam separation so that $1/r^2$ effects may be neglected in this approximation. Using the exact p-state population of Eqs.(31) the actual radiation profile including window will be proportional to (dropping the average value sign)

$$|p(z)|^2 = \frac{1}{u}\left[Ae^{-\alpha z} + Be^{-\beta z} - Ge^{-\hat{a}z}F(\delta z - \phi)\right], \tag{49}$$

where

$$A = (2A'/w\alpha)\sinh(w\alpha/2), \quad B = (2B'/w\beta)\sinh(w\beta/2),$$

$$F(\delta z - \phi) = X\cos(\delta z - \phi) - Y\sin(\delta z - \phi),$$

$$X = 2\left[a\sinh(aw/2)\cos(\delta w/2) + \delta\cosh(aw/2)\sin(\delta w/2)\right]/w(a^2+\delta^2) \tag{50}$$

$$Y = 2\left[\delta\sinh(aw/2)\cos(\delta w/2) - a\cosh(aw/2)\sin(\delta w/2)\right]/w(a^2+\delta^2).$$

The remaining factors may be found defined in Eqs. (31)

It is now a simple matter to account for a velocity dispersion, $\Delta v/v \neq 0$. Upon entering the fringe field, a length $\Delta\ell$ of the radiating beam spreads according to

$$\Delta z = \Delta\ell + \frac{\Delta v}{v} z \ . \tag{51}$$

We can therefore account for a velocity dispersion by including a z-dependent increase in the window

$$w \to w + \frac{\Delta v}{v} z \ . \tag{52}$$

This completes our development of the two-level problem and its application to the hyperfine system. We will next examine the appa-

ratus used to obtain the data and some of the difficulties encountered.

CHAPTER III

EXPERIMENTAL APPARATUS AND DATA

Production of a Pure Metastable Beam

The proton beam used in production of the metastable hydrogen beam is provided by a 50 to 130kV accelerator (Texas Nuclear Model 9501-1 Neutron Generator modified as a proton source). Two alignment magnets are placed at the output of the accelerator allowing precise vertical and horizontal positioning of the beam (see Fig. 4). The pressures at the accelerator's output are maintained from 5μT to 7.5μT ($1\mu T = 1\times10^{-6}$mmHg) during operation by a four inch diffusion pump. This replaces the less efficient system originally on the accelerator and provides a factor of four improvement in the vacuum. An electrostatic focusing lens (a quadrupole doublet, Texas Nuclear Model 9515) is employed to concentrate the diffuse beam, thereby increasing the useable beam by a factor of five at least. The proton beam is then velocity selected from the non-proton components (like H_2^+, O^+, O_2^+, N^+, etc.) and is deflected approximately 20^o from its original direction. Because alignment of this proton beam is so critical we have installed two triming magnets, one upstream and one downstream from the analyzing magnet. Each of these magnets provides adjustable vertical and horizontal deflection of the beam and are found to be indispensible

Fig. 4. Layout of apparatus. Drawn approximately to scale.

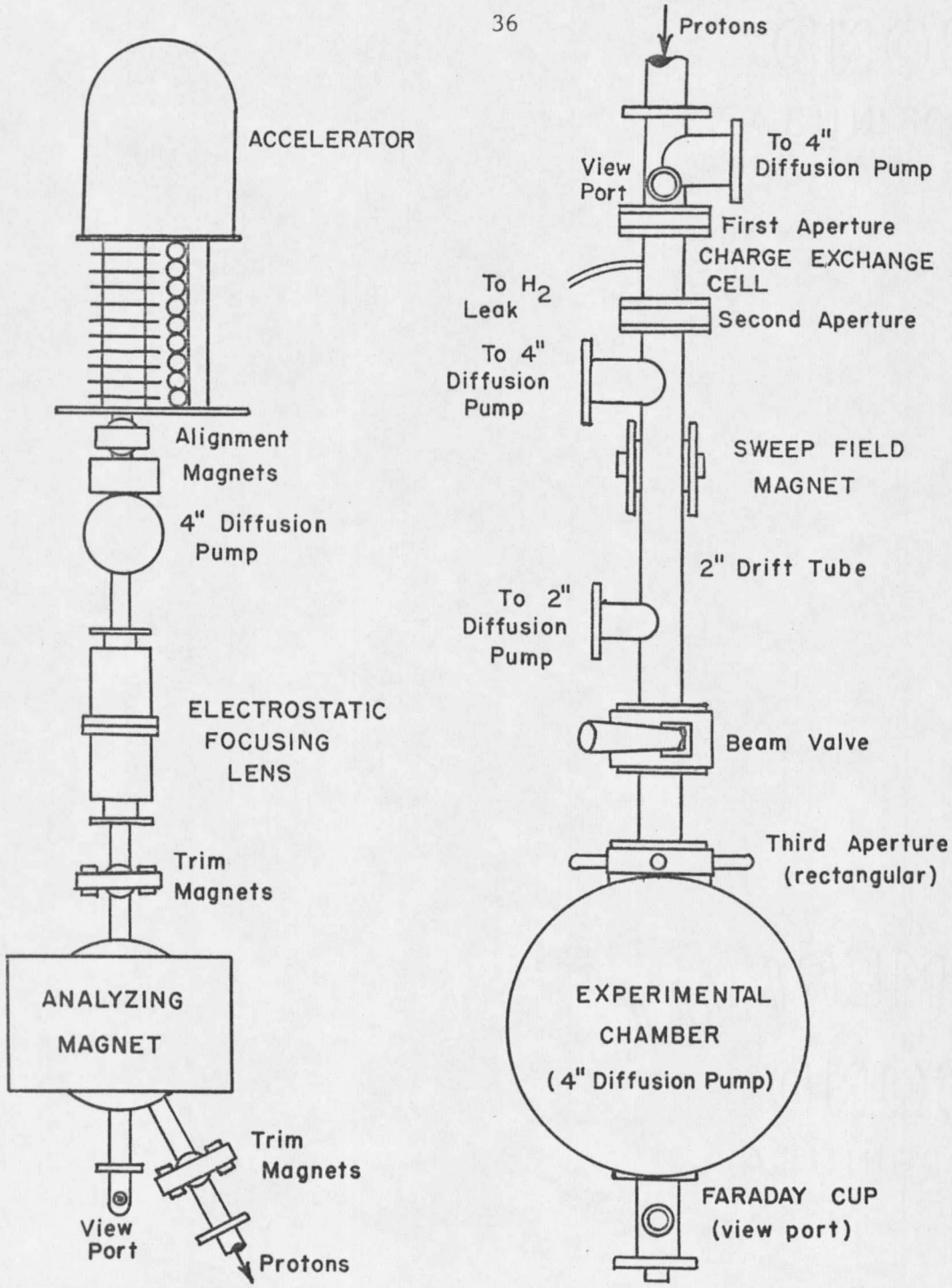

ACCELERATOR
Alignment Magnets
4" Diffusion Pump
ELECTROSTATIC FOCUSING LENS
Trim Magnets
ANALYZING MAGNET
Trim Magnets
View Port
Protons
Protons
To 4" Diffusion Pump
View Port
First Aperture
CHARGE EXCHANGE CELL
To H_2 Leak
Second Aperture
To 4" Diffusion Pump
SWEEP FIELD MAGNET
2" Drift Tube
To 2" Diffusion Pump
Beam Valve
Third Aperture (rectangular)
EXPERIMENTAL CHAMBER (4" Diffusion Pump)
FARADAY CUP (view port)

FIG. 4

in maximizing the downstream beam current especially when a new beam velocity is selected.

The proton beam is partially converted to an atomic hydrogen beam by passing through a cell where the pressures are maintained sufficiently high so that the proton is likely to acquire an electron via collisions with the background gas.[21] This charge exchange region is enclosed by two adjustable, circular apertures. The upstream (#1) aperture's diameter is 1.083±0.002mm and downstream (#2), 0.980±0.003mm. The pressures within the charge exchange cell are maintained by a Granville-Phillips leak from 30mT to 45mT (depending upon the run) to within less than 1% as monitored by an MKS Baratron pressuremeter (type 77).

Upon leaving the charge exchange cell the beam is composed of protons (which survived collisions) and hydrogen atoms in many excited states as well as ground state hydrogen. Because of very short natural lifetimes many of the excited atoms quickly decay to the ground state or one of the other longer lived s-states such as $2^2S_{\frac{1}{2}}$, $3^2S_{\frac{1}{2}}$, etc. and, therefore, don't present cascade problems downstream in the measurement regions. The protons do cause difficulties if a sufficient number are present in the beam; because they produce electric fields which quench some of the $2^2S_{\frac{1}{2}}$ metastables and, therefore, act as a source of stray electric fields. Removal of the protons is accomplished by a magnetic

field which bends the proton beam from the neutral beam. Originally an electric field was employed to deflect the proton beam, but because of charge accumulation on the plates providing spurious stray electric fields they were replaced by an external magnet.

This proton sweep field serves another purpose. The $n > 2$ s states are also metastable ($3^2S_{\frac{1}{2}}$ and $4^2S_{\frac{1}{2}}$ states have lifetimes of 160ns and 230 n s respectively [22]). With beam velocities of over 1% the speed of light this corresponds to distances of almost a meter and these states would survive to the experimental chamber if they were not quenched by the sweep field. Roughly 50% of the $2^2S_{\frac{1}{2}}$ metastables are quenched from the beam as a result of the motional electric field produced by the sweep field magnet. Since the transition probability is approximately proportional to the square of the coupling, and the square of the dipole coupling for the $n = 3, 4$ s levels to the nearest p levels are roughly six and twenty times the square of the 2s - 2p dipole coupling;[23] we may therefore be assured that upon entering the experimental chamber all states other than the $2^2S_{\frac{1}{2}}$ state have been depopulated and we have remaining an essentially pure beam of $2^2S_{\frac{1}{2}}$ metastables. Ground state atoms are present in great number but don't affect the results and may be neglected. A distance of about 60cm separates the charge-exchange cell and the experimental chamber allowing sufficient time for depopulation of all but the $2^2S_{\frac{1}{2}}$ level.

Experimental Chamber and Radiation Detection

Before entering the experimental chamber the metastable beam is collimated by a rectangular aperture. A rectangular aperture is used since it allows a wide beam to pass through the chamber's electric field regions taking advantage of the symmetry of their fields and increasing the measured radiation by up to six times the radiation obtained from a circular aperture. Each of the four plates comprising the aperture can be moved independently and for purposes of knowing where the beam is during alignment the beam current on each plate can be monitored.

Within the experimental chamber are placed four electrode configurations for the application of electric fields the the beam (see Fig. 5). The first electric field region is the quench field. Here it is possible to remove all the metastable component from the beam (for purposes of taking background counts) by applying large voltages to the plates. (Although 500V seemed to quench all metastables we use 1.5kV.)

Next the decay induction sandwich provides a spatially short electric fiels to the beam thereby allowing conversion of a fraction of the $2^2S_{\frac{1}{2}}$ metastables to the $2^2P_{\frac{1}{2}}$ atoms in a small distance. The field-free decay of the new $2^2P_{\frac{1}{2}}$ state can then be observed shortly after the sandwich because the ground plates prevent the field from ex-

Fig. 5. Electrode geometry in experimental chamber drawn approximately to scale. With enlargement of the decay induction sandwich and entrance to uniform field region.

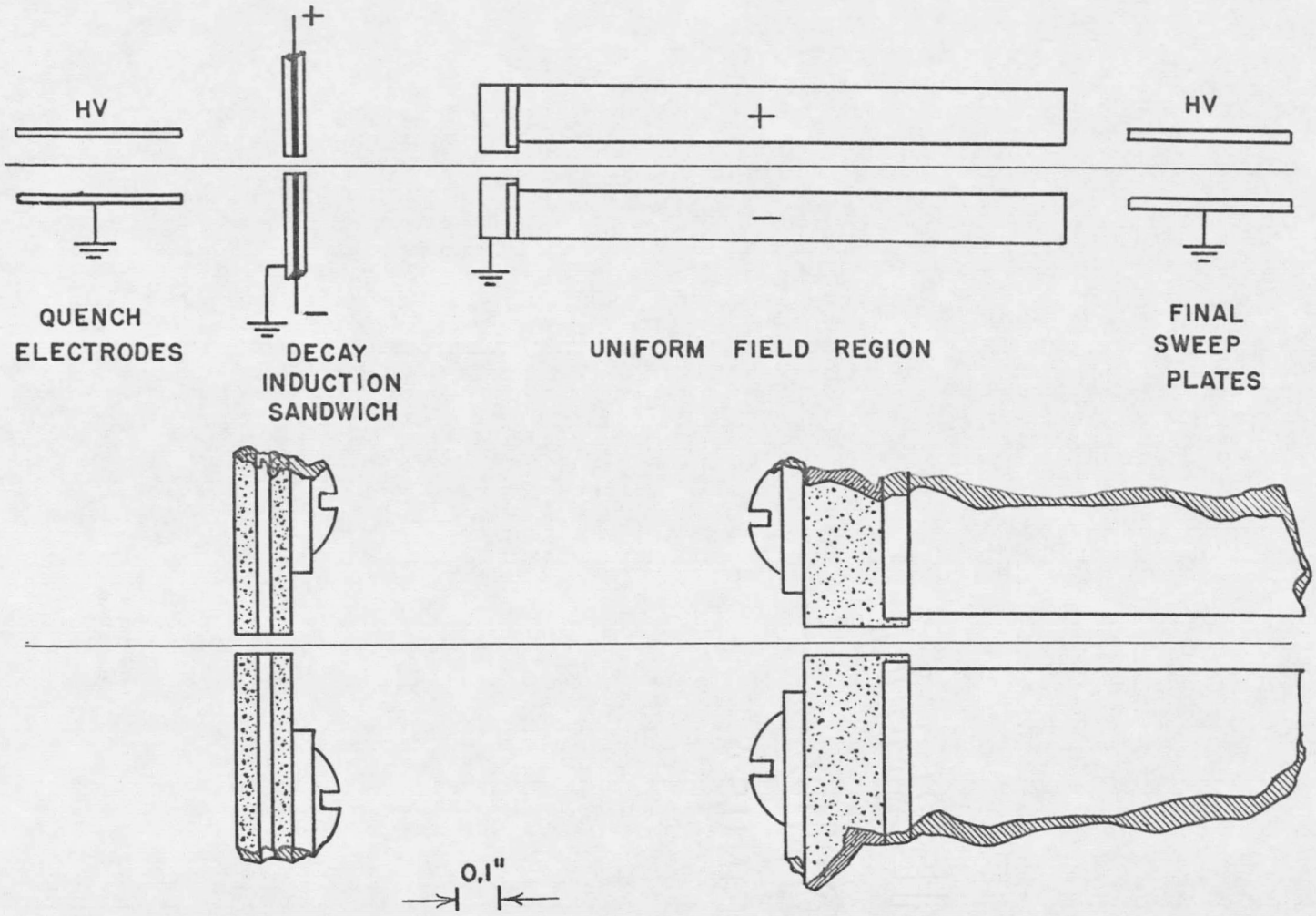

HV
+
HV
+
−
QUENCH
ELECTRODES
DECAY
INDUCTION
SANDWICH
UNIFORM FIELD REGION
FINAL
SWEEP
PLATES
0.1"

FIG. 5

tending very far downstream.

The uniform field region is designed so that the length of the fringe field was held to a minimum. If the fringe field is too long there will be no modulation in the field-induced radiation profile, therefore ground plates are added to shorten the fringe field. (In the next chapter we examine the fringe fields more carefully.)

The last field is employed to remove all traces of protons from the beam. During the course of a run the alignment of the beam would change sometimes allowing more protons to enter the experimental chamber. These few extra protons do not modify the radiation profiles enough to be measured but they are detected by the Faraday cup like hydrogen atoms. The final sweep plates are provided to assure that the Faraday cup only indicates the intensity of the hydrogen beam. 650V assures that no protons enter the Faraday cup; 1kV is used.

When a fast beam of protons of hydrogen atoms strikes a metal surface many electrons are scattered from the surface and are called secondary electrons. The Faraday cup is biased to collect these secondary electrons (see Fig. 6); the current so produced provides a measure of the hydrogen beam intensity.

The Lyman-α radiation resulting from p-state decay is monitored by a Channeltron electron multiplier (CEM, Galileo Electro-Optics, formerly Bendix). To prevent detection of ions the CEM is enclosed in

Fig. 6. Faraday cup is biased to measure the secondary electron current produced by the hydrogen beam thereby indicating its intensity. A quartz target is provided for direct viewing of the beam when the metal shield is rotated from the beam's path. A switching circuit is provided (not shown) to monitor either the proton current, or secondary electron current produced by the beam.

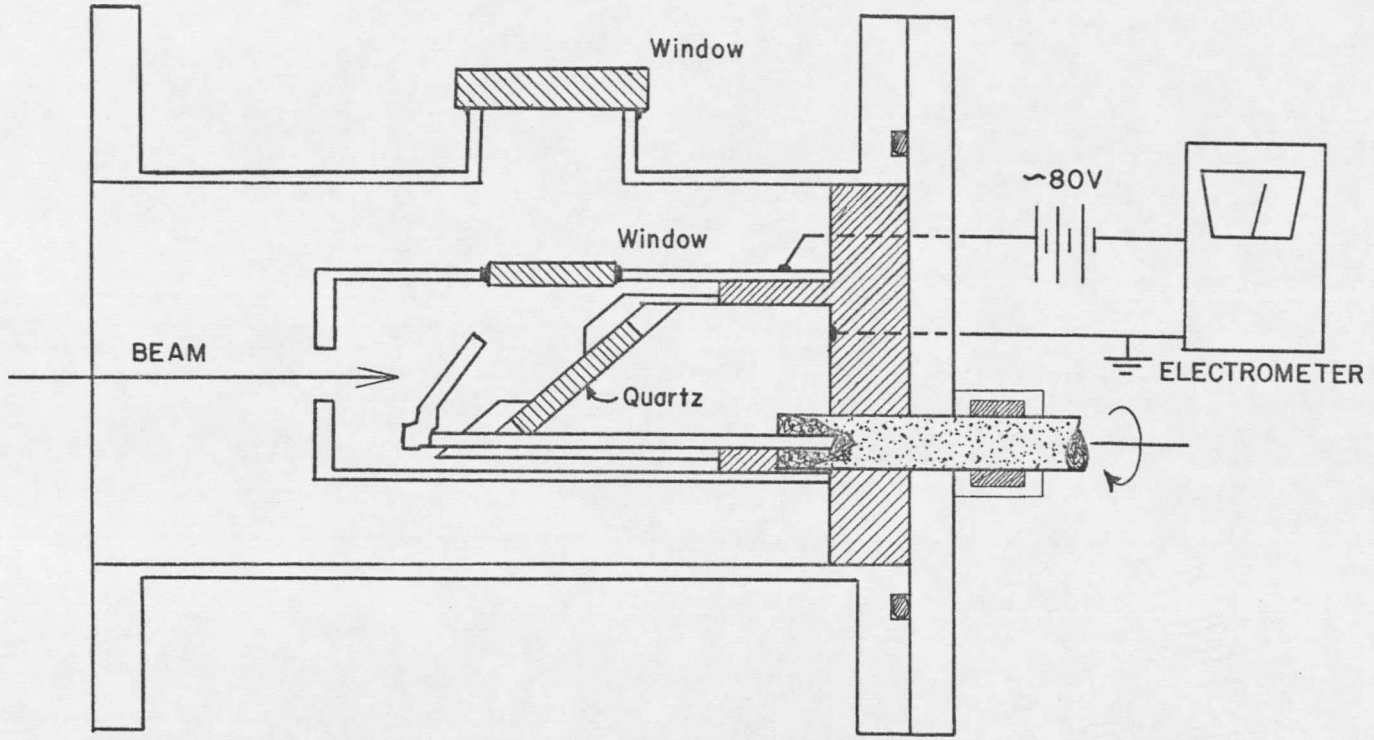


FIG. 6

a metal box and sees the beam through a LiF window. The portion of the beam observed is restricted by a slit on the cart's face. The cart assembly rolls on tracks which parallel the beam, and is held against a positioning rod by a pulley system with small weights which hang down into the throat of the diffusion pump beneath the experimental chamber. The rod extends through a feed-through to the exterior where its position is manually controlled by a micrometer head and calibrated spacers. See Fig. 7 for details of the cart and its electrical connections.

Figure 8 shows a block diagram of the counting electronics. If the beam never changed its intensity we would have been able to record the CEM counts (proportional to the Lyman-α intensity) for a preset time then change the cart's position and repeat the process obtaining a radiation profile. However, the beam is not stable either for short or long times, so the CEM counts must be recorded for a preset number of hydrogen atoms passing the detector. The Keithley Model 601 electrometer provides an output which is fed into a voltage-to-frequency converter (VFC). The frequency output of the VFC is proportional to the secondary electron current measured by the electrometer and hence to the hydrogen atom beam intensity. A Canberra Model 1790 counter-timer counts the VFC frequency pulses for a preset count. During this counting time the CEM counts are recorded in the counter's second channel. When the preset count is reached by the VFC counter both channels

Fig. 7. Lyman-α detector. The CEM cart is shown observing the rectangular beam within the uniform field region. Note that the biasing of the CEM is necessary to repel any stray electrons from detection.

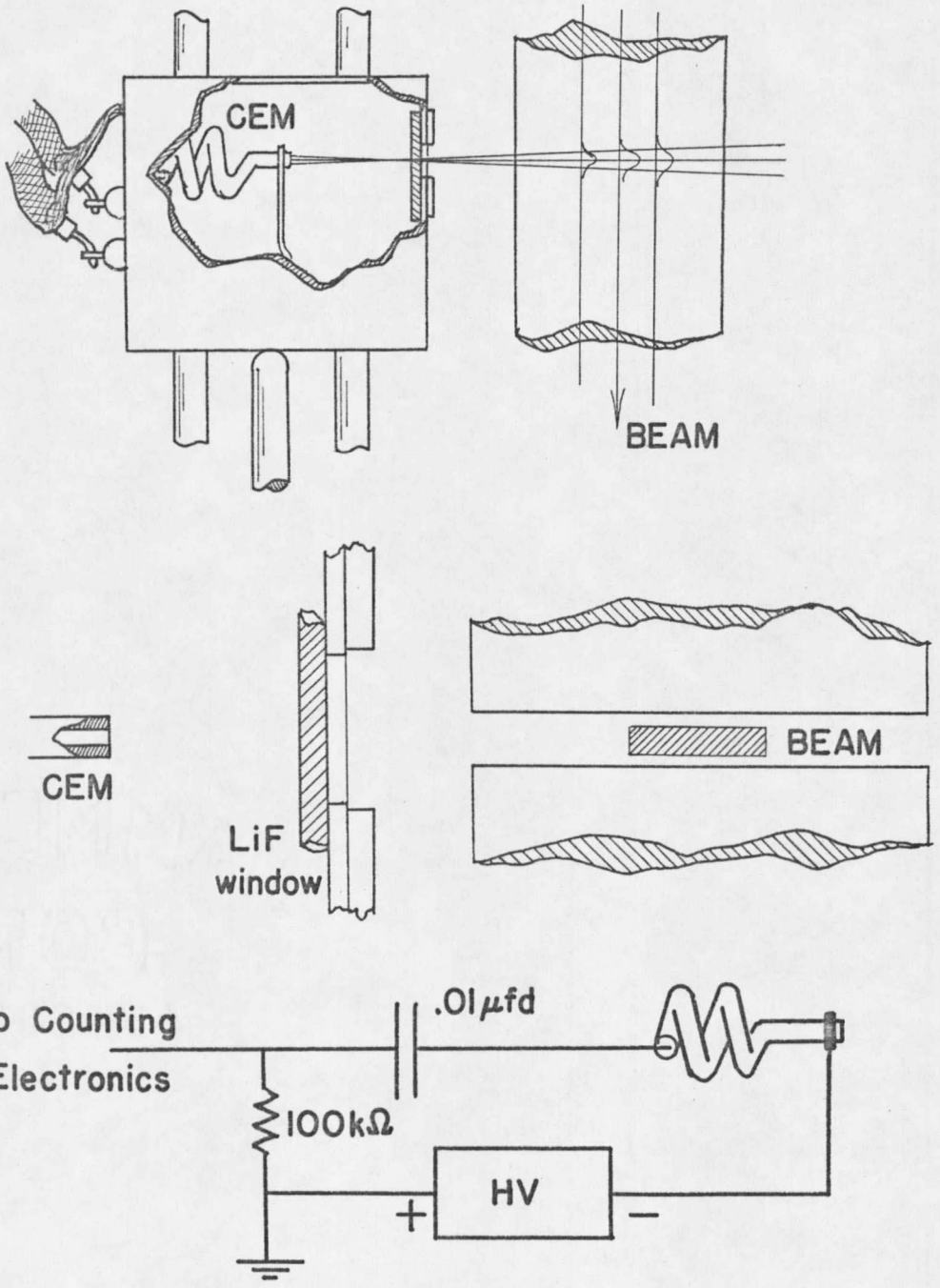

CEM
BEAM
CEM
LiF
window
BEAM
To Counting
Electronics
.01μfd
100kΩ
HV
+
−

FIG. 7

Fig. 8. Counting electronics.

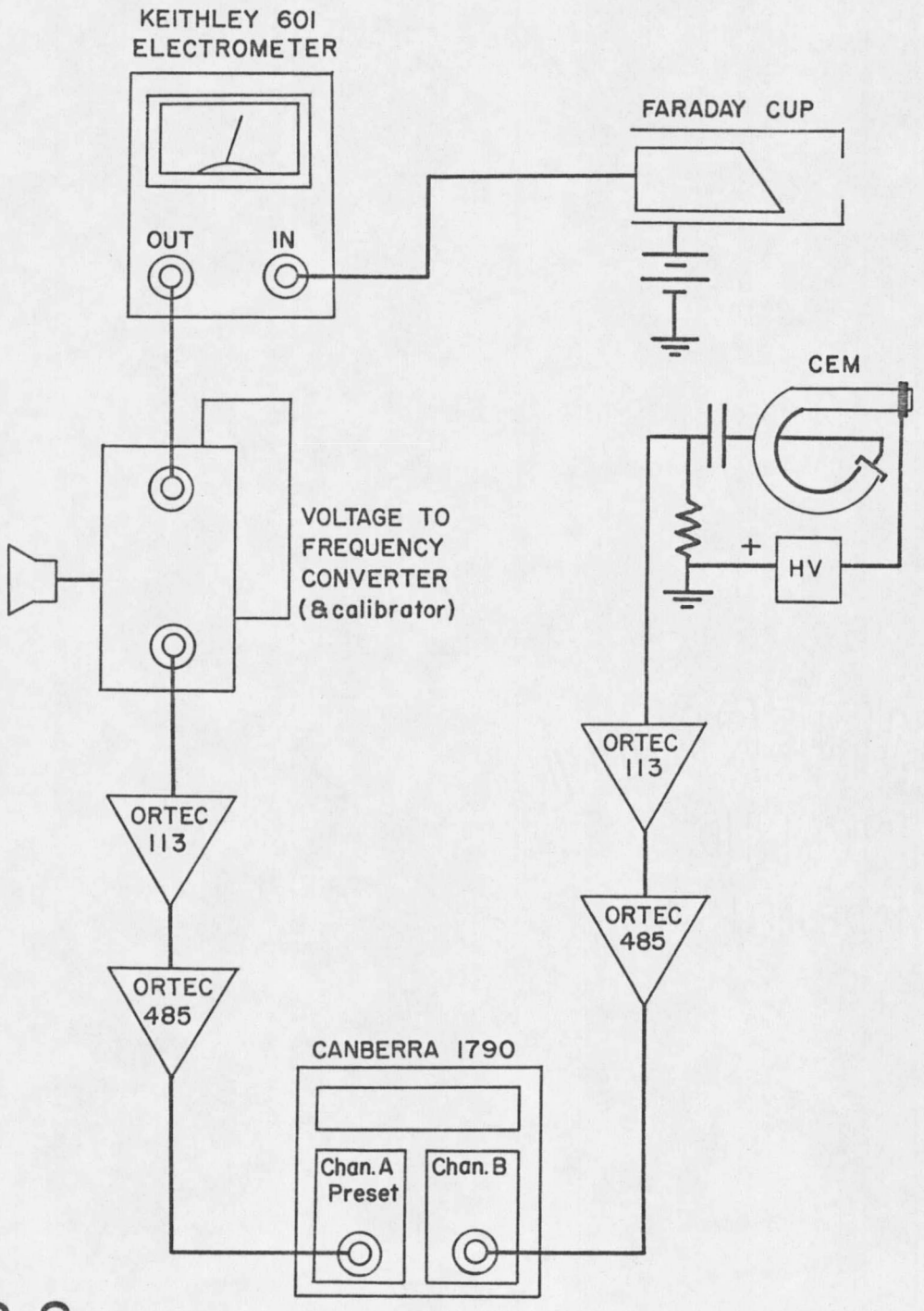

KEITHLEY 601
ELECTROMETER
OUT
IN
FARADAY CUP
CEM
+
HV
VOLTAGE TO
FREQUENCY
CONVERTER
(& calibrator)
ORTEC
113
ORTEC
485
ORTEC
113
ORTEC
485
CANBERRA 1790
Chan. A
Preset
Chan. B

FIG. 8

stop their accumulation. In this way the CEM counts are integrated against the hydrogen beam intensity.

Depending upon the run, secondary electron currents are found to range from 150nA to 950nA as measured in the Faraday cup by the electrometer. The -1V full-scale-deflection output of the electrometer corresponds to a VFC output from 3kHz to 5kHz (the higher frequency was used in the earlier runs). Provided the electrometer is zeroed for each count it has a measured precision and drift of 0.075%. The VFC is "homemade." It has a 741 operational amplifier on input driving a 566 function generator. The voltage input for calibration is controlled by another 741. The measured precision and drift is 0.11%. The VFC's audio monitor is valuable for alignment purposes and for keeping constant check on the running of the machine; for we are no longer "glued" to a meter and can concentrate on other adjustments while "listening" to the beam.

For both the free-decay (FD) and quantum beat (QB) radiation profiles, CEM counts are recorded for a preset number of hydrogen atoms then the cart is moved and the next reading is taken. Because of collisions with the molecules in the vacuum a background count is observed and must be subtracted from the signal. Ideally one would record a count with the coupling fields on then record the background count (with the coupling fields still on) while the upstream quench field

removes the metastable component. It is observed, however, that two minutes are required for the metastable intensity to return to its former size prior to turning on the quench field. To avoid excessive wait times the FD backgrounds are taken after the decay profile is obtained. If the beam touches the decay-induction sandwich then a pronounced increase in the background is observed having an exponential tail. Collisions with any part of the field electrodes is avoided as much as possible.

In the uniform field region the beam never directly hit any electrode structure and the background counts are fairly uniform. The slight nonuniformity of the background may be attributed to atoms scattered out of the beam path which collide with the ground structure at the front of the plates. Because of the uniformity of the background in this region we need only record a few background counts.

The above two-minute wait period after turning off the quench field is disturbing; for it suggests there is charging of some surface in the vicinity of the quench plates. Attempts were made to determine the source of the charging by switching the polarity of the quench plates, etc. We feel that such a charging could arise from field-induced charging of insulating surfaces within the electrode structure itself. When the fields are turned off some time is required for the charge to bleed away or be neutralized by the space charge emitted

from the beam.

Sources of Difficulties

Charging problems were observed in the data since the outset of this experiment. The first obeserved effects were found to arise from charging of the sweep-field electric field plates. Originally an electric field was employed to remove the protons from the beam before the third aperture. During running the beam produces ions as it experiences collisions with background molecules in the vacuum. If an electric field is applied to the beam these collisionally produced charged particles will respond to the field and could attach themselves to any insulator in the vicinity of the field. The effect would be to neutralize the field. When the applied field is turned off the residual field from the accumulated ions provide a field yet capable of quenching metastables. In time the charges are neutralized by the continued beam-ion production. These characteristics were finally observed in association with the operation of the electric sweep plates. The charging phenomena could account for as much as a 40% long-term drift in the signal. Because the electric plates were employed on a previous experiment with apparent success they were never suspected.[24] The problem was difficult to locate since the time constant associated with the charging was about 1 hour. Shortly after the charging was discovered the plates were replaced by an external magnet which pro-

vided a solution to this charging problem; however, it served only to unmask other difficulties in the experimental chamber.

It was discovered that the free-decay radiation count at any position was affected by the past history of the cart's location. The radiation counts would be different at the same z depending upon whether the cart had been upstream or downstream previously. After several minutes this "history" was forgotten and the signal returned to its equilibrium value. Numerous charging schemes were advanced to explain such observations. At one point we were convinced that in the absence of the cart a cloud of electrons would form ("electron fog hypothesis") on the downstream side of the decay induction sandwich. When the cart returned to take a count it provided a nearby grounded surface and the cloud would slowly disappear. This idea was rejected when it was discovered that several small holes in the face of the cart admitted electrons to the cart's interior which were eagerly counted by the CEM. Covering all holes and cracks in the cart still didn't completely solve the problem of a spurious signal, however. It was necessary to negatively bias the mouth of the CEM to repel all electrons before the "history" problem ceased.

Reproducible data could now be obtained but the free-decay curves indicated that the accelerating voltage was as much as 70% higher than the accelerator setting indicated. The logarithms of the

decay curves always seemed straight enough; so, again the charging hypotheses were resurrected. To eliminate as many insulating surfaces as possible the experimental chamber was entirely rebuilt and redesigned. All large pieces of plastic were removed. Despite these precautions the data still indicated that the beam velocity was too high. A detailed investigation ultimately revealed that Lyman-α radiation from upstream was reflecting off the beveled edge of the downstream brass slit directly into the CEM. The slits were replaced with 0.001in brass which served to eliminate the problem.

The problems of signal drift and charging have not been solved entirely. In examination of the FD results to follow we will find that the standard deviation of the "slopes" $m = \gamma/\upsilon$ exceeds the expected standard deviation by a factor of four in at least one case. Such a large deviation is felt to arise from inadequacies in the positioning device rather than stray fields. To completely eliminate all charging problems we would have to remove all insulting surfaces which are exposed to the beam--another overhaul which would require a redesigning of all electrodes. However, since the major difficulties had been solved it was felt that even at a sacrifice of accuracy we would continue and attempt completion of the measurement rather than rebuild the electrodes.

In the process of eliminating problems many factors were consid-

ered which might influence the metastable content of the beam. Vacuum pressures were not good throughout the machine except perhaps the accelerator vacuum pressures. Vacuum pressures in the accelerator, the sweep-field region, and the experimental chamber were all changed significantly in attempts to modify the signal, however, no changes were observed in the field-induced signals. The only changes were increased background counts in the experimental chamber as the experimental chamber's pressure increased. The charge-exchange-cell pressure is important, but fortunately we always operated in a plateau region and were able to maintain the pressures to within 1% of the starting pressure; so, we anticipate that there will be no measurable error introduced by the cell (see Fig. 9).

The applied voltages must be known accurately and held constant. A Data Precision (Model 2440, 4½ digit) digital voltmeter (DVM) is used to measure all voltages. Although this DVM shows only a 0.024% standard deviation on successive measurements of a standard cell during the course of a run, in comparing its readings to a Fluke DC Differential Voltmeter (Model 881A) there is a deviation of 0.134%. Such discrepancies are not responsible for the final error in the decay-rate value, however.

An important factor in reducing the metastable content of the beam is the magnetic field produced by the sweep-field magnet. In Fig.

Fig. 9. Counts vs charge-exchange-cell pressure. The charge-exchange-cell pressure is selected near the middle of the Lyman-α count plateau. The plateau region doesn't change its position significantly for beam energies from 80kV to 120kV.

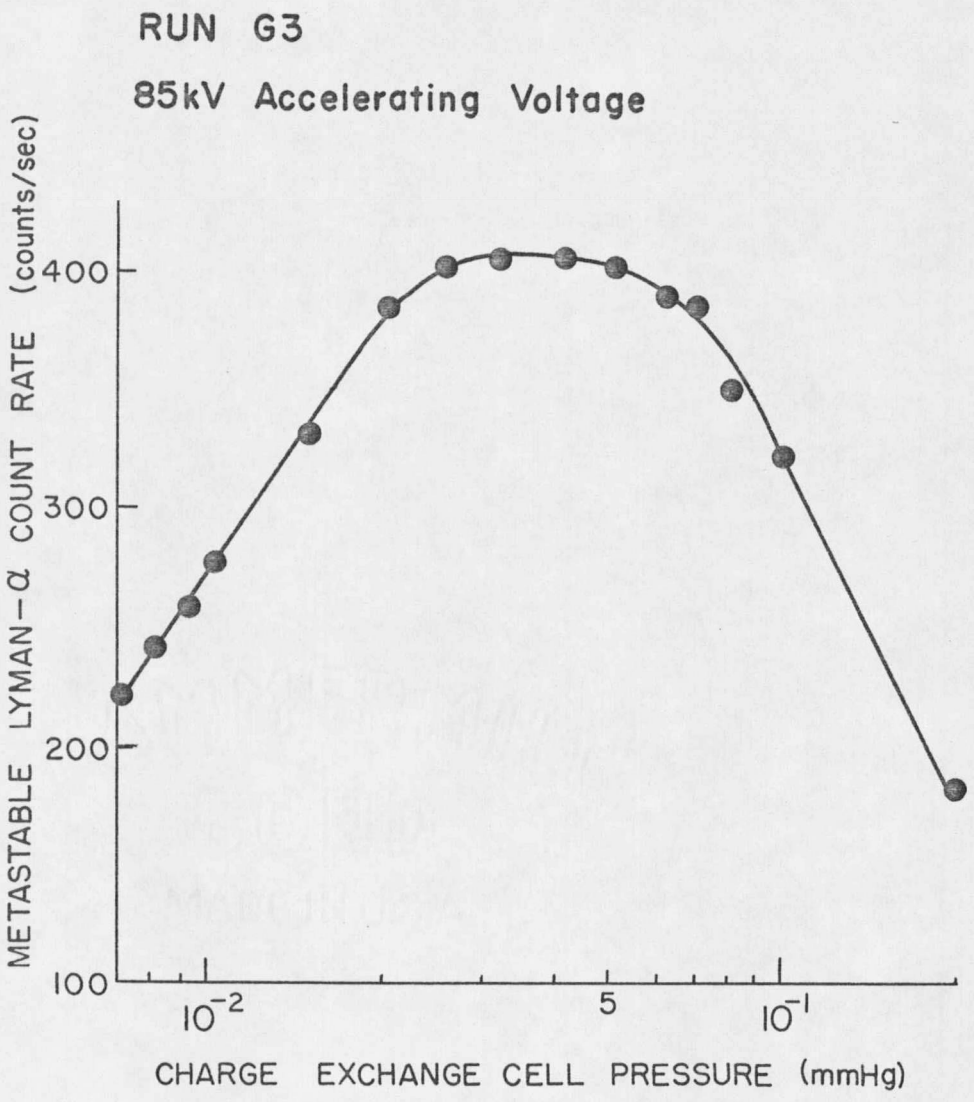

RUN G3
85kV Accelerating Voltage
METASTABLE LYMAN-α COUNT RATE (counts/sec)
400
300
200
100
10^-2
5
10^-1
CHARGE EXCHANGE CELL PRESSURE (mmHg)

FIG. 9

10 we show the metastable signal as a function of the sweep-field-magnet current. To essentially eliminate the protons from the beam requires quenching roughly 50% of the metastables. With such a slope the effects of a small change in magnet current will be reflected by the metastable content of the beam. The measured standard deviation of the magnet current during a run is 2.3×10^{-4}A (0.15%) which corresponds to an uncertainty in the counts of 15 counts out of 9000 or an uncertainty of 0.17% which is small compared to the anticipated 1.05% standard deviation associated with Poisson statistics.

Having eliminated all obvious difficulties in the apparatus and assured ourselves that random error from the equipment should be small, we can investigate the data.

Final Data

After the p state has been produced from the s state in the decay-induction sandwich we monitor the field-free decay radiation as a function of distance. We must be sure that the data is recorded only in a field-free region and that the fringe field does not extend into the data taking region. In Fig. 11 we show the radiation profile associated with the sandwich. When the field is on the profile represents the p-state population, when off, and the third aperture is opened, the radiation shows the outline of the entire electrode region.

Fig. 10. Sweep-field signal quenching. Motional quenching of metastables from proton sweep-field magnet is shown together with proton sweep characteristics.

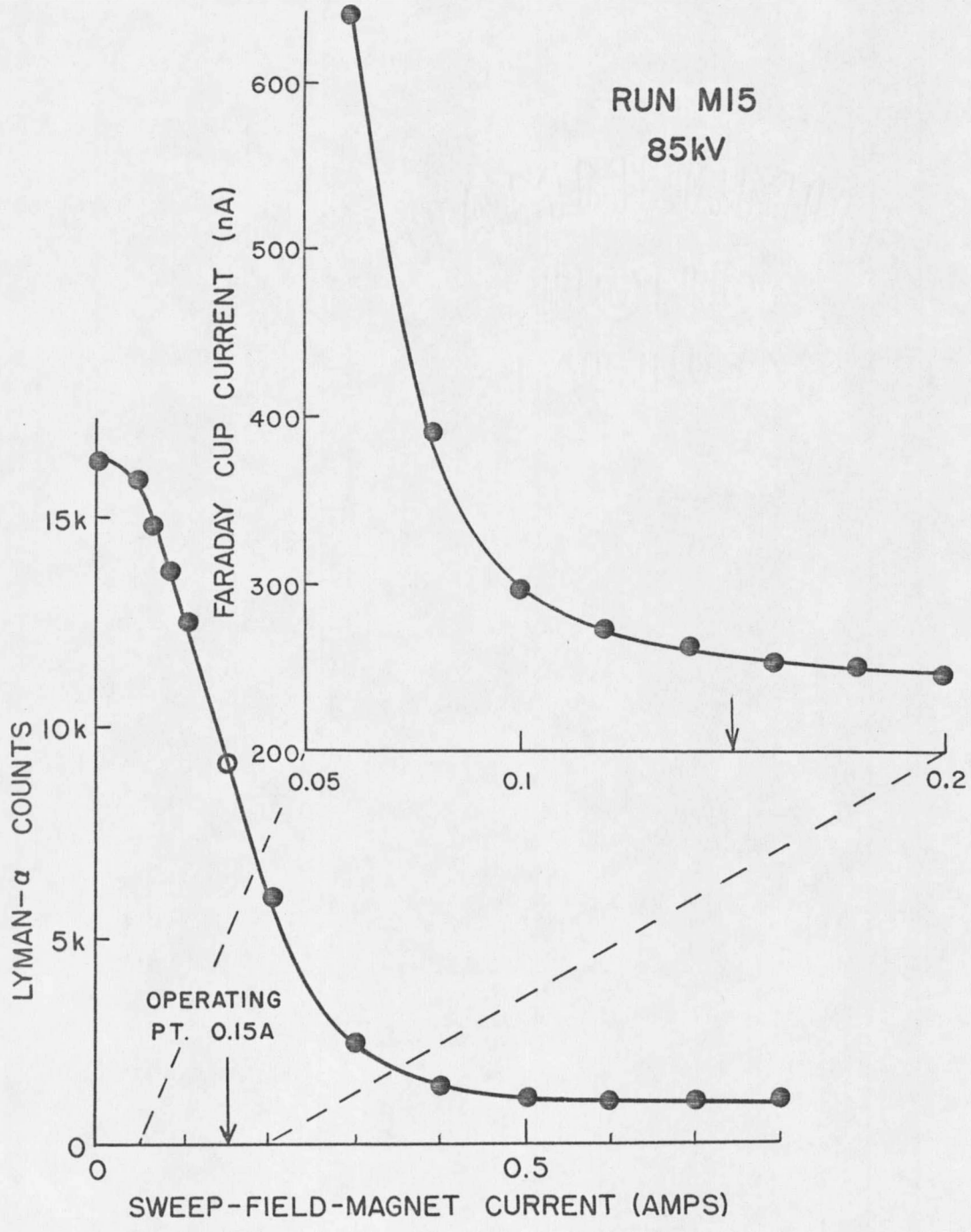

RUN M15
85kV
FARADAY CUP CURRENT (nA)
600
500
400
300
200
0.05
0.1
0.2
LYMAN-α COUNTS
15k
10k
5k
0
OPERATING
PT. 0.15A
0
0.5
SWEEP-FIELD-MAGNET CURRENT (AMPS)

FIG. 10

Fig. 11. Decay-induction sandwich. Shown drawn to scale along with the field-induced signal and the collisional background signal (indicating the position of the structure). The detail drawing shows a central field plot made in a field-mapping tank. Note the effects of a finite detector window in the observation of a signal before reaching the position where the field is nonzero.

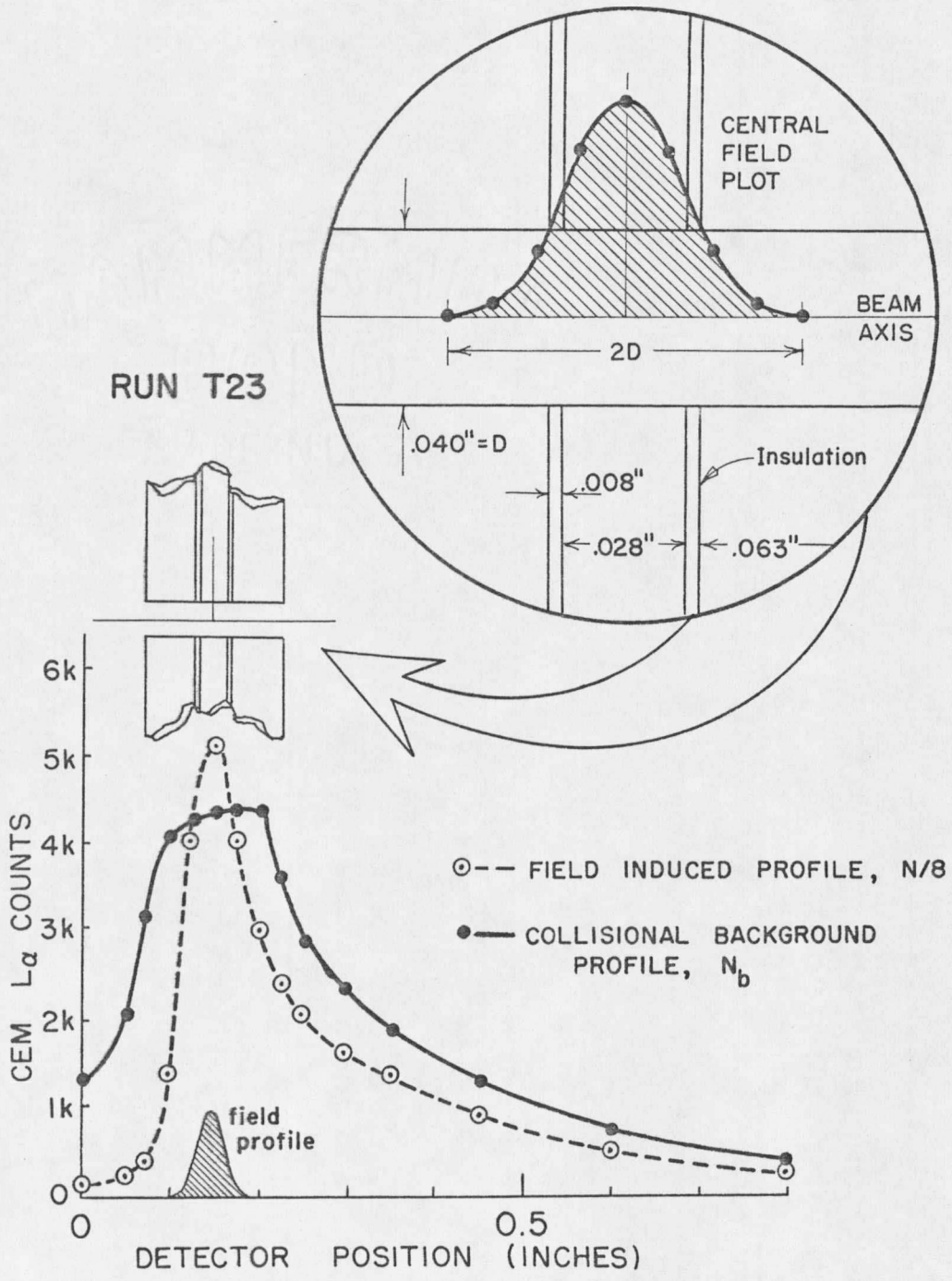

CENTRAL
FIELD
PLOT
BEAM
AXIS
2D
RUN T23
.040"=D
.008"
Insulation
.028"
.063"
6k
5k
4k
3k
2k
1k
0
CEM Lα COUNTS
FIELD INDUCED PROFILE, N/8
COLLISIONAL BACKGROUND
PROFILE, N_b
field
profile
0
0.5
DETECTOR POSITION (INCHES)

FIG. 11

Comparing the radiation profiles with the field map we see that any data taken after 0.25in is probably free of all effects of the field. To be safe we usually take all free-decay data at 0.3in or further downstream. The natural logarithm of one of the decay curves shown in Fig. 12 verifies these conclusions.

The Lyman-α signal as a function of sandwich voltage is shown in Fig. 13. The operation voltage is usually from 300V to 400V. The voltage here refers to the total applied voltage; +V/2 is applied to the upper (or lower) plate while -V/2 is applied to the lower (or upper) plate.

Several sets of free-decay data usually are taken during each run both before and after the quantum beat data are recorded. Accelerating voltages from 80kV to 120kV are used since the accelerator performs best in this range, though some of the preliminary runs were made at lower accelerating voltages. Often up to six hours of running are required before the machine settles down and runs smoothly, because of this the runs usually begin late morning and continue through the night into the next morning to take advantage of a less active line voltage during the night. In tables 2 - 5 we present the free-decay data associated with the quantum-beat runs along with a linear regression performed upon the log of the net signal

$$\ln(N - N_b) = \ln N_0 - mz \quad . \tag{53}$$

Fig. 12. Verification of field-free region. Sample data showing excessive size of signal at z = 0.2in. Data at z = 0.25in and beyond shows acceptable fit to straight line. We usually consider $z \geq 0.25$in to be the field free region to be sure of no interference from possible fringe field. The straight line is a least squares fit to the natural log of data past 0.2in. Assuming $\gamma = 6.27\times10^{8}s^{-1}$ we obtain 65kV as accelerating voltage (meter on accelerator indicated 60 - 61kV). Background was subtracted from the data used to produce the graph.

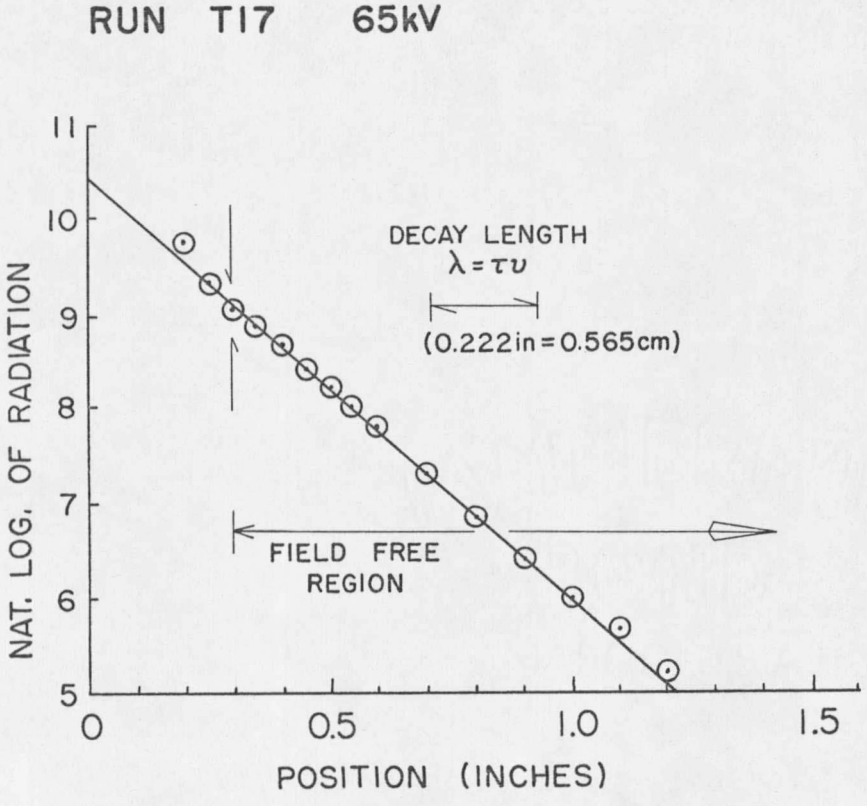

RUN T17 65kV
NAT. LOG. OF RADIATION
11
10
9
8
7
6
5
0
0.5
1.0
1.5
POSITION (INCHES)
DECAY LENGTH
λ = τυ
(0.222in = 0.565cm)
FIELD FREE
REGION

FIG. 12

Fig. 13. Free-decay radiation vs conversion voltage. The success with which the decay-induction sandwich converts metastables to p-state atoms is shown as a function of applied field strength.

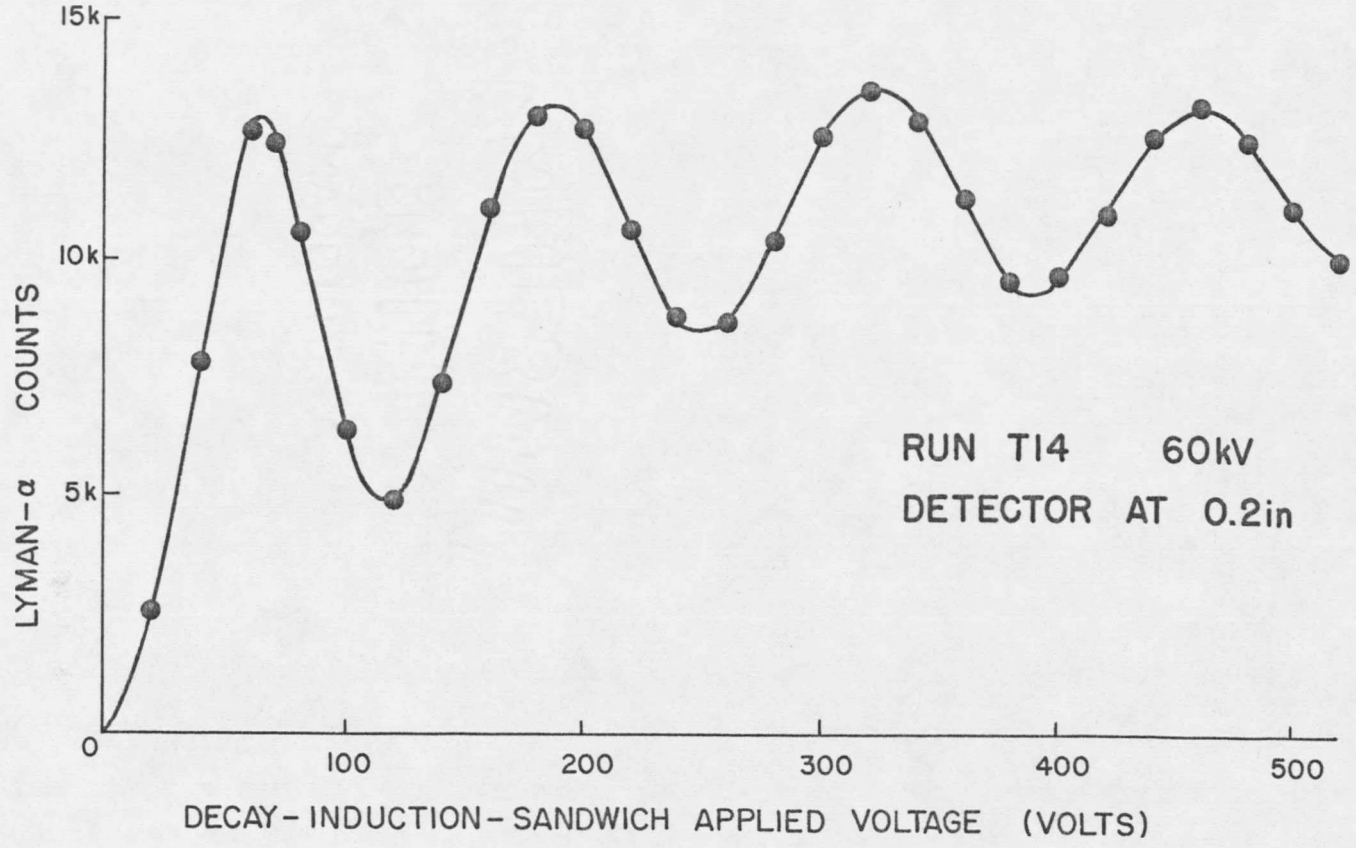

15k
10k
5k
0
LYMAN-α COUNTS
RUN T14 60kV
DETECTOR AT 0.2in
100
200
300
400
500
DECAY-INDUCTION-SANDWICH APPLIED VOLTAGE (VOLTS)

FIG. 13

TABLE 2

FREE-DECAY DATA: RUN T18

85kV ACCELERATOR SETTING

z(in)	N	N_b	z(in)	N	N_b	Log fit results
DATA SET 4: V = 320V, Ave. count time = 68s, taken before QB data						
0.25	12054	386	0.80	1466	66	
0.30	9733	249	0.90	1034	61	$m=3.8300in^{-1}=1.5079cm^{-1}$
0.35	8006	180	1.00	747	59	$\ln(N_o) = 10.3166$
0.40	6655	160	1.10	490	58	correlation coefficient
0.50	4456	104	1.20	366	57	= -0.99985
0.60	3180	81	1.30	274	72	
0.70	2196	70				
DATA SET 6: V = 330V, Ave. count time = 130s, taken after QB data						
0.30	19515	487	0.60	6145	155	$m=3.8449in^{-1}=1.5138cm^{-1}$
0.40	13225	289	0.80	2919	138	$\ln(N_o) = 11.0043$
0.50	8893	162				cor. coef.=-1.00000
DATA SET 7: V = 330V, Ave. count time = 130s, taken after QB data						
0.30	30224	222	0.60	9522	190	$m=3.8406in^{-1}=1.5120cm^{-1}$
0.40	20266	184	0.80	4561	187	$\ln(N_o) = 11.4469$
0.50	13630	164				cor. coef.=-0.99985

COMBINED RESULTS OF LOG FITS--ESTIMATE OF m

Ave. slope: $\langle m \rangle = 1.511 \pm 0.003 cm^{-1}$ ($\pm 0.2\%$). Using $\gamma = 6.27 \times 10^8 s^{-1}$ we determine that $\upsilon = 4.126 \times 10^8 cm/s$ and the accelerating voltage would be 88.85kV.

TABLE 3

FREE-DECAY DATA: RUN T19

100kV ACCELERATOR SETTING

z(in)	N	N_b	z(in)	N	N_b	Log fit results
DATA SET 9A: V = 360V, Ave. count time = 123s, taken before QB data.						
0.30	15606	163	0.80	2798	105	$m=3.5252in^{-1}=1.3879cm^{-1}$
0.40	10799	121	1.00	1385	97	$\ln(N_o) = 10.699$
0.50	7741	115				cor. coef.=-0.99991
DATA SET 9B: V = 360V, Ave. count time = 133s, taken before QB data.						
0.30	15699	196				$m=3.5236in^{-1}=1.38725cm^{-1}$
0.50	7772	104				$\ln(N_o) = 10.706$
0.80	2763	101				cor. coef.=-1.00000
DATA SET 11A: V = 360V, Ave. count time = 125s, taken after QB data.						
0.30	15828	146	0.70	3888	98	$m=3.5474in^{-1}=1.3966cm^{-1}$
0.40	11249	124	0.80	2775	96	$\ln(N_o) = 9.6286$
0.50	7803	111				cor. coef.=-0.99997
DATA SET 11B: V = 360V, Ave. count time = 125s, taken after QB data.						
0.30	15684	121	0.80	2748	96	$m=3.5420in^{-1}=1.3945cm^{-1}$
0.40	11060	100				$\ln(N_o) = 9.6157$
0.50	7695	95				cor. coef.=-0.99998
DATA SET 11C: V = 360V, Ave. count time = 128s, taken after QB data.						
0.30	15683	134	0.80	2733	96	$m=3.5443in^{-1}=1.3954cm^{-1}$
0.40	10945	112				$\ln(N_o) = 9.6147$
0.50	7775	103				cor. coef.=-0.99999

$\langle m \rangle = 1.3923 \pm 0.004 cm^{-1}$ (±0.3%) giving Accel. Vlts. = 104.7kV

TABLE 4

FREE-DECAY DATA: RUN T22

90kV ACCELERATOR SETTING

z(in)	N	N_b	z(in)	N	N_b	Log fit results
DATA SET 3E: V = 360V, Ave. count time = 379s, taken before QB data.						
0.30	37174	346	0.50	17448	299	$m=3.8467in^{-1}=1.5144cm^{-1}$
0.40	25344	289	0.70	8194	294	$lnN_o=11.670$, c.c.=-.99999
DATA SET 3F: same but Ave. count time = 386s						
0.30	36579	365	0.50	17273	297	$m=3.7714in^{-1}=1.4848cm^{-1}$
0.40	25266	294	0.70	8310	281	$lnN_o=11.630$, c.c.=-.99998
DATA SET 3H: same but Ave. time = 369s						
0.30	37114	328	0.50	17373	302	$m=3.7742in^{-1}=1.4859cm^{-1}$
0.40	25209	344	0.70	8385	283	$lnN_o=11.638$, c.c.=-.99994
DATA SET 3I: same but Ave. time = 375s						
0.30	36508	399	0.50	17395	331	$m=3.7874in^{-1}=1.4911cm^{-1}$
0.40	25082	314	0.70	8235	300	$lnN_o=11.633$, c.c.=-.99998
DATA SET 6A: V = 360V, Ave. count time = 414s, taken after QB data.						
0.30	33984	330	0.50	15785	305	$m=3.8327in^{-1}=1.5090cm^{-1}$
0.40	23432	340	0.70	7573	284	$lnN_o=11.754$, c.c.=-.99994
DATA SET 6B: same but Ave. time = 411s						
0.30	33925	337	0.50	15636	309	$m=3.9059in^{-1}=1.5377cm^{-1}$
0.40	23016	280	0.70	7340	295	$lnN_o=11.593$, c.c.=-1.0000

$\langle m \rangle = 1.504 \pm 0.021 cm^{-1}$ (±1.4%) giving Accel. Vlts. = 89.72kV

TABLE 5

FREE-DECAY DATA: RUN T23

105kV ACCELERATOR SETTING

z(in)	N	N_b	z(in)	N	N_b	Log fit results
DATA SET 3A: V = 360V, Ave. count time = 167s, taken before QB data.						
0.30	19616	186	0.50	9703	145	$m=3.4762in^{-1}=1.3686cm^{-1}$
0.40	13662	179	0.70	4926	109	$lnN_o=10.9085$, c.c.=-.99990
DATA SET 3B: same						
0.30	19231	159	0.50	9696	146	$m=3.4464in^{-1}=1.3568cm^{-1}$
0.40	13502	136	0.70	4899	110	$lnN_o=10.886$, c.c.=-.99997
DATA SET 3C: same but Ave. time = 165s						
0.30	19209	179	0.50	9738	128	
0.30	19318	163	0.50	9716	161	$m=3.4525in^{-1}=1.3593cm^{-1}$
0.30	19125	158	0.70	4939	107	$\ln(N_o) = 10.8941$
0.40	13740	135	0.70	4907	110	cor. coef. = -0.99995
0.40	13836	176	0.70	4877	107	
DATA SET 5: same but Ave. time = 140s, taken after QB data.						
0.30	19275	408	0.50	9886	155	$m=3.4771in^{-1}=1.3689cm^{-1}$
0.40	13811	271	0.70	4894	191	$lnN_o=10.901$, c.c.=-.99966

$\langle m \rangle = 1.3634 \pm 0.0063 cm^{-1}$ (±0.46%) giving Accel. Vlts. = 109.2kV

Later we perform fits to an exponential function; the log fits serve only for illustration and obtaining approximate values. Figure 14 shows a sample of the free-decay data for a single run on a log plot.

The quantum-beat data are recorded in much the same way as the free-decay data only a smaller step in position is made. The optimum voltage is obtained by recording the first peak and valley counts at several voltages. We demonstrate the results in Fig. 15. About 100V applied to the uniform-field plates usually produces the best results. The loss of modulation at higher voltages is a result of the demodulating effects of the detector window. Eventually for sufficiently high fields the spatial wavelength of the oscillation would be the size of the window so that no quantum beats would be observed.

As for the decay-induction plates the voltage on the uniform-field plates is symmetrically divided between the plates (+V/2 on one; -V/2 on the other). The quantum-beat data is presented for each run in tables 6 - 9. The recorded backgrounds are averages of a few recordings. A plot of run T23 is shown in Fig. 16.

We have discussed the essential features of the apparatus and the difficulties encountered in obtaining the data. We now need to analyze these data we have just presented and extract a lifetime measurement from them. We conclude this chapter with a summary of the operating conditions in table 10.

Fig. 14. Free-decay data for Run T18 is shown on a natural log plot. See table 2 for a listing of data.

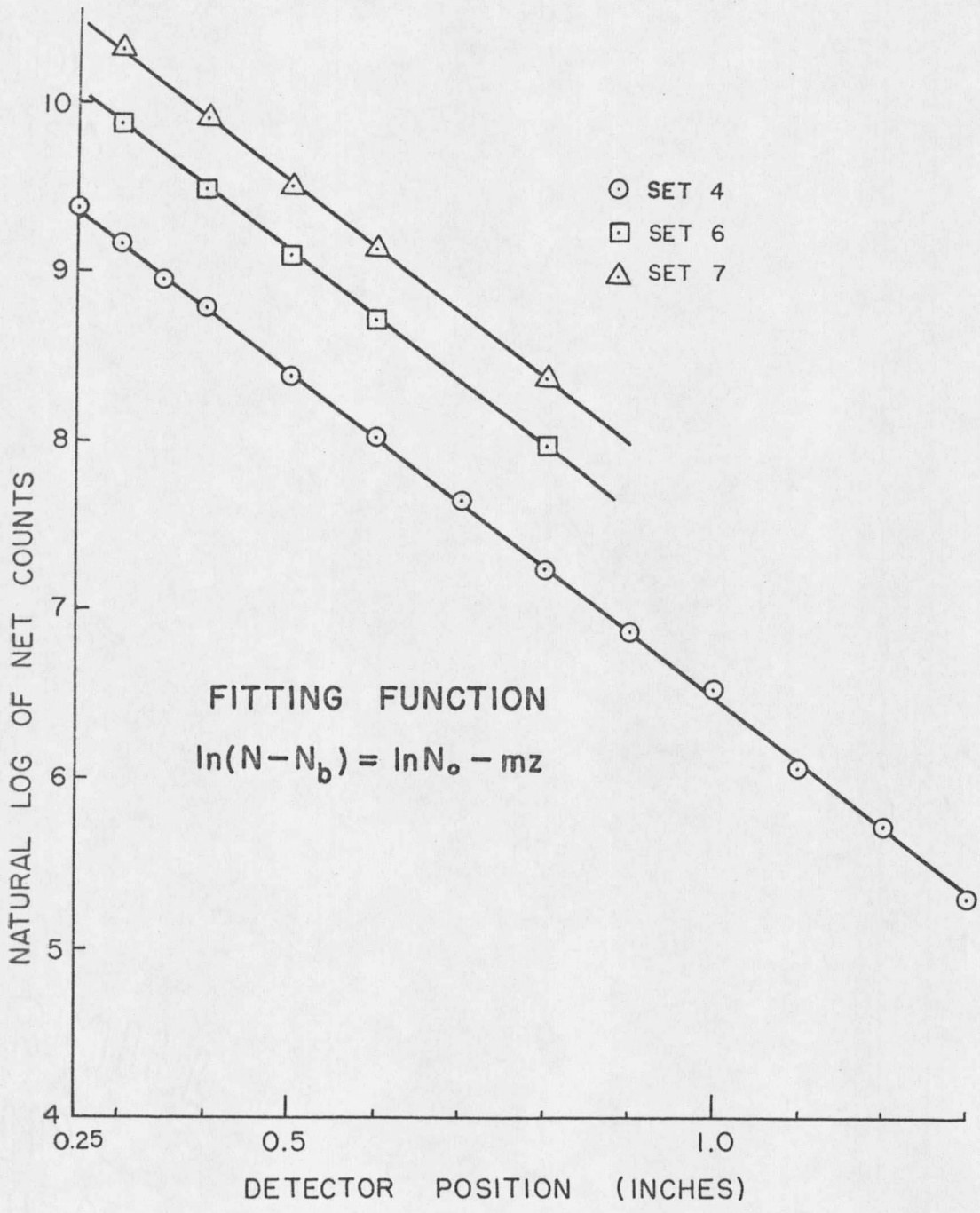

SET 4
SET 6
SET 7
FITTING FUNCTION
$\ln(N-N_b) = \ln N_o - mz$
NATURAL LOG OF NET COUNTS
10
9
8
7
6
5
4
0.25
0.5
1.0
DETECTOR POSITION (INCHES)

FIG. 14

Fig. 15. Quantum-beat modulation. The peak radiation intensity, initial modulation and signal-to-noise ratio is shown as a function of voltage applied to the uniform vield plates.

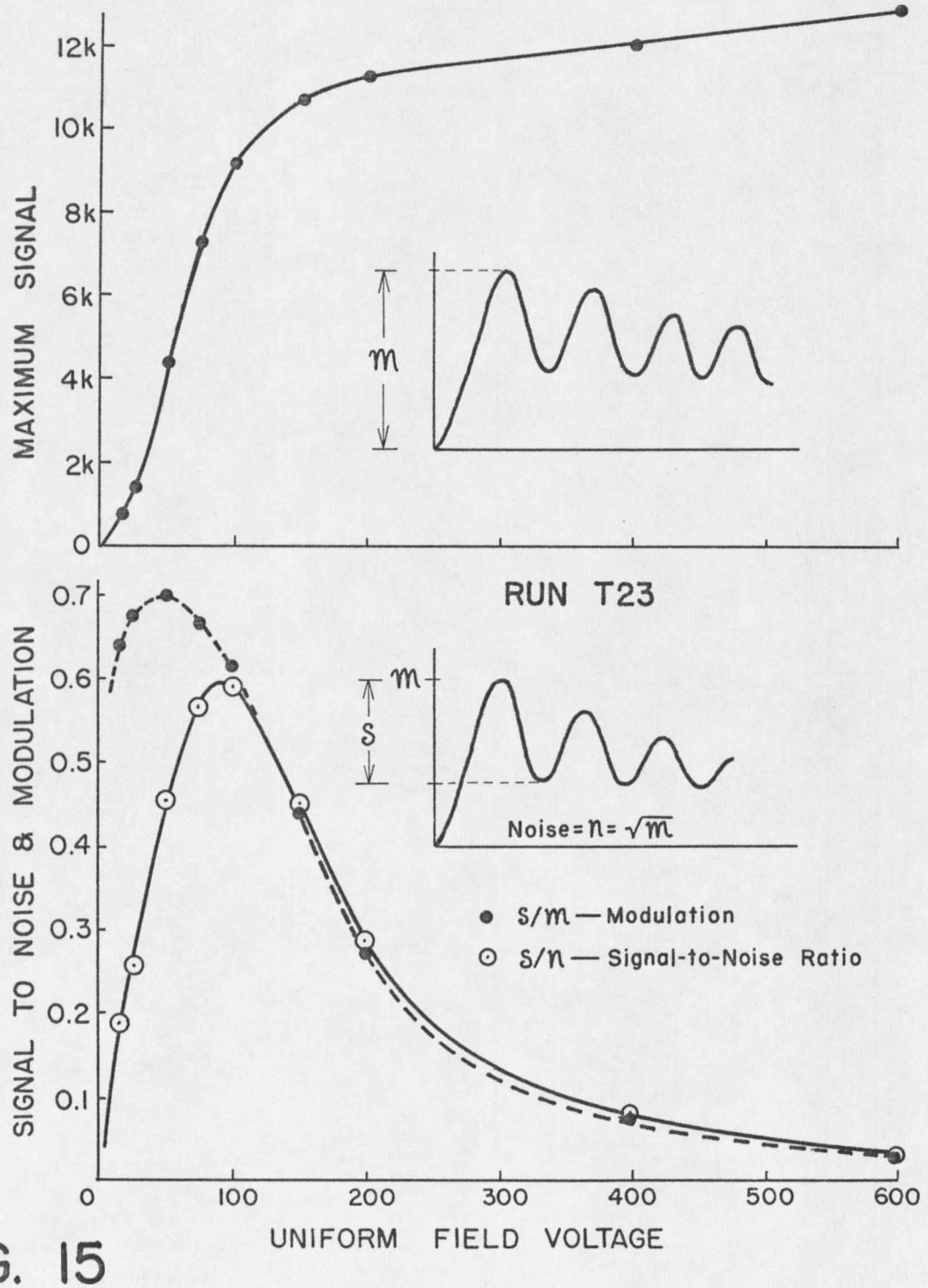

MAXIMUM SIGNAL
12k
10k
8k
6k
4k
2k
0
m
RUN T23
SIGNAL TO NOISE & MODULATION
0.7
0.6
0.5
0.4
0.3
0.2
0.1
m
S
Noise = n = √m
S/m — Modulation
S/n — Signal-to-Noise Ratio
0
100
200
300
400
500
600
UNIFORM FIELD VOLTAGE

FIG. 15

TABLE 6

QUANTUM-BEAT DATA: RUN T18

z(in)	N	z(in)	N	z(in)	N	z(in)	N	z(in)	N	z(in)	N
1.50	161	1.78	6221	2.01	6503	2.24	3553	2.47	3040	2.70	2607
1.55	191	1.79	5030	2.02	6425	2.25	3735	2.48	2699	2.71	2483
1.57	251	1.80	4844	2.03	5958	2.26	3967	2.49	2618	2.72	2364
1.58	357	1.81	5955	2.04	4876	2.27	4183	2.50	2840	2.73	2162
1.59	641	1.82	7398	2.05	4109	2.28	4198	2.51	2856	2.74	2104
1.60	1127	1.83	8496	2.06	3776	2.29	3960	2.52	3012	2.75	1970
1.61	2383	1.84	9137	2.07	4072	2.30	3838	2.53	3018	2.76	2067
1.62	4099	1.85	8276	2.08	4764	2.31	3359	2.54	2963	2.77	2131
1.63	6671	1.86	6976	2.09	5387	2.32	3082	2.55	2736	2.78	2284
1.64	9144	1.87	5450	2.10	5836	2.33	3124	2.56	2521	2.79	2310
1.65	11186	1.88	4514	2.11	5561	2.34	3441	2.57	2579	2.80	2247
1.66	12003	1.89	4534	2.12	4950	2.35	3621	2.58	2478	2.81	2125
1.67	11325	1.90	5418	2.13	4364	2.36	3680	2.59	2591	2.82	1984
1.68	9412	1.91	6614	2.14	3857	2.37	3499	2.60	2759	2.83	1810
1.69	7220	1.92	7410	2.15	3664	2.38	3472	2.61	2840	2.84	1838
1.70	5548	1.93	7675	2.16	4005	2.39	3188	2.62	2688	2.85	1887
1.71	5189	1.94	6848	2.17	4358	2.40	3068	2.63	2643	2.86	2041
1.72	6195	1.95	5710	2.18	4869	2.41	2985	2.64	2478	2.87	2075
1.73	8043	1.96	4676	2.19	4943	2.42	3047	2.65	2388	2.88	2136
1.74	9665	1.97	4104	2.20	4595	2.43	3184	2.66	2190	2.89	2021
1.75	10277	1.98	4211	2.21	4257	2.44	3373	2.67	2232	2.90	1979
1.76	9693	1.99	5108	2.22	3857	2.45	3357	2.68	2346		
1.77	8039	1.20	5877	2.23	3510	2.46	3180	2.69	2385		

Approximate background counts = 150±30

TABLE 7

QUANTUM-BEAT DATA: RUN T19

z(in)	N	z(in)	N	z(in)	N	z(in)	N
1.60	787	1.83	4085	2.06	5811	2.29	4180
1.61	1593	1.84	5096	2.07	6251	2.30	3930
1.62	2933	1.85	6733	2.08	6199	2.31	3423
1.63	5002	1.86	7805	2.09	5388	2.32	3224
1.64	7369	1.87	8601	2.10	4939	2.33	3217
1.65	9830	1.88	8261	2.11	4073	2.34	3315
1.66	11456	1.89	7417	2.12	3437	2.35	3738
1.67	11730	1.90	5897	2.13	3533	2.36	3863
1.68	10946	1.91	4419	2.14	3934	2.37	3901
1.69	8816	1.92	3752	2.15	4476	2.38	3948
1.70	6389	1.93	3781	2.16	4886	2.39	3636
1.71	4596	1.94	4567	2.17	5302	2.40	3381
1.72	3967	1.95	5669	2.18	5177	2.41	3117
1.73	4545	1.96	6757	2.19	4959	2.42	3027
1.74	5937	1.97	7231	2.20	4259	2.43	2967
1.75	7960	1.98	7075	2.21	3702	2.44	3182
1.76	9462	1.99	6377	2.22	3374	2.45	3404
1.77	10074	2.00	5268	2.23	3316	2.46	3346
1.78	9648	2.01	4283	2.24	3473	2.47	3613
1.79	7974	2.02	3778	2.25	3963	2.48	3349
1.80	6258	2.03	3588	2.26	4436	2.49	3336
1.81	4489	2.04	4096	2.27	4587	2.50	3025
1.82	4011	2.05	4990	2.28	4521		

Approximate background counts = 74±18

TABLE 8

QUANTUM-BEAT DATA: RUN T22

z(in)	N	z(in)	N	z(in)	N	z(in)	N
1.60	1740	1.83	10001	2.06	8770	2.29	5486
1.61	3588	1.84	11988	2.07	7759	2.30	5812
1.62	6268	1.85	13221	2.08	6668	2.31	6080
1.63	9919	1.86	13254	2.09	5925	2.32	6336
1.64	13881	1.87	11785	2.10	5904	2.33	6275
1.65	16768	1.88	9866	2.11	6434	2.34	5881
1.66	18342	1.89	7826	2.12	7227	2.35	5575
1.67	17797	1.90	6689	2.13	7815	2.36	5167
1.68	15418	1.91	6429	2.14	8090	2.37	4958
1.69	11898	1.92	7615	2.15	8037	2.38	4933
1.70	8847	1.93	9373	2.16	7509	2.39	5154
1.71	7282	1.94	10604	2.17	6605	2.40	5502
1.72	7675	1.95	11228	2.18	5913	2.41	5737
1.73	10173	1.96	10785	2.19	5592	2.42	5709
1.74	12928	1.97	9390	2.20	5897	2.43	5408
1.75	15144	1.98	7898	2.21	6454	2.44	5130
1.76	15857	1.99	6569	2.22	7005	2.45	4781
1.77	14701	2.00	6319	2.23	7241	2.46	4504
1.78	11998	2.01	6435	2.24	7131	2.47	4447
1.79	9250	2.02	7484	2.25	6687	2.48	4677
1.80	7493	2.03	8771	2.26	6091	2.49	4830
1.81	6695	2.04	9361	2.27	5565	2.50	5224
1.82	7777	2.05	9335	2.28	5383		

Approximate background counts = 146±29

TABLE 9

QUANTUM-BEAT DATA: RUN T23

z(in)	N	z(in)	N	z(in)	N	z(in)	N
1.60	1926	1.77	17584	1.94	7477	2.11	7940
1.61	3527	1.78	16914	1.95	9367	2.12	6758
1.62	6249	1.79	14125	1.96	11228	2.13	6130
1.63	10228	1.80	11039	1.97	12425	2.14	6262
1.64	14676	1.81	8244	1.98	12403	2.15	6892
1.65	17729	1.82	6760	1.99	11990	2.16	7824
1.66	20136	1.83	7189	2.00	10434	2.17	8831
1.67	20266	1.84	8818	2.01	8449	2.18	9030
1.68	18445	1.85	11544	2.02	6982	2.19	8896
1.69	14584	1.86	13480	2.03	6465	2.20	8374
1.70	10878	1.87	14928	2.04	6615	2.21	7413
1.71	7944	1.88	14753	2.05	7642	2.22	6631
1.72	7152	1.89	13153	2.06	9011	2.23	6006
1.73	8270	1.90	10815	2.07	10271	2.24	5803
1.74	11180	1.91	8458	2.08	10495	2.25	6118
1.75	14106	1.92	6695	2.09	10325		
1.76	17073	1.93	6511	2.10	9274		

Approximate background counts = 210±42

Fig. 16. Quantum-beat data for Run T23 is presented. See table 9 for details.

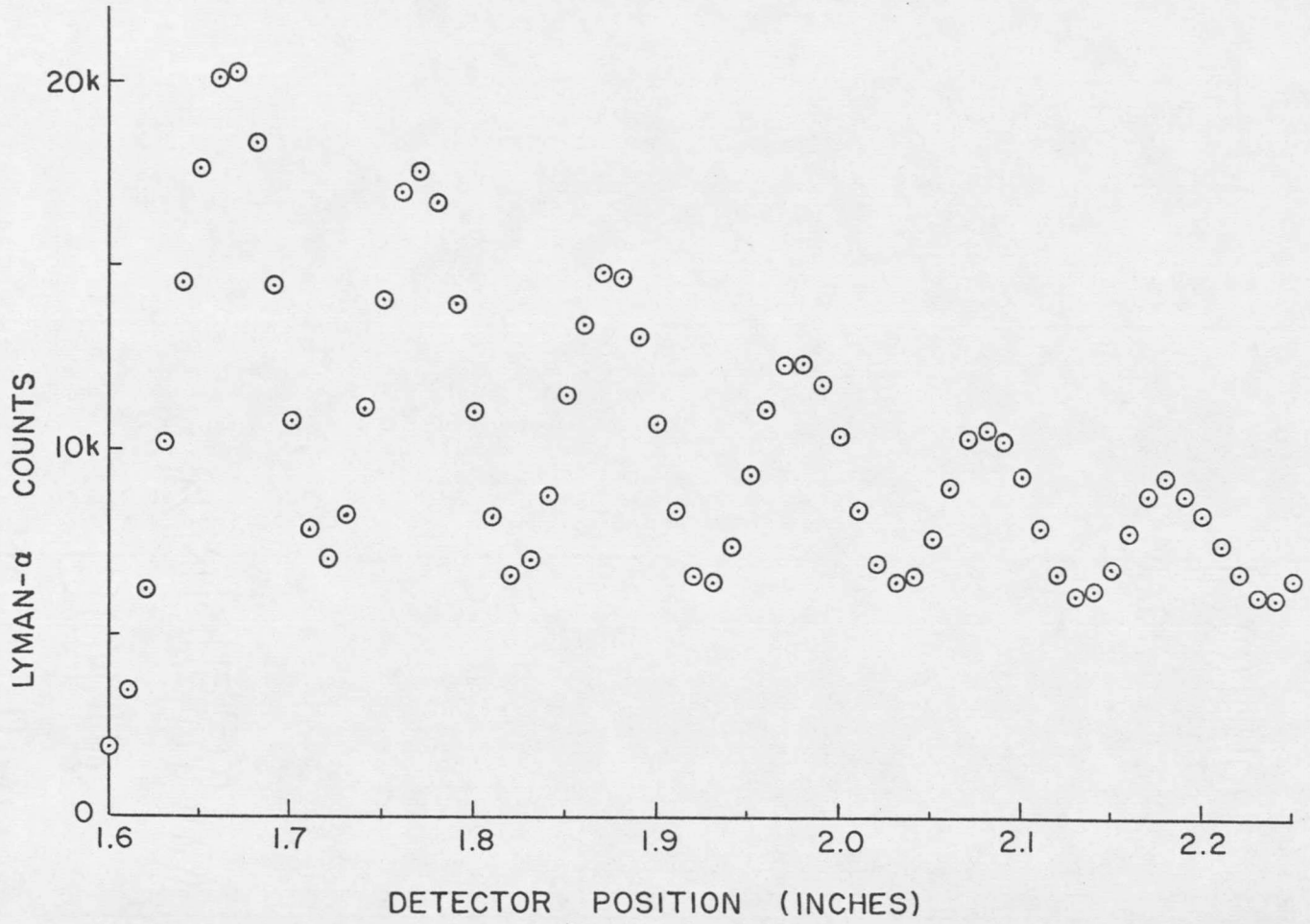

20k
10k
0
LYMAN-α COUNTS
1.6
1.7
1.8
1.9
2.0
2.1
2.2
DETECTOR POSITION (INCHES)

FIG. 16

TABLE 10

TYPICAL OPERATING CONDITIONS: RUN T23

Accelerator Voltage Setting = 105kV

Extraction = 0.7mA, Focus = 0.68mA, Leak = 0.75mA

Accel. vacuum pressure = 8μT (initially) to 6μT

Beam current #1 aperture = 200μA (includes sec. elect.)

Faraday cup current = 500nA (#3 aperture open)

V_{CEM} = 3kV, V_{quench} = 1kV, $V_{final\ sweep\ plates}$ = 1.5kV

Sweep-field-magnet current = 0.150A

Experimental chamber vacuum pressure = 5μT down to 2μT

Charge-exchange-cell pressure = 45mT

CHAPTER IV

ANALYSIS OF DATA

Least-Squares Fitting

In extracting values for "unknown" parameters from the data presented in the previous chapter we choose to fit the theory to the data by minimizing the weighted square deviation between the data and theory accomplished by adjusting the "unknown" parameters, i.e., we adjust the "unknown" parameters so that χ^2 is minimized where

$$\chi^2 = \sum_{i=1}^{N} [y_i - f(a_j; z_i)]^2/\sigma_i^2 \qquad (54)$$

and y_i is the i^{th} data point ($i = 1,2,\ldots,N$) having an estimated standard deviation of σ_i (for counting $\sigma_i=\sqrt{y_i}$, Poisson statistics) which was taken at position z_i; $f(a_j,z_i)$ is the theory function depending upon the unknown parameters a_j ($j = 1,2,\ldots,J$). Ideally a fit is "completed" when the parameters a_j are adjusted so that the gradient of χ^2 with respect to the parameters is zero specifying a minimum of the χ^2 hypersurface. In making these fits one must be careful to determine just how unique the fit parameters are. When $f(a_j,z_i)$ is very nonlinear and the number of fit parameters is large ($J > 5$) there may be several choices of the a_j which serve to define relative minima of χ^2. The problem is further complicated if the theory also depends upon parameters which are not free to be fit. In general we can write

$f(a_j, b_k; z_i)$ where we've included a set of parameters b_k, k=1,2,...,K which are known, e.g., the applied voltage, hyperfine-frequency state separations, etc. As the number of a_j and b_k increase we must be very careful in selecting our starting values of a_j and in determining the values of a_j and in establishing the values of b_k.

In what follows we will be referring to the reduced χ^2 defined by

$$\chi^2_\nu = \chi^2/(N-J) \tag{55}$$

where $\nu = N - J$ is called the number of degrees of freedom. Usually when a good fit is obtained the reduced χ^2 will be approximately equal to one. If χ^2_ν is less than one we shouldn't consider that a better fit has been obtained, rather, we've merely fit a statistically unusual set of data. Conversely, if χ^2_ν is much greater than one we need not conclude that the theory does not adequately describe the data, for again, any single set of data may be "unusual." If on the other hand, χ^2_ν is found to be large for all data sets analyzed we would then be led to conclude that the theory does not adequately describe the data.

Ultimately we need to establish estimations of the standard deviations associated with the fitted parameters. If the fitting function is linear in the parameters it can be shown that the standard deviation associated with fit parameter a_j may be estimated by [25]

$$\sigma_{a_j} = \epsilon_{jj} \tag{56}$$

where ϵ_{jj} is the diagonal element of the inverse of the χ^2 curvature matrix

$$\epsilon_{ij} = \alpha_{ij}^{-1}, \qquad \alpha_{ij} = \frac{1}{2}\frac{\partial^2 \chi^2}{\partial a_i \partial a_j} . \tag{57}$$

Such a derivation is based upon writing

$$\sigma_{a_j}^2 = \sum_i \left[\sigma_i^2 (Da_j/Dy_i)^2 \right], \tag{58}$$

where the derivative means "change in the fit result, Da_j when the i^{th} data point y_i changes by Dy_i." For nonlinear fitting functions we can approximate χ^2 with a χ^2 which is linear in the a_j if we are very near to the minimum χ^2 ($a_j : \nabla\chi^2 = 0$). Such estimates of the standard deviations σ_{a_j} are not always good, especially if the fitting function is specified by known parameters whose uncertainties also contribute to the fit-parameter error. A method which accounts for all possible uncertainty in the data and known parameters is to analyze new sets of data and parameters which have been generated from the experimental data. This simulation method varies the dependent variables y_i, the independent variables z_i, and the known parameters b_j in a random fashion according to a normal distribution consistent with their estimated errors.[26] These new sets of data are then fit. Each set of simulated data generates a different set of fit parameters; the standard deviation of the fit parameters produced in this manner provide a good estimation of the expected error associated with the fit parameters. If the fitting function is very nonlinear, as in our QB theory, such a

simulation method can cost upwards of several hundred dollars of computer time for only a few (~20) simulations. Because of the cost such simulations are only provided for a few of the fits.

Analysis of Free-Decay Data: Determination of γ/υ

The fitting function we use in determining the decay-rate velocity ratio is

$$N(z) = N_0 e^{-mz} + N_b(z) \tag{59}$$

where $m = \gamma/\upsilon$ and N_0 are to be determined by the fit, and $N(z)$ and $N_b(z)$ are the free decay signal and background respectively. Fitting such a simple function is an easy matter for almost any nonlinear routine. In table 11 we show the fit results for all the runs along with the standard deviation of the fits for each run. Included with these results is the accelerating voltage and velocity if we assumed a value for $\gamma = 6.27\times10^8 s^{-1}$ (its "accepted" value). Notice that the accelerating voltage determined in this way is higher than what is indicated by the actual accelerator setting. This discrepancy was observed numerous times prior to taking the final data and is not characteristic of only the final data. We show the results of data simulation on several fits.

Quantum-Beat Data

The analysis of the quantum-beat (QB) data is considerably more involved than the analysis of the free-decay data. We have developed a

TABLE 11

FIT RESULTS FOR FREE-DECAY DATA

Run	Data Set	m (cm^{-1})	Fit results
T23 (105kV)	3A	1.36859	$\bar{m} = 1.3619 cm^{-1}$
	3B	1.35683	$\sigma_m = 0.0093(\pm 0.69\%) cm^{-1}$
	3C	1.35925	Accel. Volts = 109.4kV
	5	1.36892	$\upsilon = 4.578 \times 10^8 cm/s$
T22 (90kV)	6A	1.51163	
	6B	1.53890	$\bar{m} = 1.5048 cm^{-1}$
	3E	1.51281	$\sigma_m = 0.0205(\pm 1.4\%) cm^{-1}$
	3F	1.4853	Accel. Volts = 89.60kV
	3H	1.49187	$\upsilon = 4.143 \times 10^8 cm/s$
	3I	1.4883	
T19 (100kV)	9A	1.38432	$\bar{m} = 1.3915 cm^{-1}$
	9B	1.38750	$\sigma_m = 0.0053(\pm 0.4\%) cm^{-1}$
	11A	1.39630	Accel. Volts = 104.8kV
	11B	1.39363	$\upsilon = 4.481 \times 10^8 cm/s$
	11C	1.39550	
T18 (85kV)	4	1.54330	$\bar{m} = 1.5288 cm^{-1}$
	6	1.51723	$\sigma_m = 0.0133(\ 0.869\%) cm^{-1}$
	7	1.52581	Accel. Volts = 86.81kV
			$\upsilon = 4.068 \times 10^8 cm/s$

Data simulations: set T22-3E, $\sigma_m \sim 0.8\%$; set T18-4, $\sigma_m \sim 0.34\%$

theory which should be capable of describing all the details of the QB curve. We have allowed for separate initial conditions for each hyperfine two-level system, calculated the effects of a detector window, anticipated the effects of a velocity dispersion, and made provisions for estimating the effects of the fringe field. With such machinery we should be able to fit the theory to the data and thereby extract a value for the decay rate γ. There are many difficulties in making such a fit, however.

The QB theory (chapter 2) is developed for a uniform field. Therefore, we would not want to insist on fitting any part of the curve which resides within the fringe field. This requires our knowing the shape of the fringe field and the anticipated radiation profile (p-state population) within it bounds. We can determine the fringe field by mapping the electric field of a scale model in a field-mapping tank. The model is a 33X enlargement of the actual plate configuration (a plate separation of 4in corresponds to the actual separation of 0.121in). The mapping probe consists of two thin wires ($\sim$1.5cm long) separated by about 1mm. When the probe is dipped into the water the potential difference between the wires serves as a measure of the electric field (60Hz AC is used). The tank is first tested on a simple parallel-plate capacitor, and the results agreed very well with the calculated fringe field of the simple capacitor (see Fig. 17).

Fig. 17. Parallel-plate-capacitor field map. The central field of a simple parallel-plate capacitor is mapped and compared to the field calculated from an ideal capacitor. The actual field is expected to have a wider fringe field because the plates have a finite thickness.

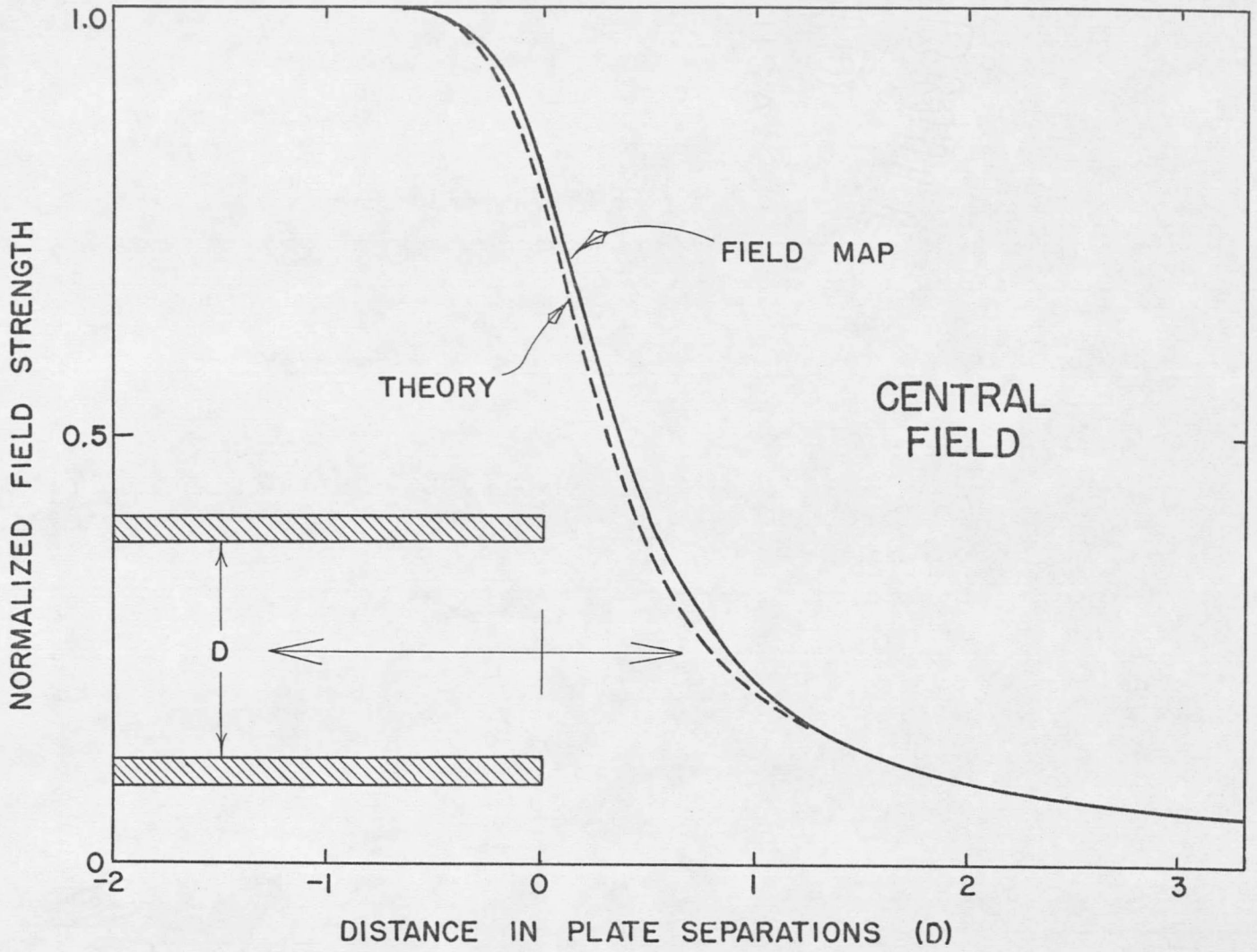

1.0
0.5
0
NORMALIZED FIELD STRENGTH
FIELD MAP
THEORY
CENTRAL
FIELD
D
-2
-1
0
1
2
3
DISTANCE IN PLATE SEPARATIONS (D)

FIG. 17

In Fig. 18 we show a similar map for the electrode configuration of the uniform field region. We do not account for the field component along the axis in this analysis; it will be a simple matter to extend our results if we find it necessary to do so. It is not necessary to worry about the field fringing transverse (horizontal) to the beam, for the field is sufficiently uniform over a region larger than the beam will occupy (see Fig. 19).

The average fringe field profile as seen by the beam would lie between the field profiles of the central and edge fringe field. If we use the off-axis field as an approximate average fringe field and perform a computer integration of the amplitude equations through this fringe field we obtain an indication of where we can safely say the field is uniform relative to the data. We show the results of such a procedure in Fig. 20 for the voltage and beam velocity associated with Run T23. We see that the first peak occurs within the fringe field. Comparing the position of this peak with the data of Run T23 we feel safest in starting a fit of our data from 1.70in and beyond (the field has reached 99% of its full value). We thereby lose the information contained in the first peak, unfortunately.

The requisite hyperfine state initial conditions could be obtained by performing a computer simulation (as was just done) for each of the hyperfine states and for each of the runs. Such a method lacks

Fig. 18. Uniform-field fringe fields along beam. Electrode configuration and size of beam drawn to scale.

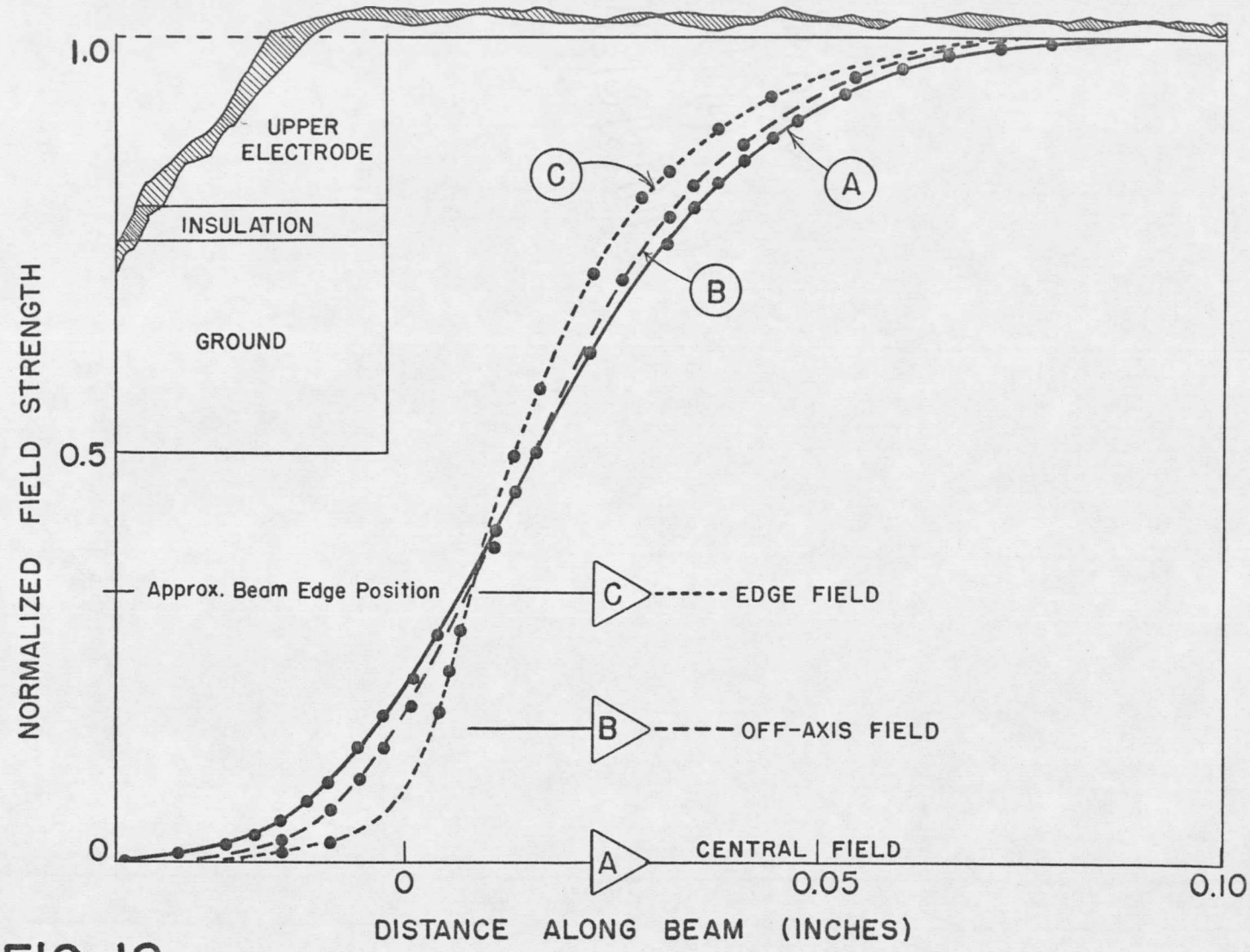

1.0
0.5
0
NORMALIZED FIELD STRENGTH
UPPER ELECTRODE
INSULATION
GROUND
C
A
B
Approx. Beam Edge Position
C
EDGE FIELD
B
OFF-AXIS FIELD
A
CENTRAL FIELD
0
0.05
0.10
DISTANCE ALONG BEAM (INCHES)

FIG. 18

Fig. 19. Uniform-field fringe field across beam.

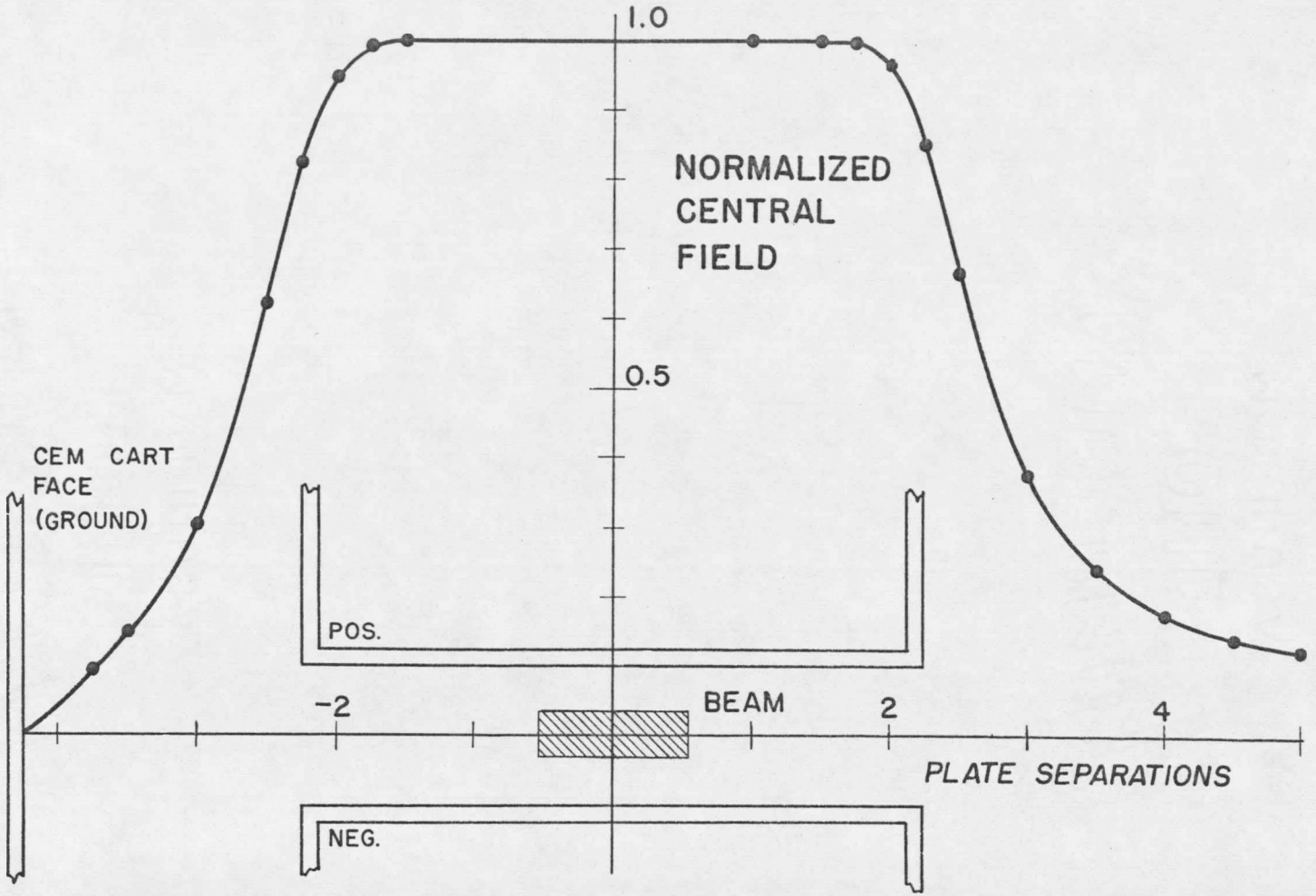

1.0
NORMALIZED
CENTRAL
FIELD
0.5
CEM CART
FACE
(GROUND)
POS.
-2
BEAM
2
4
PLATE SEPARATIONS
NEG.

FIG. 19

Fig. 20. First radiation peak in fringe field. If we start the fit at 99% full field we need to begin fitting at z = 1.70in in the data obtained. The simulation of the problem is an average of hyperfine populations and not a fine-structure calculation.

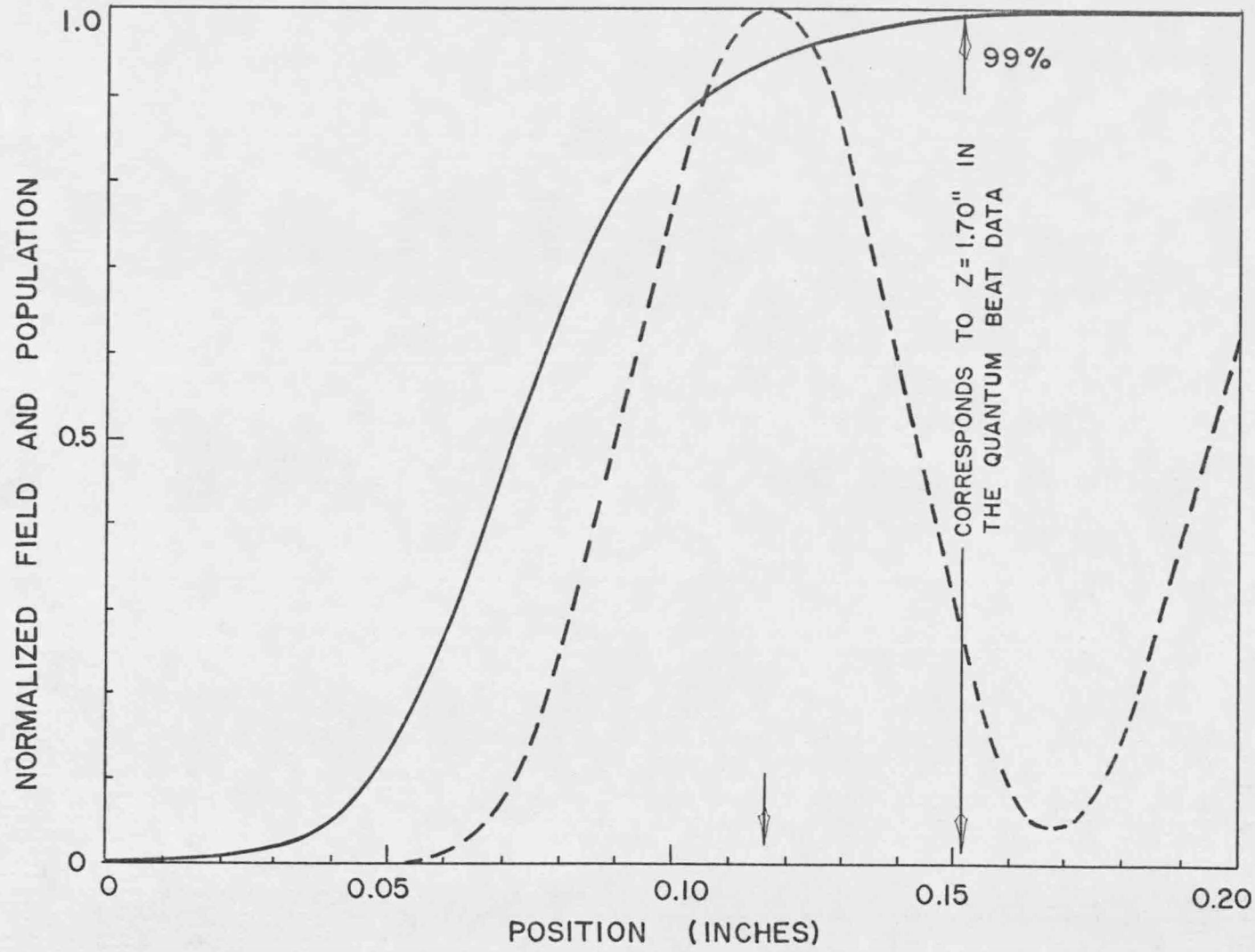

1.0
0.5
0
NORMALIZED FIELD AND POPULATION
0
0.05
0.10
0.15
0.20
POSITION (INCHES)
99%
CORRESPONDS TO Z = 1.70" IN
THE QUANTUM BEAT DATA

FIG. 20

flexibility, however, for we could not change the length of the fringe field without a great deal of trouble. Instead we employ the analytical fringe field developed in chapter 2. The only parameter we don't know is the equivalent half-width-half-maximum length (HWHM) of the hyperbolic secant fringe field so that the amplitudes calculated analytically are a good approximation to the "computer" amplitudes. The simplest way to do this is to perform several amplitude calculations for different HWHM and then compare the results to computer solutions. In this way we determine the best HWHM to use is 0.0246in. Figure 21 shows how nicely the p-state populations compare. As a check we perform computer simulations of the problem for each run and similarly compare the results of the hyperfine average with the analytical method's hyperfine average. The results are in excellent agreement. We can now estimate the changes produced in the amplitudes because of changes in the fringe field, the velocity, voltage, etc. as well as quickly obtain the amplitudes for each hyperfine state. Such flexibility proves to be most valuable in selection of the proper fit.

One problem has not been discussed. With the hyperbolic secant fringe field the two level system always feels the field because of the exponential tail. On the other hand, the fringe field used in the computer simulation of the problem probably didn't extend far enough. The probabilities of the s and p states are not affected by such a differ-

Fig. 21. Analytical and actual fringe-field comparison. The solid lines represent a computer simulation of the entrance of the beam into the fringe field for the measured fringe-field profile. The dashed lines represent the problem using the analytical (Rosen-Zener) solution.

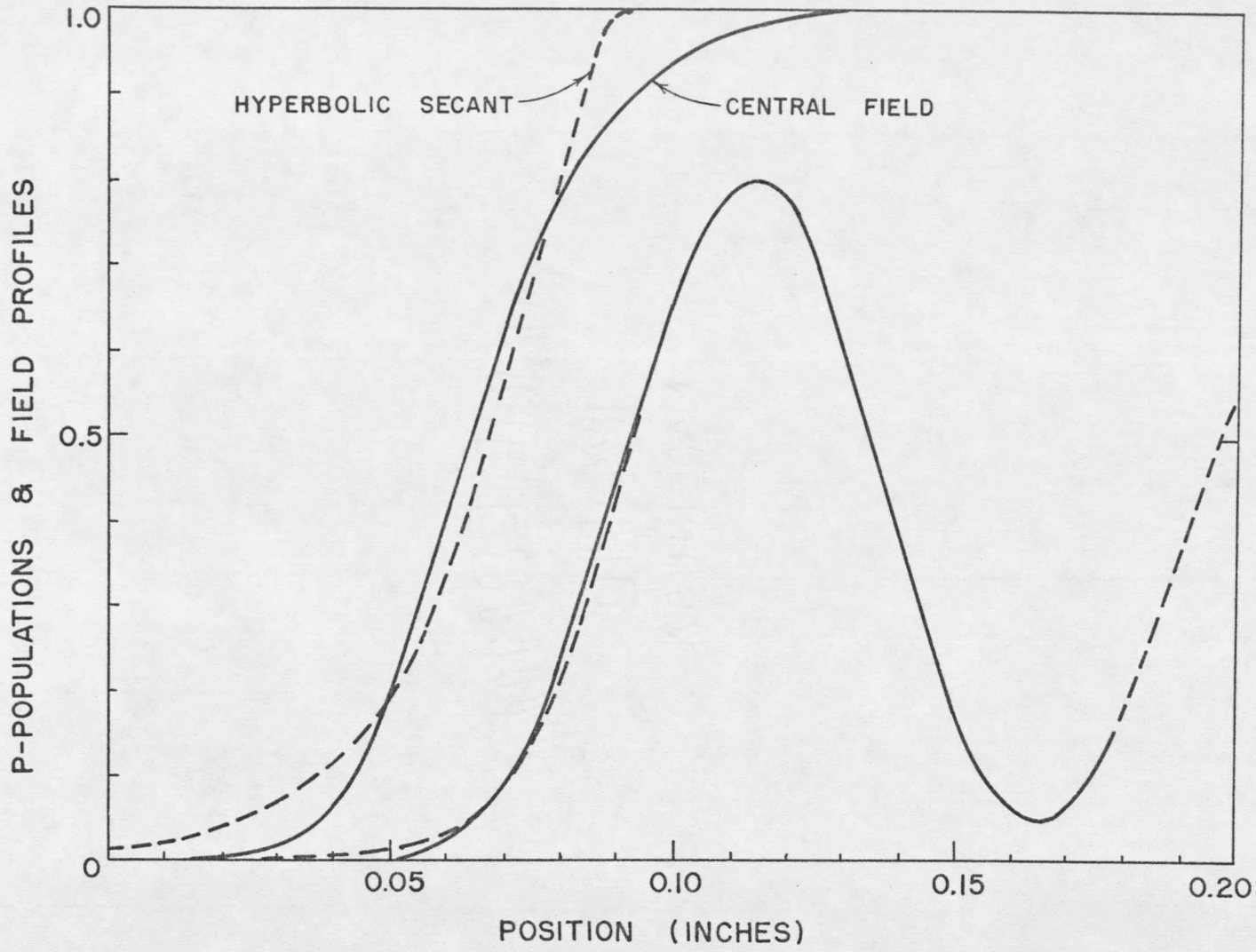

1.0
0.5
0
HYPERBOLIC SECANT
CENTRAL FIELD
P-POPULATIONS & FIELD PROFILES
0.05
0.10
0.15
0.20
POSITION (INCHES)

FIG. 21

ence but the phases definitely are. Referring back to the weak field expressions for the amplitudes we notice that the phase which accumulates in the s state is proportional to the square of the field while as soon as the p state is produced its phase accumulates as ωt--see Eqs. (16) through (18). The phase difference is therefore very uncertain, and the phase difference established by the computer simulation of the problem is probably as small as the actual phase difference can be. Provided the phase difference is increased as $\omega_i t$ for each hyperfine state, we should be able to find the best phase difference by starting with the phase difference manufactured by the computer simulation.

Calculation of Window, Velocity Dispersion, and $2^2P_{3/2}$ Contribution

Now that we have a means of estimating the hyperfine initial state amplitudes we need to provide an estimate of the detector window size. In Fig. 22 we show a scale drawing of the detector, slit, and beam. We need to determine the observation profile produced by a slit moving across the circular detector as viewed from the beam. The problem can be solved analytically but the derivation is quite uninteresting; so we only quote the results. In terms of the distances specified in Fig. 22 the normalized detection profile is given by the following expression:

Fig. 22. Detector window geometry. We measure a = 0.040in, b = 0.0084in, A = 0.507in, and B is designed to be 0.728in at the center of the beam (beam diameter is 0.250in).

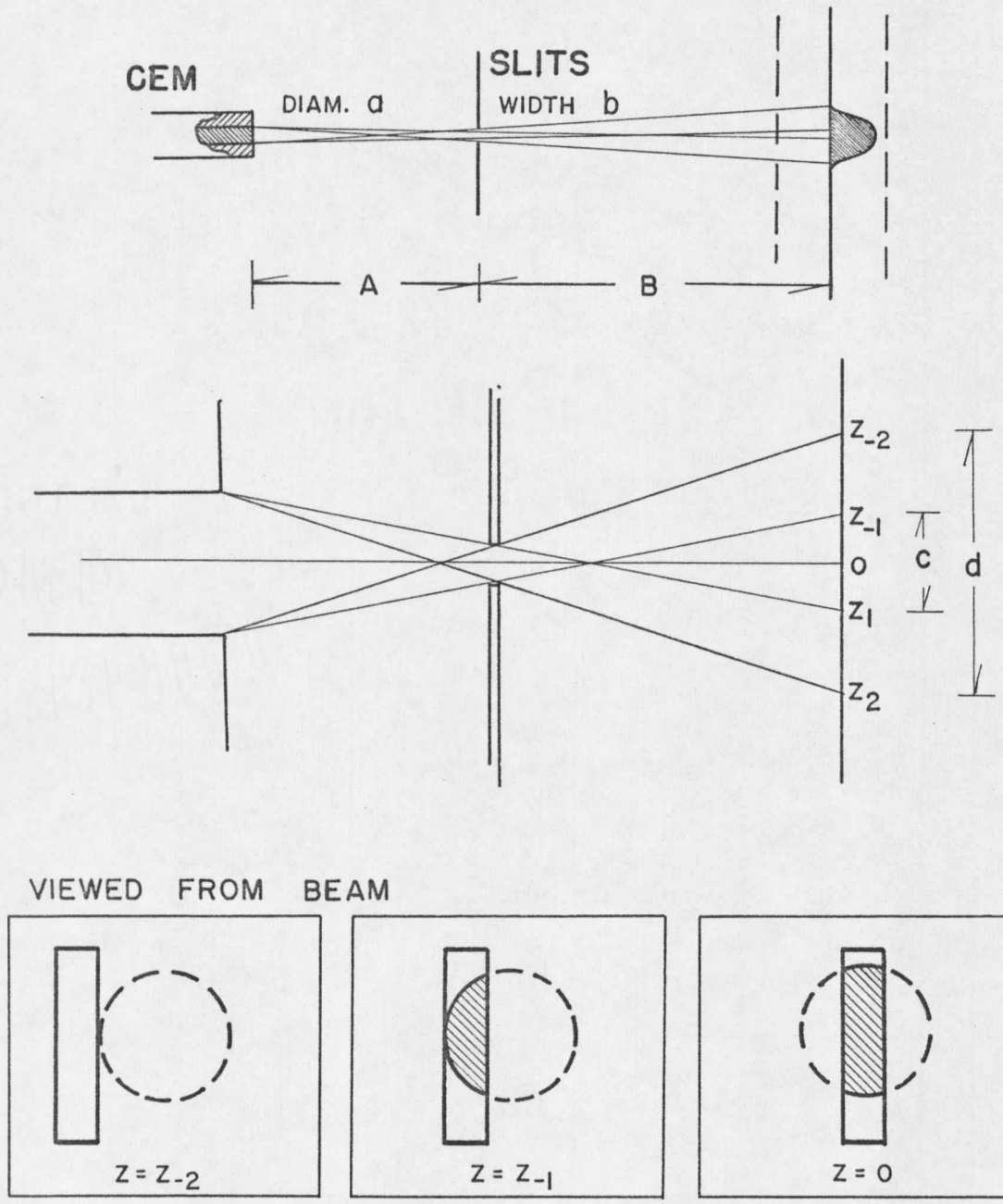

CEM
DIAM. a
SLITS
WIDTH b
A
B
Z_{-2}
Z_{-1}
0
Z_1
Z_2
c
d
VIEWED FROM BEAM
Z = Z_{-2}
Z = Z_{-1}
Z = 0

FIG. 22

$$\alpha(z) = \begin{cases} \frac{1}{N}\left[F(|x|+\Delta x/2) - F(|x|-\Delta x/2)\right], & -\frac{c}{2} < z < \frac{c}{2} \\ \frac{1}{N}\left[F(|x|+\Delta x/2) - F(|x|-\Delta x/2)\right], & \frac{c}{2} \le z \le \frac{d}{2} \end{cases} \tag{60}$$

where

$$F(w) = w\sqrt{r^2-w^2} + r^2 \sin^{-1}(w/r),$$
$$N = \Delta x\sqrt{r^2-(\Delta x/2)^2} + 2r^2 \sin^{-1}(\Delta x/2), \tag{61}$$
$$x = zA/B\ ,\ \Delta x = b(A+B)/B,\ r = a/2$$

The area is given by

$$S = \frac{1}{N}\left\{\pi r^2(d-c)/2 + 2(B/A)\left[G(Q) - G(P)\right]\right\}, \tag{62}$$

where

$$Q = AC/2B + \Delta x/2\ ,\quad P = Ad/2B - \Delta x/2,$$
$$G(w) = -\sqrt{r^2-w^2} - (r^2-w^2)^{3/2}/3 + w\sin^{-1}(w/r). \tag{63}$$

In Fig. 23 we show the actual window area compared to a rectangular profile with the same area and how the area changes across the beam.

Unfortunately, this careful measurement of the window was not helpful. Almost all fit attempts demanded that the window was larger than predicted. The window calculated is for a beam traveling through the center of the field region. It was discovered that the beam was actually closer to the cart than anticipated resulting in a window of length 0.047in. There is reason to believe the fits, however. We can get an idea of the size of the window from Fig. 11. The extent to which radiation produced at the center of the sandwich is observed by the detector before the detector reaches the center electrode position indi-

Fig. 23. Detector-window profile. The variation of the detector window across the beam is shown as a function of distance of detector cart from the beam.

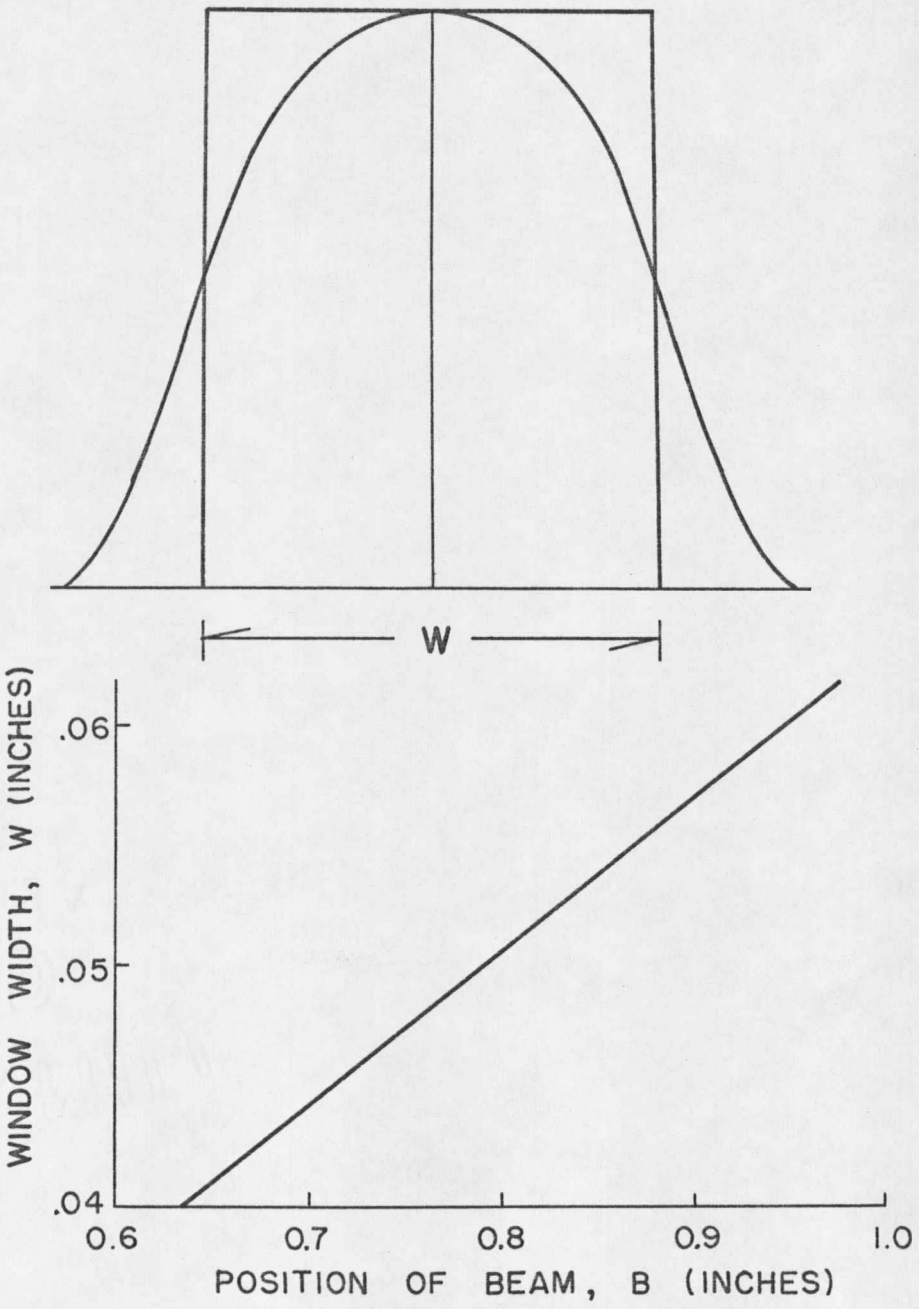

W
WINDOW WIDTH, W (INCHES)
.06
.05
.04
0.6
0.7
0.8
0.9
1.0
POSITION OF BEAM, B (INCHES)

FIG. 23

cates the window's size. It is clear that the window could be larger than estimated, especially when we realize that the beam doesn't have a uniform crossection and the maximum intensity could range over the entire width of the beam or there could be a "hot spot"; such conditions were observed to vary from run to run--the intensity distribution across the beam could be observed via the quartz target in the Faraday cup. It is clear that we cannot fix the window, therefore, and it is regraded as a free (or fitted) parameter.

The velocity dispersion arises from the inherent velocity distribution produced by the rf ion source as well as any 60Hz ripple from the accelerator power supply. Fortunately, the velocity dispersion hardly changes the fit results, for we can only guess that $\Delta\upsilon/\upsilon$ ranges from 0.003 to 0.007. The 60Hz ripple introduces roughly a 0.2% dispersion. Fit results are shown with and without a velocity dispersion for Run T23 only.

As discussed in chapter 2 the lowest order approximation of the effects of the $2^2P_{3/2}$ state is the slight increase in the decay rate $\gamma \rightarrow \gamma(1+2\eta^2)$ where η is the ratio of the Lamb shift to the $2^2P_{3/2}$-$2^2S_{\frac{1}{2}}$ level separation ($\eta = 0.1067$). Therefore, we anticipate that the effective decay rate within the uniform field region will be 2.28% higher than if the $2^2P_{3/2}$ level were not present. This means that the input value of the γ/υ ratio obtained from the free-decay data will have to

be increased by this amount and that the resulting value of γ obtained from the fit will then have to be decreased by the same amount. The contribution from the $2^2P_{3/2}$ level amounts to an important correction.

Fitting Function and Results

The fitting function which we use is the net p population of Eq. (49) with minor modifications. To avoid any confusion we explicitly exhibit the fitting function at the risk of repetition

$$|\rho(z)|^2 = \frac{N}{4}\left[2(A_s)_1^2|\rho(\omega_1;z)|^2 + (A_s)_3^2|\rho(\omega_3;z)|^2 + (A_s)_4^2|\rho(\omega_4;z)|^2\right], \tag{64}$$

where

$$|\rho(\omega_i;z)|^2 = \frac{1}{u}\left[Ae^{-\alpha(z-z_0)} + Be^{-\beta(z-z_0)} - Ge^{-a(z-z_0)}F(\delta(z-z_0)-\phi)\right],$$

and

$$a = m/2\,,\quad \alpha = a(1-\xi),\quad \beta = a(1+\xi),\quad \delta = a\zeta,\quad \Delta = \Delta_i + 2\pi\frac{\omega_i}{\omega_{fs}}\Delta\,,$$

$$\xi = R - \kappa S,\quad \zeta = \kappa R + S\,,\quad R = \sqrt{u}\cos(\theta/2),\quad S = \sqrt{u}\sin(\theta/2),$$

$$u = \sqrt{x^2+y^2},\quad x = 1 + 4q^2(\kappa^2-1)/(1+\kappa^2)^2,\quad y = 8q^2\kappa/(1+\kappa^2)^2,$$

$$\theta = \tan^{-1}(y/x),\quad \kappa = 2\omega_i/\gamma\,,\quad q = E/\left[\gamma(3.588736\times10^{-8}\,\text{volts}\cdot\text{cm}^{-1}\cdot\text{s})\right],$$

$$E = V_0/d\,,\quad \omega_i = \omega_{s_i} - \omega_{p_i}\,,\quad Q^2 = q^2/(1+\kappa^2),\quad P = \rho q/(1+\kappa^2),\quad \rho_i = \rho(\rho)_i,$$

$$A' = Q^2 + \rho^2(u+1-2R)/4 + P\left[(\zeta-\kappa)\cos\Delta + (1-\xi)\sin\Delta\right],$$

$$B' = Q^2 + \rho^2(u+1+2R)/4 - P\left[(\zeta+\kappa)\cos\Delta - (1+\xi)\sin\Delta\right],$$

$$C = 2Q^2 - \rho^2(u-1)/2 - 2P\left[\kappa\cos\Delta - \sin\Delta\right],$$

$$D = \rho^2 S + 2P\left[\xi\cos\Delta + \zeta\sin\Delta\right],\quad G = \sqrt{C^2+D^2},\quad \phi = \cos^{-1}(C/G),$$

$$A = (2A'/w\alpha)\sinh(w\alpha/2),\quad B = (2B'/w\beta)\sinh(w\beta/2),$$

$$F(\delta z-\phi) = \left[X\cos(\delta z-\phi) - Y\sin(\delta z-\phi)\right.,$$

$$X = 2\left[a\sinh(aw/2)\cos(\delta w/2) + \delta\cosh(aw/2)\sin(\delta w/2)\right]/w(a^2+\delta^2),$$

$$Y = 2\left[\delta\sinh(aw/2)\cos(\delta w/2) - a\cosh(aw/2)\sin(\delta w/2)\right]/w(a^2+\delta^2).$$

The value for $m = \gamma/\upsilon$ is the value obtained from the free-decay data with the 2.28% correction. The hyperfine amplitudes enter in the form

$$(A_s)_i\,,\quad (\rho)_i = (A_p)_i/(A_s)_i\,,\quad \Delta_i = (\Delta)_i + 2\pi\omega_i(\Delta-1)/\omega_{fs} \tag{65}$$

where $(A_s)_i$, $(A_p)_i$, $(\Delta)_i$ are the amplitude maxima and phase difference estimated from the fringe-field analysis for the hyperfine two-level problem associated with the hyperfine level separation ω_i. The Δ factor allows us to change the phase difference in a similar fashion as $\omega_i T$ would allow where T is the unknown extra time spent in the fringe field. The factor ρ allows our changing all the amplitude magnitude ratios by the same factor; it provides a means of making corrections to the ratio without releasing many parameters. z_o corresponds to the point at which the data fit is started (z_o = 1.70in); the difference $z-z_o$ corresponds to t = 0 when z = 1.70in.

It must be emphasized that much time has been spent in establishing exactly how to make a fit. By not being careful we could fit almost any γ. However, the basis for the rejection of a fit was how well it compared with the estimated parameters. The overall amplitude N, initial position z_o, and window don't make statements about the physics; however, if a fit shows ρ = 2.75 whereas we think it should be ρ = 1, then we have a reason to reject the fit.

The justification for this method arises from the fringe-field analysis. The amplitudes are the most uncertain parameters that contain information about the physics of the problem. By sufficiently adjusting these amplitudes or allowing them to be free we can change the shape of the curve to fit almost anything. However, because of the analytical fringe field solution we can estimate how much these initial amplitudes will change because of possible errors made, e.g. an error of 10% in the HWHM estimation. It turns out that the amplitudes and phase differences are relatively insensitive to small changes in the voltage, velocity, HWHM of the fringe field, etc. In this way we can reject a fit if the fitted parameters significantly deviate from what is expected or what we can allow. Fortunately the fits are easily separated as being reasonable or not.

The most successful method of fitting is to start by freeing the parameters which don't contain information about the physics--N, z_o, and w. Next the phase is released. Then the decay rate is released and the fit concluded when the fractional change in all the parameter values between successive fits is less than 10^{-4}. This fit scheme is then checked by the release sequence N, z_o, then Δ, then w, and finally the decay rate γ.

The initialization of the fits are summarized in table 12 and the fit sequences are shown in tables 13 - 16. We illustrate how a fit

TABLE 12

FITTING-FUNCTION INITIALIZATION

Parameters common to all fits:

$\rho = 1$	$\omega_1 = 6.832875\times10^9 s^{-1}$
$z_o = 1.70$in	$\omega_3 = 7.204749\times10^9 s^{-1}$
$w = 0.060$in	$\omega_4 = 5.717252\times10^9 s^{-1}$
$\gamma+2\% = 6.3925\times10^8 s^{-1}$	$d = 0.1213$in

Parameters unique to each fit:

Parameter	QB23 105kV	QB22 90kV	QB19 100kV	QB18 85kV
N	37200	33600	21500	22000
Δ	0.476	0.444	0.468	0.424
V_o	100	100	100	110.02
m + 2%(2.28%)	3.53808in	3.9091in	3.6149in	3.9716in
A_{s_1}	0.893	0.920	0.915	0.938
A_{s_3}	0.907	0.941	0.926	0.942
A_{s_4}	0.841	0.911	0.873	0.917
ρ_1	0.384	0.288	0.305	0.206
ρ_3	0.347	0.204	0.274	0.200
ρ_4	0.519	0.283	0.422	0.260
Δ_1	-1.49	-1.68	-1.62	-2.7
Δ_3	-1.59	-2.42	-1.81	-3.0
Δ_4	-1.00	-1.41	-1.105	-2.0
N_b	210	146	74	150
σ_{N_b}	43	42	18	30

TABLE 13

QUANTUM-BEAT FIT RESULTS: RUN T18

$N = 41932$ $z_o = 1.70902\text{in}$	$\chi^2_\nu = 300$	
$N = 53625$ $z_o = 1.70536\text{in}$ $\Delta = 0.3224$	$\chi^2_\nu = 4.9$	$N = 42170$ $z_o = 1.7084\text{in}$ $w = 0.06775\text{in}$ — $\chi^2_\nu = 125$
$N = 53412$ $z_o = 1.70534\text{in}$ $\Delta = 0.32594$ $w = 0.05167\text{in}$	$\chi^2_\nu = 4.8$	$N = 53391$ $z_o = 1.7053\text{in}$ $w = 0.05184\text{in}$ $\Delta = 0.32626$ — $\chi^2_\nu = 4.8$
$N = 52698$ $z_o = 1.70379\text{in}$ $\Delta = 0.32594$ $w = 0.05620\text{in}$ $\gamma' = 6.4571\times10^8\text{s}^{-1}$	$\chi^2_\nu = 2.18$	$N = 52698$ $z_o = 1.70397\text{in}$ $w = 0.05620\text{in}$ $\Delta = 0.33925$ $\gamma' = 6.4571\times10^8\text{s}^{-1}$ — $\chi^2_\nu = 2.18$

Assuming a 0.5% velocity dispersion we get $\gamma' = 6.4614\times10^8\text{s}^{-1}$, $\chi^2_\nu = 2.17$. Results for 10 data simulations (no velocity dispersion) are as follows:

$$\gamma' = 6.4351\times10^8\text{s}^{-1}, \quad \sigma_{\gamma'} = 0.0751\times10^8\text{s}^{-1} \quad (\text{or } \pm 1.17\%),$$

where γ' is the uncorrected result ($\gamma' = \gamma + 2.28\%$).

TABLE 14

QUANTUM-BEAT FIT RESULTS: RUN T19

$N = 46127$ $z_o = 1.7080\text{in}$	$\chi^2_\nu = 113$	
$N = 49471$ $z_o = 1.70983\text{in}$ $\Delta = 0.34298$	$\chi^2_\nu = 71$	$N = 46642$ $z_o = 1.7083\text{in}$ $w = 0.06352\text{in}$
$N = 48384$ $z_o = 1.7084\text{in}$ $\Delta = 0.39303$ $w = 0.06222\text{in}$	$\chi^2_\nu = 37$	$N = 48362$ $z_o = 1.7085\text{in}$ $w = 0.06237\text{in}$ $\Delta = 0.39314$
$N = 40409$ $z_o = 1.7028\text{in}$ $\Delta = 0.37645$ $w = 0.06311\text{in}$ $\gamma' = 6.6457\times10^8\,\text{s}^{-1}$	$\chi^2_\nu = 4.27$	$N = 49409$ $z_o = 1.7028\text{in}$ $w = 0.06311\text{in}$ $\Delta = 0.37645$ $\gamma' = 6.6457\times10^8\,\text{s}^{-1}$

TABLE 15

QUANTUM-BEAT FIT RESULTS: RUN T19

$N = 26688$ $z_o = 1.7122\text{in}$	$\chi^2_\nu = 115$	
$N = 30348$ $z_o = 1.7116\text{in}$ $\Delta = 0.35182$	$\chi^2_\nu = 11.4$	$N = 26838$ $z_o = 1.71176\text{in}$ $w = 0.06511\text{in}$
$N = 30088$ $z_o = 1.7113\text{in}$ $\Delta = 0.3626$ $w = 0.05531\text{in}$	$\chi^2_\nu = 9.62$	$N = 30058$ $z_o = 1.7112\text{in}$ $w = 0.05585\text{in}$ $\Delta = 0.3635$
$N = 29979$ $z_o = 1.70915\text{in}$ $\Delta = 0.37126$ $w = 0.05759\text{in}$ $\gamma' = 6.4760\times10^8\,\text{s}^{-1}$	$\chi^2_\nu = 6.12$	$N = 29979$ $z_o = 1.70195\text{in}$ $w = 0.05759\text{in}$ $\Delta = 0.37126$ $\gamma' = 6.4760\times10^8\,\text{s}^{-1}$

TABLE 16

QUANTUM-BEAT FIT RESULTS: RUN T18

$N = 29306$ $z_o = 1.7081\text{in}$	$\chi^2_\nu = 61.1$	
$N = 29215$ $z_o = 1.7080\text{in}$ $\Delta = 0.5154$	$\chi^2_\nu = 47$	$N = 29318$ $z_o = 1.7090\text{in}$ $w = 0.06119\text{in}$
$N = 28857$ $z_o = 1.7069\text{in}$ $\Delta = 0.55177$ $w = 0.06148\text{in}$	$\chi^2_\nu = 29$	$N = 28893$ $z_o = 1.7069\text{in}$ $w = 0.06165\text{in}$ $\Delta = 0.5524$
$N = 29242$ $z_o = 1.6999\text{in}$ $\Delta = 0.5567$ $w = 0.06207\text{in}$ $\gamma' = 6.6746\times10^8\,\text{s}^{-1}$	$\chi^2_\nu = 3.46$	$N = 29244$ $z_o = 1.6999\text{in}$ $w = 0.06205\text{in}$ $\Delta = 0.5566$ $\gamma' = 6.6751\times10^8\,\text{s}^{-1}$
Requiring a smaller Δ during fit.	$N = 29625$ $z_o = 1.7000\text{in}$ $\Delta = 0.3027$ $w = 0.06451\text{in}$ $\gamma' = 6.6834\times10^8\,\text{s}^{-1}$	

looks in comparison with the data in Fig. 24. If we make the 2.28% correction in these γ values we obtain the following final results for the decay rate of the $2^2P_{\frac{1}{2}}$ state in hydrogen:

$$\left.\begin{aligned} \gamma_{23} &= 6.3098\times10^8 s^{-1} \\ \gamma_{22} &= 6.4942\times10^8 s^{-1} \\ \gamma_{19} &= 6.3283\times10^8 s^{-1} \\ \gamma_{18} &= 6.52695\times10^8 s^{-1} \end{aligned}\right\} \quad \begin{aligned} \gamma &= 6.415(\pm0.112)\times10^8 s^{-1} \\ \tau &= 1.559(\pm0.027)\text{ns}. \end{aligned} \tag{66}$$

The standard deviation of the final value is rather large amounting to ±1.74%. Our value for the decay rate is higher than the generally accepted value of $\gamma = 6.27\times10^8 s^{-1}$. The deviation is 2.39%. We note also that the fitted phase differences are slightly larger than estimated by the computer simulation of the problem. This corresponds with the fringe field having an extent which is slightly larger than what we could measure in the field mapping tank.

The uncertainty in γ is not surprizing in view of the rather disappointing standard deviations associated with the values for $m=\gamma/\upsilon$ from the free-decay data. However, what is surprizing is the 2.4% deviation from the accepted value. Because of the difficulties we encounter in establishing our γ value via this method, verification of this value by an independent analysis of these data would serve to strengthen our confidence.

Fig. 24. Fit for Run T23 compared to the data.

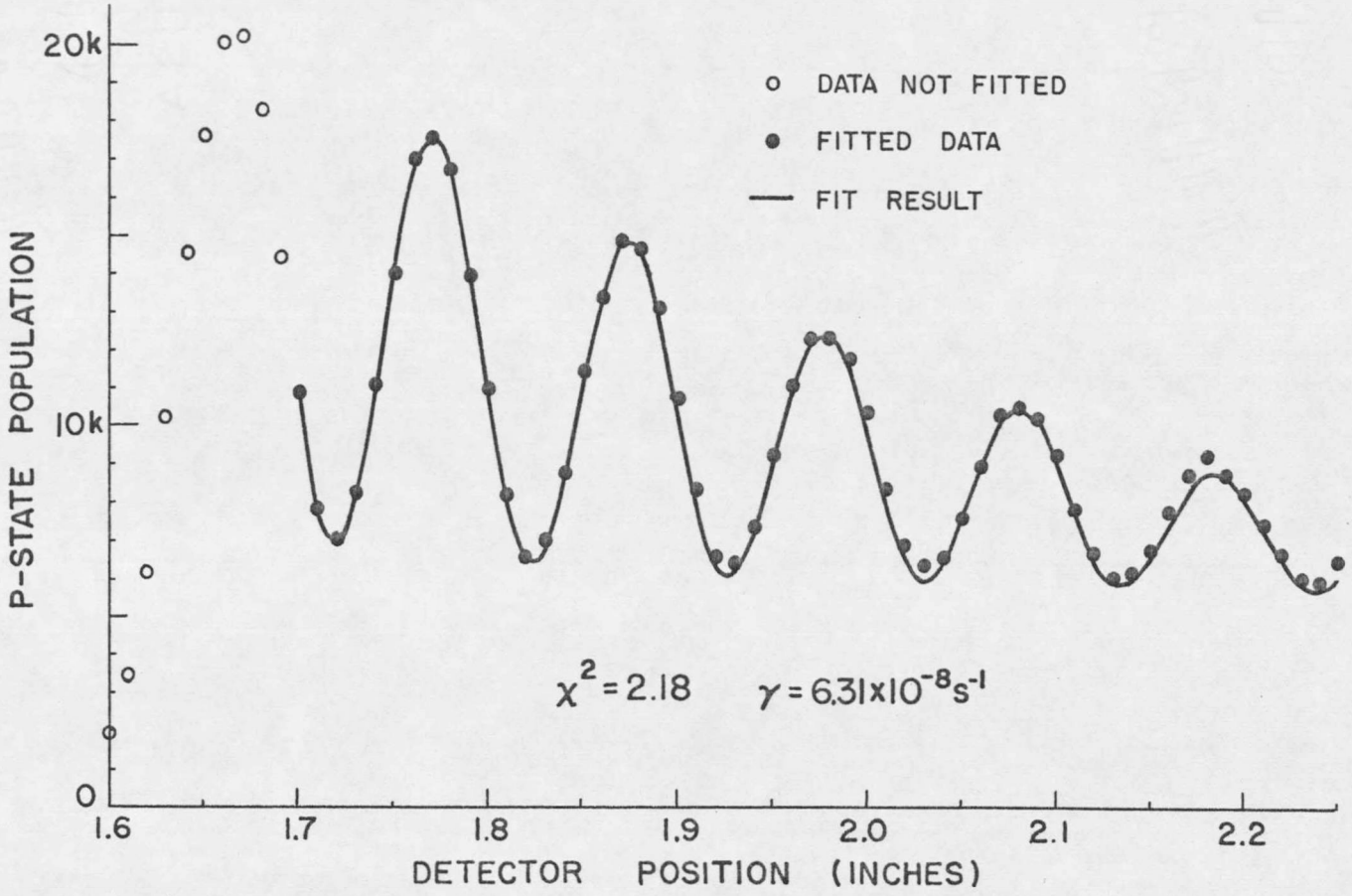

20k
10k
0
P-STATE POPULATION
DATA NOT FITTED
FITTED DATA
FIT RESULT
$\chi^2 = 2.18$
$\gamma = 6.31 \times 10^{-8} s^{-1}$
1.6
1.7
1.8
1.9
2.0
2.1
2.2
DETECTOR POSITION (INCHES)

FIG. 24

Independent Check with Profile Fit

We can provide an independent analysis by fitting the curve with a general profile function of the form

$$R(z) = N\left[e^{-\alpha z} + B e^{-\beta z} - G e^{-az}\cos(\delta z - \phi)\right] \tag{67}$$

where all the parameters (N, α, β, a, δ, ϕ) are free. We are interested in determining the value for δ as it represents the frequency of the modulation. In the high-frequency approximation, Eq. (30), we find

$$\delta = \omega\sqrt{1+4\epsilon^2}/v \ , \quad \epsilon = E/E_o \tag{68}$$

where E_o = 477.345volts/cm. If we solve for the velocity

$$v = \omega\sqrt{1+4\epsilon^2}/\delta \tag{69}$$

then we have a means of measuring the velocity if we establish δ via a fit, since we know the fine-structure splitting ω_{fs} and the applied field E. In table 17 we show the results of such a fit and the predicted velocities. Using the free-decay result for $m = \gamma/v$ we can determine the decay rate ($\gamma = mv = m\omega\sqrt{1+4\epsilon^2}/\delta$). The results of the profile fit are

$$\left.\begin{aligned} \gamma_{23} &= 6.4219\times10^8 s^{-1} \\ \gamma_{22} &= 6.5016\times10^8 s^{-1} \\ \gamma_{19} &= 6.3839\times10^8 s^{-1} \\ \gamma_{18} &= 6.4664\times10^8 s^{-1} \end{aligned}\right\} \begin{aligned} &\overline{\gamma} = 6.4435(\pm0.0514)\times10^8 s^{-1} \\ &\text{2.84\% higher than } 6.27\times10^8 s^{-1}. \end{aligned} \tag{70}$$

Although the standard deviations of these values are 0.8% of the aver-

TABLE 17

QUANTUM-BEAT PROFILE FITS

Run	Accel. Setting (kV)	Fit vel. υ ($\times 10^8$ cm/s)	Inferred Accel. Volts (kV)	Inferred γ ($\times 10^8 s^{-1}$)	χ^2_υ
T23	105	4.715	116.0	6.4219	2.36
T22	90	4.321	97.46	6.5016	4.77
T19	100	4.588	109.9	6.3839	3.33
T18	85	4.230	93.40	6.4664	4.00

age value we are encouraged to find only a 0.45% deviation between the two methods of obtaining the decay rate using our data.

Because of the above agreement we feel that we can claim that our method of determining γ is successful and that the analysis of the fringe field is correct. The experiment has been successful in this respect. However, either previous calculations and measurements of γ are insufficient, or there remains a hidden systematic error. We will now consider the possibilities.

Possible Systematic Errors and Improvements

The accuracy of the free-decay data and the resulting values for $m = \gamma/\upsilon$ are important to the final determination of the decay rate. In beam-foil experiments attention must be given cascades from higher levels before the lifetime of any single state may be determined. If cascades were present in this experiment their effects would be to lengthen the tail of the free-decay profile thereby decreasing the slope m. Cascades would, if present, produce a value for the decay rate which would be lower than the actual value contrary to our results. As explained in chapter 3 since no $n \geq 3$ states should survive passage to the experimental chamber we need not consider cascades further.

Another problem which could plague the free-decay data would be stray fields, motional electric fields from stray magnetic fields or electric fields from charged surfaces. If a charged surface should

arise in the supposed field-free region we anticipate that the ions kicked from the path of the beam would move in such a way to neutralize that surface. Thus after several minutes we expect any charge fields to be eliminated. To determine what any other stray field could do to the free-decay data we invoke the high-frequency approximation (small-field approximation). To lowest order in $\varepsilon = E/E_0$ the p-state population in presence of a small electric field is given by

$$|p(z)|^2 = e^{-\gamma' z/v} - 2\varepsilon^2 e^{-\gamma z/2v}\left[e^{-\gamma z/2v} - \cos\omega t\right], \tag{71}$$

where

$$\gamma' = \gamma(1-\varepsilon^2), \tag{72}$$

and ω is the finestructure splitting ($6.6469\times10^9 s^{-1}$). The presence of any stray field is seen to decrease the measured value of the decay rate ($\gamma' < \gamma$). In addition oscillations of the decay profile should be present. To get an idea of what stray field might be observed via the oscillations, a field of 75.5V/cm would decrease the measured decay rate γ' by 2.5% ($\varepsilon = 0.158$). In Fig. 25 we show what typical data would look like with a 50V/cm and a 100V/cm uniform stray field. We feel that any stray field larger than 50V/cm would be observable in the oscillations produced; a 50V/cm field would provide for a 1.1% correction to the decay rate.

The earth's magnetic field and other stray magnetic fields produce motional fields given by

$$E_H = kvH/c \tag{73}$$

Fig. 25. Quasi-free decay. The effects of a stray field upon a typical free-decay curve is shown.

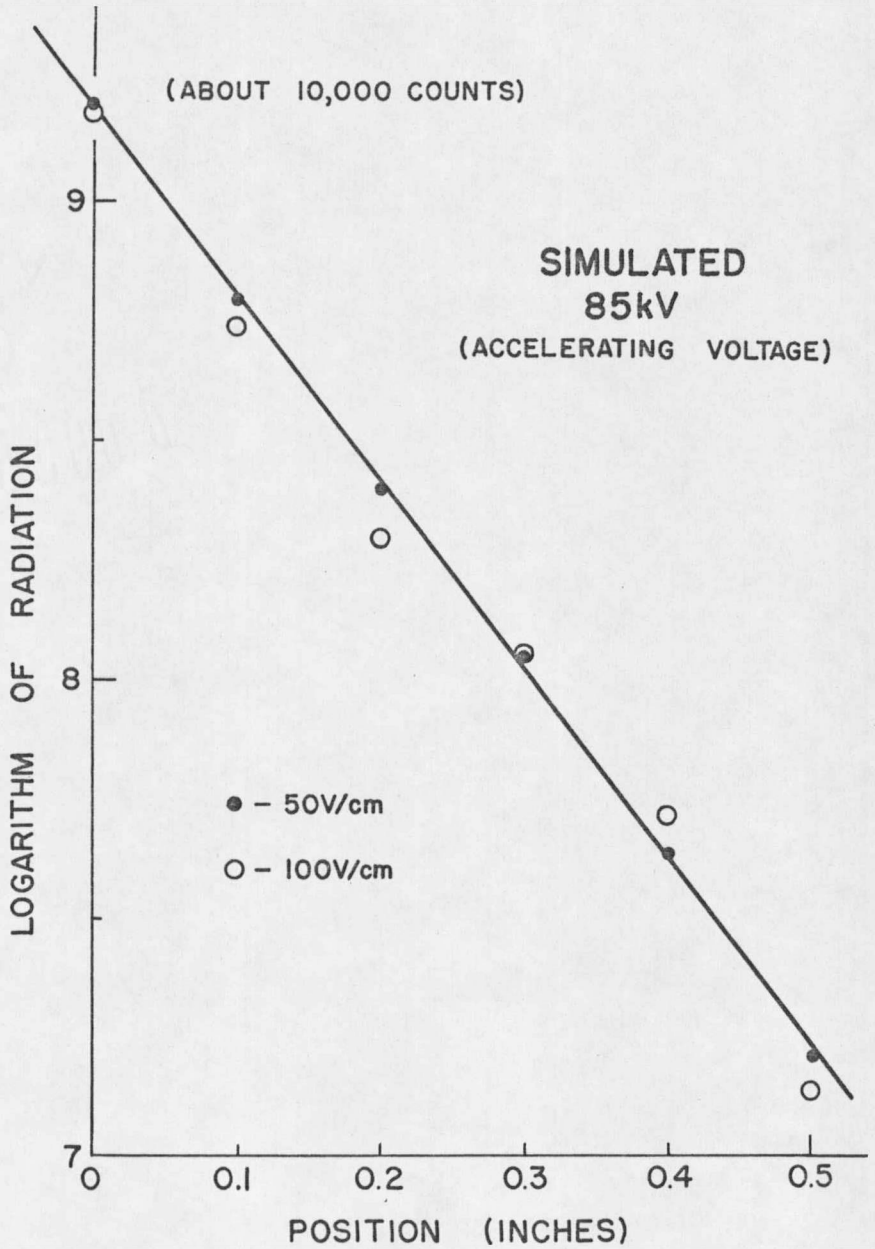

(ABOUT 10,000 COUNTS)
SIMULATED
85kV
(ACCELERATING VOLTAGE)
LOGARITHM OF RADIATION
9
8
7
● – 50V/cm
○ – 100V/cm
0
0.1
0.2
0.3
0.4
0.5
POSITION (INCHES)

FIG. 25

where

$$k = 299.776 \text{Volts/G}\cdot\text{cm}. \tag{74}$$

The stray magnetic fields were always less than 1Gauss. With beam velocities of 4×10^8cm/s the motional electric fields would be 4V/cm which is totally ignorable. We may therfore eliminate the possibility of stray fields entirely. Not only do they change the decay rate in the wrong way if we wish to explain our observations, but they would manifest themselves in the form of oscillations which are not observed.

This does not mean the the free-decay data are free from difficulties. An unexplained excessively large standard deviation is found in the sets of free-decay data for any run. For example, in Run T22 six sets of free-decay data are taken. The standard deviation of the six values for the slope m is 1.37%. During the analysis of data set 3E in run T22 we perform a simulation and find that the expected error in the inferred decay rate should be 0.8%. For the six similar sets the standard deviation of the means would be 0.33% ($\sigma_\mu = \sigma/\sqrt{n}$). The observed standard deviation is over four times larger. We feel that this unexpected error arrises from the detector positioning device and is not indicative of a more subtle systematic correction which we have neglected.

A possible solution to the discrepancy is seen to arise in specifying the fields for the QB data--the uniform field region. In the

high-frequency approximation the beam velocity is given by Eq. (69)

$$v = \omega\sqrt{1+4\epsilon^2}/\delta, \tag{75}$$

and γ is obtained from the free-decay data as $\gamma = mv$. Reducing the velocity would lower the inferred decay rate. If the electric field within the uniform field region were smaller we would infer a smaller velocity. In this approximation the electric field is related to the velocity by

$$E = (E_o/2)\left[\left(\frac{v\delta}{\omega}\right)^2 - 1\right]^{1/2}. \tag{76}$$

If we assume the free-decay results for run T23 are correct and that $\gamma = 6.27\times10^8 s^{-1}$ the beam velocity is 4.5780×10^8cm/s. Using the profile fit value for δ we find that the voltage applied to the plates would be $V = 95.49$V which is 5% lower than the 100V used (plate separation is 0.1213in or 0.3081cm). If the plates were oxidized and if this oxide layer--or oil layer from oil diffusion pump, although it was cold trapped with LN_2 except during warm up, and the plates were cleaned prior to Run T23--could hold a small charge the fields could be reduced by beam-ion charge neutralization. We calculate the capacitance of the uniform field plates (10.16cm × 2.54cm; $C = A\epsilon_o/d$) to be $C_{UFR} = 7.4$pfd. A four volt change in the field could be produced by a surfance charge accumulation of 2.97×10^{-11}C. We measure a beam-ion current to these plates of 46pA per plate. At such a current it would take on the order of one second to charge the surface, and switching the polarity of the

plates would not show the charging time constant in the Lyman-α counts since counting times are always of the order of minutes.

Although the earth's magnetic field produces motional quenching fields near 4V/cm, the motional field is for the most part perpendicular to the uniform field's direction. For this reason we may ignor the contribution from the earth's magnetic field (or other stray magnetic fields).

Having explored the possibilities for systematic errors we conclude this chapter with several suggestions which would serve to reduce or eliminate the problems associated with this measurement. We feel that record precisions could be provided by rebuilding the machine with the following changes:

1.) Better vacuums: Because beam-ion production and charging have been an observed problem it would be reduced greatly by decreasing the experimental chamber's pressures. This would also reduce the background counts. A stainless steel experimental chamber with ion pumps is recommended.

2.) Shielding all insulating surfaces that are in direct view of the beam is recommended--even the thin plastic spacers separating electrodes and ground plates.

3.) A new CEM cart positioning device which would essentially eliminate the positioning error should be included. In the data simu-

lation associated with the fit of free-decay data E3 of Run T22 we assume that the positioning precision is 0.00051in and the simulated precision of γ is 0.8%. If we reduce the error associated with the position to zero the precision of γ decreases to 0.7%.

4.) In attempts to eliminate all surface charging, all electrode and grounded surfaces which are near the beam should be gold plated.

6.) A serious source of error is the spacing between the plates of the uniform field region. The precision for γ is only as good as the accuracy of this spacing. Accurate spacing must be provided, however, without exposing insulating surfaces to the beam.

A comment is in order concerning the fitting. It would have been a great benefit in carefully fitting such nonlinear curves to have each parameter's size controlled in a continuously variable manner as input to the computer (using an analog-to-digital conversion). Such a feature would aid in establishing initial values of parameters which are unknown, and if the fits could be continuously displayed on a video monitor against the data one could quickly develop a feel for the fit and the function.

CHAPTER V

CONCLUSION

In the foregoing analysis we measure the lifetime of the 2p state in hydrogen by carefully analyzing spontaneous radiation in a field-free region and in an electric field region. The field-free decay (FD) exhibits simple exponential structure; whereas the decay radiation is modulated while in the uniform electric-field region giving rise to quantum beats (QB). The QB data are employed in two ways to give similar results for the lifetime. We first use the information from the FD curves to allow us to adjust the decay rate value so that the QB theory fits the data. We obtain $(6.415\pm0.112)\times10^{8}s^{-1}$ as the decay rate from this method. Secondly we determine the frequency of the QB oscillations whereby we infer the beam velocity. Then by using the FD results we determine the decay rate to be $(6.444\pm0.051)\times10^{8}s^{-1}$. Averaging these results we obtain $\gamma = (6.429\pm0.087)\times10^{8}s^{-1}$ for the decay rate of the 2p state where the standard deviation obtains from the average variance $\sigma^2 = \frac{1}{2}(\sigma_1^2 + \sigma_2^2)$. The corresponding lifetime is

$$\tau = (1.555\pm0.021)\text{ns}$$

which is 2.5% shorter than our calculated value of 1.596ns and exhibits a standard deviation of 1.35%.

In obtaining this result we not only account for the hyperfine structure of the $2^2S_{\frac{1}{2}}$ and $2^2P_{\frac{1}{2}}$ levels as well as the effects of the $2^2P_{3/2}$ level, but we also take care to account for the fringe field of the uniform field region. With such attention it is rather surprising to find a 2.5% discrepancy between our result and both theory and previous experiment. There is only one possible experimental condition which could serve to explain such a variance--that of beam-ion charging of the uniform-field-region plates thereby reducing the effective field applied by the plates. However, since such charging mechanisms must also modify the background radiation in ways which are not observed, we have no recourse but to trust our result.

It is doubtful that previous experiment and theory could be in error in that they have failed to provide an accurate value for the lifetime. Objections may be raised against the beam-foil experiments since they do not analyze a detailed theory involving cascade effects and state preparation but are simple fits involving two exponential functions or an exponential plus a constant. However, because the 2p decay is noticeably distinct from the 3p decay such objections may have little weight. Even so, the calculation of the 2p lifetime seems to be sound enough so that any difficulties there would certainly manifest themselves in other realms of atomic measurement. For these reasons our attention and suspicion turns to the two-level theory.

Recall that the two-level theory which we employ--the Bethe-Lamb theory--assumes that the decay of the p state is accurately provided for by the inclusion of a damping term in the amplitude equation for the p state. The probability of the n = 2 level is not conserved and the $1^2S_{\frac{1}{2}}$ ground state serves only as a graveyard for the p-state atoms which decay. As Keller and Robiscoe point out, such assumptions fail to account for any effects which arise from Stark coupling of the p state with the ground state.[27] Such ground-state coupling may become important when the matrix elements are no longer small compared to the natural level width $\hbar\gamma/2$ as in this experiment ($\hbar\gamma/2 \simeq 3\times10^{-19}$ergs whereas $V_{sp} \simeq 4\times10^{-18}$ergs). Thus, a full analysis of the three-level problem will provide a more accurate picture and may resolve the differences between our result and those obtained previously.

Our measurement of the 2p lifetime in hydrogen provides experimental evidence that the Bethe-Lamb theory needs modification before it can be applied to problems with stronger coupling. This suggests that a full, Weisskopf-Wigner treatment of the three-level problem should be a next step in our attempts to better understand spontaneous radiation as it manifests itself in the simplest atomic system.

APPENDIX 1

CALCULATION OF LIFETIME

One application of time-dependent perturbation theory is in the calculation of spontaneous transition probabilities in the dipole approximation. The spontaneous transition probability of a state A decaying to state B may be written [28]

$$W_{AB} = \frac{4}{3}\alpha \frac{\omega^3}{c^2} |\vec{r}_{BA}|^2 \tag{77}$$

where $\alpha = e^2/\hbar c$, $\vec{r}_{BA} = \langle B| \vec{r} |A\rangle$ and $\vec{r}$ is the position vector. The lifetime of state A (τ_A) may then be written as

$$\gamma = 1/\tau_A = \sum_i W_{AB_i} \tag{78}$$

where B_i represents all the final states to which the state A may decay. If there are N states comprising a level A then we speak of the lifetime of level A as an average of the lifetimes for each state in the level. Thus

$$\tau = \frac{1}{N}\sum_k \tau_{A_k} = \frac{1}{N}\sum_k \left[\sum_i W_{A_k B_i}\right]^{-1} \tag{79}$$

assuming an equal population of the initial states A_k.

The $2^2P_{\frac{1}{2}}$ fine-structure level is composed of four hyperfine states as is the $1^2S_{\frac{1}{2}}$ ground state (the final state). In order to calculate the lifetime we must evaluate the transition probabilities for these hyperfine transitions which leads us first to a calculation of $|\vec{r}_{BA}|^2$.

Following Sakuri we write [29]

$$|\vec{r}_{BA}|^2 = \left| -\frac{(x_{BA} + i y_{BA})}{\sqrt{2}} \right|^2 + \left| \frac{x_{BA} - i y_{BA}}{\sqrt{2}} \right|^2 + |z_{BA}|^2 \tag{80}$$

The initial states A are the hyperfine $2^2P_{\frac{1}{2}}$ (2p) states and the final states B are the hyperfine $1^2S_{\frac{1}{2}}$ (1s) states. In appendix 2 we examine the possible couplings between the 2p and the $2^2S_{\frac{1}{2}}$ (2s) hyperfine system. The conlusions obtained there are applicable to the 2p - 1s system, for we are considering the same angular momentum structure in a different n level. We only need to remember that the 2p - 1s fine-structure splitting (analogous to the Lamb shift) is larger and the 1s hyperfine splitting is also larger than the corresponding state separations associated with the n = 2 system. The non-zero matrix elements in table 20 of appendix 2 arise from orthogonality of spin states of the electron and the nucleus. In an analogous manner the matrix elements, Eq. (80), associated with the 2p - 1s system may be written in terms of three elements $\langle 1S_o | V | 2P_{1,0,-1} \rangle$. Using the wavefunction

$$|1S_o\rangle = \frac{1}{\sqrt{\pi}} a^{-3/2} e^{-r/a}, \tag{81}$$

where $a = a_o(1 + m_e/M_p)$ and a_o is the Bohr radius, we calculate

$$\begin{aligned} M_z &= \langle 1S_o | z | 2P_o \rangle = \mathcal{M} \\ M_+ &= \langle 1S_o | (x+iy)/\sqrt{2} | 2P_{-1} \rangle = \mathcal{M} \\ M_- &= \langle 1S_o | (x-iy)/\sqrt{2} | 2P_{+1} \rangle = \mathcal{M} \end{aligned} \tag{82}$$

as the only nonzero elements for the elementary wavefunctions (not hy-

perfine wavefunctions). Here

$$= 2^8 a/3^5\sqrt{2} = (0.744935)a. \tag{83}$$

The hyperfine matrix elements will then be $1/\sqrt{3}$ times the above elements (see table 20). There will accordingly be three transitions out of each hyperfine 2p state. The square of the coupling for each transition is the same having the value

$$V^2 \equiv |\vec{r}_{BA}|^2 = \frac{1}{3}(0.554929)a^2. \tag{84}$$

There are three frequencies associated with these transitions

$$\begin{aligned} \omega_a &= \omega_\alpha\left[1+(\Delta\omega_2/4\omega_\alpha)-(\Delta\omega_1/4\omega_\alpha)\right] \\ \omega_b &= \omega_\alpha\left[1+(\Delta\omega_2/4\omega_\alpha)-(3\Delta\omega_1/4\omega_\alpha)\right] \\ \omega_c &= \omega_\alpha\left[1-(3\Delta\omega_2/4\omega_\alpha)-(\Delta\omega_1/4\omega_\alpha)\right], \end{aligned} \tag{85}$$

where $\omega_\alpha = 1.5495\times10^{16}s^{-1}$ is the fine-structure 2p - 1s splitting [30] and $\Delta\omega_1$, $\Delta\omega_2$ are the hyperfine splittings of the 1s and 2p states respectively--$\Delta\omega_1 = 8.922\times10^9 s^{-1}$(1420MHz) and $\Delta\omega_2 = 3.719\times10^8 s^{-1}$(59.2MHz). Because the transition level splitting is so large compared to the hyperfine splittings, these frequencies will be considered to be equal, i.e., to better than 1ppm we let

$$\omega_\alpha = \omega_a = \omega_b = \omega_c. \tag{86}$$

The summations of the transition probabilities will then all be equal

$$\sum_i W_{A_k B_i} = 4\alpha V^2 \omega_\alpha{}^3/c^2, \quad k=1,2,3,4. \tag{87}$$

The lifetime, Eq (79), may then be determined to be [31]

$$\tau = 1.5961\times10^{-9}s.$$

A similar result (τ = 1.596ns) is calculated by Chupp, Dotchin, and Pegg.[5] We note that several approximations have been used to obtain this result as pointed out by Bethe and Salpeter[32]: 1.) we use the nonrelativistic Schrödinger theory, 2.) only the lowest order terms in the expansion for the interaction of the electron with the radiation field is used, and 3.) the dipole approximation is employed. All of these approximations should be good for the problem at hand.

APPENDIX 2

HYPERFINE STRUCTURE OF THE N = 2 LEVEL

The elementary wavefunctions of hydrogen are described by three quantum numbers (q.n.) n, ℓ, m_ℓ. The principle q.n. n determines the energy of the level (in cgs units)

$$\langle H \rangle = E_n = -\alpha^2 c^2 \mu / 2n^2, \tag{89}$$

where $\alpha = e^2/\hbar c$ is called the fine-structure constant and μ is the reduced mass $\mu = M_p m_e/(M_p + m_e)$. The q.n. ℓ describes the total orbital angular momentum of the electron

$$\langle \mathbb{L}^2 \rangle = \hbar^2 \ell(\ell+1), \quad \ell = 1, 2, \cdots, n; \tag{90}$$

and m_ℓ is the q.n. which specifies the component of the angular momentum which may be observed in some particular direction (magnetic q.n.), say z direction,

$$\langle L_z \rangle = \hbar m_\ell, \quad m_\ell = -\ell, -\ell+1, \cdots, 0, 1, 2, \cdots, \ell. \tag{91}$$

Such a formulation of the hydrogen atom neglects the contributions to the energy which arise from the spin of both the electron and the nucleus, however, the wavefunctions obtained form a basis for generating wavefunctions of the more complete systems. The elementary wavefunctions for the n = 2 level will be of interest to us in this calculation; so using the notation

$$\Psi_{n\ell m_\ell} = \psi_{n\ell m_\ell} e^{-i\omega_n t}, \tag{92}$$

where $\omega_n = E_n/\hbar$, the spatial parts are given by

$$\begin{aligned}
\psi_{z00} &= |2S_0\rangle = (4\sqrt{2\pi}\, a^{3/2})^{-1}(2-\rho)\, e^{-\rho/2} \\
\psi_{z11} &= |2P_1\rangle = -(8\sqrt{\pi}\, a^{3/2})^{-1}\rho e^{-\rho/2} \sin\theta\, e^{i\phi} \\
\psi_{z10} &= |2P_0\rangle = (4\sqrt{2\pi}\, a^{3/2})^{-1}\rho e^{-\rho/2}\cos\theta \\
\psi_{z1-1} &= |2P_{-1}\rangle = (8\sqrt{\pi}\, a^{3/2})^{-1}\rho\, e^{-\rho/2}\sin\theta\, e^{-i\phi}
\end{aligned} \tag{93}$$

where $\rho = 2r/na$ $(n = 2)$ and $a = (m_e/\mu)a_o$ where a_o is the Bohr radius $a_o = \hbar^2/e^2 m_e$. The reader is referred to the literature for the other hydrogenic wavefunctions.[33]

When placed in an electric field which is sufficiently uniform (the spatial variations in the applied field are very small compared to atomic dimensions) the proton-electric pair looks like a dipole. The energy of such a dipole is $W = -\vec{p}\cdot\vec{E}$ where $\vec{p} = -e\vec{r}$ is the dipole moment, or

$$W = e\vec{r}\cdot\vec{E}. \tag{94}$$

Because of the spherical symmetry of the problem and the specific complex nature of the wavefunctions, it is useful to write $\vec{r}$ and $\vec{E}$ in spherical coordinates. The vector product can be written as

$$\vec{r}\cdot\vec{E} = r\left[\tfrac{1}{2}\sin\theta\,(E_- e^{i\phi} + E_+ e^{-i\phi}) + \cos\theta\, E_z\right], \tag{95}$$

where

$$E_\pm = E_x \pm i E_y. \tag{96}$$

Using the wavefunctions of Eqs. (93) the only nonzero, Stark matrix

elements coupling the states are straightforwardly calculated to be [34]

$$\langle 2P_1|W|2S_0\rangle = (3ae/\sqrt{2})E_-$$

$$\langle 2P_0|W|2S_0\rangle = -3ae\,E_z \tag{97}$$

$$\langle 2P_{-1}|W|2S_0\rangle = -(3ae/\sqrt{2})E_+ .$$

These results will provide the basis for the fine-structure and hyperfine-structure matrix elements. We note the verification of the selection rules $\Delta\ell = \pm 1$, $\Delta m_\ell = \pm 1,0$ for a dipole transition. We also note that if the electric field lies totally along the quantization axis (z axis) then the electric field couples only two states and two-level theory sufficiently handles the problem. If the electric field lies in the plane perpendicular to the quantization axis then three-level theory would be needed; for arbitrary electric field we would have a four-level problem.

The fine structure of the hydrogen atom may be explained by considering the contribution to the energy level structure coming from the interaction of the electron's spin and orbital angular momentum. With the introduction of spin $\vec{S}$ the actual total angular momentum is

$$\vec{J} = \vec{L} + \vec{S}. \tag{98}$$

We may now find wavefunctions which are eigenfunctions of $\vec{L}^2$, $\vec{S}^2$, $\vec{J}^2$, and J_z in terms of products of the elementary n, ℓ, m_ℓ wavefunctions and spin-state wavefunctions χ_+ denoting spin up and χ_- denoting spin

down.[34] The transformation relating the n, ℓ, m_ℓ and s, m_s wavefunctions ($s = \frac{1}{2}$, $m_s = \pm\frac{1}{2}$) and the n, ℓ, s, j, m_j wavefunctions--hereafter referred to as fine-structure wavefunctions--is the Clebsch-Gordan transformation. The resulting fine-structure wavefunctions for the n = 2 level are found to be [35]

$$
\begin{aligned}
|2S_{1/2}\rangle &= \begin{cases} |2S_0\rangle\chi_+ , & \text{for } m_j = +1/2 \\ |2S_0\rangle\chi_- , & m_j = -1/2 \end{cases} \\
|2P_{1/2}\rangle &= \begin{cases} -\sqrt{\frac{1}{3}}\,|2P_0\rangle\chi_+ + \sqrt{\frac{2}{3}}\,|2P_1\rangle\chi_- , & m_j = +1/2 \\ -\sqrt{\frac{2}{3}}\,|2P_{-1}\rangle\chi_+ + \sqrt{\frac{1}{3}}\,|2P_0\rangle\chi_- , & m_j = -1/2 \end{cases} \\
|2P_{3/2}\rangle &= \begin{cases} |2P_1\rangle\chi_+ , & m_j = +3/2 \\ \sqrt{\frac{2}{3}}\,|2P_0\rangle\chi_+ + \sqrt{\frac{1}{3}}\,|2P_1\rangle\chi_- , & m_j = +1/2 \\ \sqrt{\frac{1}{3}}\,|2P_{-1}\rangle\chi_+ + \sqrt{\frac{2}{3}}\,|2P_0\rangle\chi_- , & m_j = -1/2 \\ |2P_{-1}\rangle\chi_- , & m_j = -3/2 \end{cases}
\end{aligned}
\tag{99}
$$

Again, we are interested in the Stark coupling bewteen the states. Because of the orthogonality of the spin wavefunctions the fine-structure matrix elements are just proportional to the elements already calculated. Table 18 summarizes the results.

In order to account for the spin of the nucleus and its contribution to the problem we proceed in a way similar to the fine-structure

TABLE 18

FINE-STRUCTURE DIPOLE MATRIX ELEMENTS

$$V = \langle \psi' \mid e\,\vec{r}\cdot\vec{E} \mid \psi \rangle$$

ψ	ψ'					
$2^2S_{\frac{1}{2}}$	$2^2P_{\frac{1}{2}}$		$2^2P_{3/2}$			
m_j	1/2	-1/2	3/2	1/2	-1/2	-3/2
$\frac{1}{2}$	$-\sqrt{\frac{1}{3}}\,V_z$	$-\sqrt{\frac{2}{3}}\,V_+$	V_-	$\sqrt{\frac{2}{3}}\,V_z$	$\sqrt{\frac{1}{3}}\,V_+$	0
$-\frac{1}{2}$	$\sqrt{\frac{2}{3}}\,V_-$	$\sqrt{\frac{1}{3}}\,V_z$	0	$\sqrt{\frac{1}{3}}\,V_-$	$\sqrt{\frac{2}{3}}\,V_z$	V_+

$$V_z = \langle 2P_o \mid e\,\vec{r}\cdot\vec{E} \mid 2S_o \rangle = -3\,a\,e\,E_z$$

$$V_- = \langle 2P_1 \mid e\,\vec{r}\cdot\vec{E} \mid 2S_o \rangle = (3/\sqrt{2})\,a\,e\,E_-$$

$$V_+ = \langle 2P_{-1} \mid e\,\vec{r}\cdot\vec{E} \mid 2S_o \rangle = -(3/\sqrt{2})\,a\,e\,E_+$$

complication. We seek to find eigenfunctions of the total angular momentum

$$\vec{F} = \vec{I} + \vec{J} \tag{100}$$

where $\vec{I}$ is the spin angular momentum of the nucleus and $\vec{J} = \vec{L} + \vec{S}$ represents the total angular momentum of the electron. Hyperfine wavefunctions may now be determined which are eigenfunctions of $\vec{L}^2$, $\vec{J}^2$, $\vec{F}^2$, and F_z by considering product wavefunctions of the above electronic fine-structure wavefunctions and nuclear spin-up, η_+, spin-down η_-, wavefunctions. A Clebsch-Gordan transformation may again be made to obtain the hyperfine wavefunctions in terms of the fine-structure wavefunctions which may then be expressed in terms of the elementary wavefunctions. The results may be found in table 19. We may now calculate the dipole matrix elements using these hyperfine wavefunctions. The results are in table 20.

As explained in the main text, since we choose the electric field to be along the quantization axis the hyperfine problem reduces to four two-level problems involving the matrix element

$$V = \sqrt{3}\, a\, e\, E \tag{101}$$

where $E = V_o/d$ with V_o, the applied voltage and d, the plate separation of the parallel plates. Noting that

$$a = (1 + m_e/M_p)a_o, \tag{102}$$

where a_o is the Bohr radius we may calculate [3]

TABLE 19

HYPERFINE WAVEFUNCTIONS

$$\psi_{HFS} = |\ell j\ f\ m_f\rangle = \sum_k A_k \mid \ell\ m_\ell\rangle|m_s\rangle|m_i\rangle$$

			A_k	ℓ	1								0	
				m_ℓ	1		0		-1		0	
				m_s	$\frac{1}{2}$	$-\frac{1}{2}$	$\frac{1}{2}$	$-\frac{1}{2}$	$\frac{1}{2}$	$-\frac{1}{2}$	$\frac{1}{2}$	$-\frac{1}{2}$
ℓ	j	f	m_f	m_i	$\frac{1}{2}$ $-\frac{1}{2}$	$\frac{1}{2}$ $-\frac{1}{2}$	$\frac{1}{2}$ $-\frac{1}{2}$	$\frac{1}{2}$ $-\frac{1}{2}$	$\frac{1}{2}$ $-\frac{1}{2}$	$\frac{1}{2}$ $-\frac{1}{2}$	$\frac{1}{2}$ $-\frac{1}{2}$	$\frac{1}{2}$ $-\frac{1}{2}$
1	$\frac{3}{2}$	2	2		1							
			1			e	e		c			
			0					g		d	d	
			-1									c
			-2									
		1	1			a	-h		-g			
			0					g		d	-d	
			-1									g
	$\frac{1}{2}$	1	1				b		-d			
			0					d		-g	g	
			-1									d
		0	0					d		-g	-g	
0	$\frac{1}{2}$	1	1									
			0									
			-1									
		0	0									

													1	
													c	c
													c	-c

$a = \sqrt{3/4}$, $b = \sqrt{2/3}$, $c = \sqrt{1/2}$, $d = \sqrt{1/3}$, $e = \sqrt{1/4}$, $g = \sqrt{1/6}$, $h = \sqrt{1/12}$

TABLE 20

HYPERFINE-STRUCTURE DIPOLE MATRIX ELEMENTS

$$V = \langle \psi'(\ell, j, f, m_f | \, e\vec{r} \cdot \vec{E} \, | \psi(\ell, j, f, m_f \rangle$$

				ψ											
			ℓ	1											
			j	3/2 ($2^2P_{3/2}$)								1/2 ($2^2P_{1/2}$)			
$\psi'(2^2S_{1/2})$			f	2					1			1			0
ℓ	j	f	m_f	2	1	0	-1	-2	1	0	-1	1	0	-1	0
0	1/2	1	1	V_-	$\sqrt{\frac{1}{2}}V_z$	$\sqrt{\frac{1}{6}}V_+$	0	0	$-\sqrt{\frac{1}{6}}V_z$	$-\sqrt{\frac{1}{6}}V_+$	0	$-\sqrt{\frac{1}{3}}V_z$	$-\sqrt{\frac{1}{3}}V_+$	0	$\sqrt{\frac{1}{3}}V_+$
			0	0	$\sqrt{\frac{1}{2}}V_-$	$\sqrt{\frac{2}{3}}V_z$	$\sqrt{\frac{1}{2}}V_+$	0	$\sqrt{\frac{1}{6}}V_-$	0	$-\sqrt{\frac{1}{6}}V_+$	$\sqrt{\frac{1}{3}}V_-$	0	$-\sqrt{\frac{1}{3}}V_+$	$-\sqrt{\frac{1}{3}}V_z$
			-1	0	0	$\sqrt{\frac{1}{6}}V_-$	$\sqrt{\frac{1}{2}}V_z$	V_+	0	$\sqrt{\frac{1}{6}}V_-$	$\sqrt{\frac{1}{6}}V_z$	0	$\sqrt{\frac{1}{3}}V_-$	$\sqrt{\frac{1}{3}}V_z$	$\sqrt{\frac{1}{3}}V_-$
		0	0	0	0	0	0	0	$\sqrt{\frac{2}{3}}V_-$	$\sqrt{\frac{2}{3}}V_z$	$\sqrt{\frac{2}{3}}V_+$	$-\sqrt{\frac{1}{3}}V_-$	$-\sqrt{\frac{1}{3}}V_z$	$-\sqrt{\frac{1}{3}}V_+$	0

$$\sqrt{3}\, a\, e = 4.404873(52)\times 10^{-18}\,\text{esu}\cdot\text{cm}. \tag{103}$$

With the conversion

$$\frac{\text{esu}\cdot\text{cm}^{-2}}{\text{volt}\cdot\text{cm}^{-1}} = 299.79250(10) \tag{104}$$

we find

$$\sqrt{3}\, a\, e = 1.469307(13)\times 10^{-20}\,\text{erg}\cdot\text{cm}\cdot\text{volt}^{-1};$$

in which case we will want to measure the electric field in units of V/cm.

We have yet to specify the energy level separations ω_i associated with the hyperfine system involving the 2s and 2p levels. The hyperfine energy contribution may be written in terms of a constant times the q.n. which specify the state [36]

$$\mathcal{E}_{hfs} = K\frac{f(f+1) - i(i+1) - j(j+1)}{j(j+1)(2\ell+1)} \tag{105}$$

The hyperfine splitting for the 2s level has been measured [37] to be

$$\Delta w = 177.55686(\pm 0.3\text{ppm})\text{MHz}. \tag{107}$$

With the help of Eq. (106) we may then determine the 2p splitting to be $\Delta w/3$. The two-level hyperfine state separations in angular frequency units may now be determined to be

$$\omega_1 = \omega_2 = 2\pi(\mathcal{S} + \Delta w/6) = 6.832875\times 10^9\,\text{s}^{-1},$$

$$\omega_3 = 2\pi(\mathcal{S} + \Delta w/2) = 7.204749\times 10^9\,\text{s}^{-1},\quad \omega_4 = 2\pi(\mathcal{S} - 5\Delta w/6) = 5.717252\times 10^9\,\text{s}^{-1},$$

where $\mathcal{S}$ is the Lamb shift (known to $\sim$20ppm).

FOOTNOTES

[1]W. Wein, Ann. Physik 60, 39 (1919); 66, 16 (1921); 73, 32 (1924); 83, 1 (1927). It is in the last reference that the Lyman-α transition lifetimes are measured.

[2]L. Kay, Phys. Let. 5, 36 (1963); Proc. Phys. Soc (london) 85, 163 (1965). S. Bashkin, Nuc. Instr. Methods 28, 88 (1964).

[3]An excellent review of beam-foil spectroscopy has been made by J. Martinson and A. Gaupp, Phys. Reports (section C of Phys. Let.) 15, 113 (1974) and more recently by H. G. Berry, Rep. Prog. Phys. (GB) 40, 155 (1977). A very recent review of lifetime measurements may be found in R. E. Imhof and F. H. Read, Rep. Prog. Phys. (GB) 40, 1 (1977).

[4]W. S. Bickel and A. S. Goodman, Phys. Rev. 148, 1 (1966)

[5]E. L. Chupp, L. W. Dotchin and D. J. Pegg, Phys. Rev. 175, 44 (1968); see also A. Gaupp, "Quantenbeats an n = 2 Niveau des Wasserstoffs bei Äusseren Feldern" (Ph.D. Thesis, Free University of Berlin, 1973, unpublished), where he obtains $\tau = (1.60\pm0.04)$ns ($\pm 2.5\%$).

[6]C. R. Stroud, Jr. and E. T. Jaynes, Phys. Rev. A 1, 106 (1970)

[7]P. W. Milonni and W. A. Smith, Phys. Rev. A 11, 814 (1975)

[8]S. R. Lundeen and F. M. Pipkin, Phys. Rev. Let. 34, 1368 (1975); see also D. A. Andrews and G. Newton, Phys. Rev. Let. 37, 1254 (1976); R. T. Robiscoe and T. W. Shyn, Phys. Rev. Let. 24, 559 (1970);

and the Lamb papers, the last of a series of six papers is E. S. Dayhoff, S. Triebwasser, and W. E. Lamb, Phys. Rev. 89, 106 (1953).

[9]G. Astner et al., Z. Physik A 279, 1 (1976).

[10]The observation of both zero-field and field-induced quantum beats are now important tools in making level separation measurements in atomic systems. See Ref. 3. Also consider discussions given by H. J. Andrä, Physica Scripta (Sweden) 9, 257 (1974). Stark Lyman beats are discussed in detail by M. J. Alguard and C. W. Drake, Phys. Rev. A 8, 27 (1973).

[11]S. Klarsfeld, Phys. Lett. 30A, 382 (1969).

[12]A. S. Davydov, Quantum Mechanics (NEO Press, Ann Arbor, Michigan, 1966), Chap. 9, Sec. 74, p. 289, Eq. (74.9).

[13]E. U. Condon and G. H. Shortley, The Theory of Atomic Spectra (Cambridge University Press, New York, 1970), Chap. 5, p. 133.

[14]Davydov, Ref. 12, Sec 76, p. 294, Eq. (76.6).

[15]V. Weisskopf and E. Wigner, Z. Physik 63, 54 (1930); 65, 18 (1930).

[16]Many experimets have based their analysis upon these phenomenological two-level equations--often referred to as the Bethe-Lamb equations. Perhaps the most notable experiments are the Lamb-shift experiments (see Ref. 8). A discussion of the appropriateness of the Weisskopf-Wigner damping is found in M. P. Silverman and F. M. Pipkin,

J. Phys. B 5, 2236 (1972).

[17]H. K. Holt and I. A. Sellin, Phys. Rev. A 6, 508 (1972).

[18]T. W. Shyn, W. L. Williams, R. T. Robiscoe, and T. Rebane, Phys. Rev. Let. 22, 1273 (1969). They quote $\Delta E_H - S = \nu_{3/2} = 9911.213 \pm 0.058$MHz.

[19]R. T. Robiscoe, Phys. Rev. A 17, 247 (1978).

[20]M. Abromovitz and I. A. Stegun, eds., Handbook of Mathematical Functions, Applied Mathematics Series 55 (National Bureau of Standards, U.S. Government Printing Office, 1965), Chap. 15.

[21]Cross section measurements have been made by J. E. Bayfield, Phys. Rev. 182, 115 (1969).

[22]Condon and Shortley, Ref. 13, p. 136.

[23]Condon and Shortley, Ref. 13, p. 133.

[24]J. M. Wessner, "An Experimental Test of Semiclassical Radiation Theories" (Ph.D. Thesis, Montana State University, 1972). The results are published in J. M. Wessner, D. K. Anderson, and R. T. Robiscoe, Phys. Rev. Let. 29, 1126 (1972).

[25]P. R. Bevington, Data Reduction and Error Analysis for the Physical Sciences (McGraw-Hill, New York, paperback, 1969), Chap. 8, p. 154. This book contains much information on nonlinear curve fitting as well as excellent discussions on data analysis. It provided the

basis for all computer programs used to analyze our data. An excellent introduction to data analysis may be found in H. D. Young, Statistical Treatment of Experimental Data (McGraw-Hill, New York, paperback, 1962).

[26]We are indebted to M. A. Hamilton for the suggestion of the simulation method, Private communications. A normal distribution can be generated from the uniform distribution on the interval (0,1) via the Box-Muller method as described in T. G. Newan and P. L. Odell, The Generation of Random Variables, Griffin's Statistical Monographs & Courses, Ed. Alan Stuart, Number 29 (Hafner Pub. Co., New York, 1971).

[27]O. A. Keller and R. T. Robiscoe, Phys. Rev. 188, 82 (1969).

[28]J. J. Sakuri, Advanced Quantum Mechanics (Addison-Wesley, Reading Mass., 1967), p. 43, with appropriate adjustment of units. See also H. A. Bethe and E. E. Salpeter, Quantum Mechanics of One- and Two-Electron Atoms (Springer-Verlag, Berlin, 1957), p. 250.

[29]Sakuri, Ref. 27, p. 43.

[30]C. E. Moore, Atomic Energy Levels (National Bureau of Standards, U.S. Government Printing Office, 1949), Vol. 1. $\omega_\alpha = 2\pi ck$, where k is given as the wavenumber $k_{\frac{1}{2}} = 8.2258907\times10^4 cm^{-1}$.

[31]We use values of the constants as given by B. N. Taylor, W. H. Parker, and D. N. Langenberg, Rev. Mod. Phys. 41, 375 (1969).

[32]Bethe and Salpeter, Ref. 27, p. 249.

[33]The normalization for the hydrogenic wavefunctions have now become standard. Though notation may differ the following references agree upon the explicit functional forms of the wavefunctions: N. Tralli and F. R. Pomilla, Atomic Theory: Introduction to Wave Mechanics (McGraw-Hill, New York, 1969), Chap. 5; L. I. Schiff, Quantum Mechanics (McGraw-Hill, New York, 1968), pp. 80, 94; E. Merzbacher, Quantum Mechanics (John Wiley & Sons, New York, 1970), pp. 185, 209, 430; Davidov, Ref. 12, pp. 24, 139; R. H. Dicke and J. P. Wittke, Introduction to Quantum Mechanics (Addison-Wesley, Reading, Mass., 1960), pp. 148, 162; Condon and Shortley, Ref. 13, pp. 52, 117, the radial functions are always less than zero in only this work; J. L. Powell and B Crasemann, Quantum Mechanics (Addison-Wesley, Reading, Mass., 1961), Chap. 7.

[34]For the details of addition of two angular momenta refer to any of the texts in Ref. 32.

[35]These calculations have been verified by R. T. Robiscoe, private communication. See also G. W. Series, Phys. Rev. 136, 684 (1964); and R. K. Wangsness, Phys. Rev. 149, 60 (1966).

[36]Bethe and Salpeter, Ref. 27, p. 110.

[37]J. Heberle, H. Reich, and P. Kusch, Phys. Rev. 101, 612 (1956).

MONTANA STATE UNIVERSITY LIBRARIES
3 1762 10010938 6

[redacted]
D378
K287
cop.2

Kelley, Edward F
Radiative mean life-time measurement in N=2 hydrogen

DATE	ISSUED TO
	L. Snively Physics Dept. 36
	[redacted]

D378
K287
cop 2